AGE-DEPENDENT CHANGES IN GLUCO-GLYCERONEOGENESIS AND FAT SYNTHESIS SUSTAIN COPULATION FITNESS IN *C. elegans* MALES

A Dissertation

by

JIMMY FERREIRA GONÇALVES

Submitted to the Office of Graduate and Professional Studies of
Texas A&M University
in partial fulfillment of the requirements for the degree of

DOCTOR OF PHILOSOPHY

Chair of Committee,	Luis René Garcia
Committee Members,	Jason Karpac
	Jerome Menet
	Bruce Riley
Head of Department,	Thomas McKnight

May 2021

Major Subject: Biology

ABSTRACT

Genetics, diet, and environment alter stereotypical cognitive and locomotive decline with age. In *C. elegans* males, dysregulated metabolism contributes to behavioral decline due to increases in neuromuscular excitability. Behavioral decline can also be exacerbated by excessive metabolic production of ROS disrupting calcium handling and damaging biomolecules. Previous work showed age-dependent increases in metabolic genes encoding PEPCK (*pck-1/2*) and Stearoyl CoA fatty acid desaturases (*fat-5/6/7*). In order to understand how shifts in fuel utilization result in behavioral dysfunction, we addressed the role of increased gluco- and glyceroneogenesis (*pck-1/2*) and fatty acid synthesis (*fat-6/7*) in sustaining mating behavior over the first 48 hours of adulthood.

Through mating potency and fitness assays, we found that during early adulthood, epidermal PEPCK maintains the metabolic needs of neuromuscular circuitry regulating male mating behavior. We used glucose supplementation to show epidermal PEPCK-dependent gluconeogenesis supports neuromuscular function on day 1 of adulthood. To explore how PEPCK is regulated we characterized a mutant of succinate dehydrogenase (SDHA), subunit A of complex II of the electron transport chain, shown to increase PEPCK levels. We found, in SDHA mutants, increases in the transcript levels of metabolic genes involved in shunting metabolites away from the TCA cycle. Finally, we found that inhibition of ETC and TCA cycle separately did not elevate PEPCK to similar levels seen in SDHA suggesting metabolic disruption of both pathways are necessary to induce PEPCK based gluco-glyceroneogenesis.

We addressed the role of fatty acid synthesis in maintaining mating behavior during the first 48 hrs of adulthood. We observed, using mating potency and fitness assays, day 2 epidermal FAT-6, used in fatty acid synthesis, circumvents increased fatty acid oxidation disrupting the neuromuscular circuitry regulating male mating behavior. We observed aging males underwent food deprivation dependent degradation of FAT-6, which was compensated by transcriptionally active *fat-6* on day 2 of adulthood. Furthermore, using Markov modeling we found the preference for food in aging wild type males decreases on day 2 of adulthood. Finally, the lack of FAT-6 and FAT-7 results in dysregulation of ERG K^+ channels which inappropriately hyperpolarizes the mating circuitry responsible for spicule insertion.

DEDICATION

This work is dedicated to my daughter Olivia Gene Gonçalves. You are 1 year 4 months 4 days old and unable to understand this written work. But know I naively did all this for you. My work is more than worm mating behavior. It sets the foundation for you to do more. Let there be no doubt you stand on the shoulders of giants and I have every faith that you will rise to the challenge. You are and will always be my greatest discovery.

ACKNOWLEDGEMENTS

I would like to give a special thank you to my committee chair, Dr. Garcia. You have helped define my style and thought process for scientific discovery. You have pushed me creatively and given me room to independently grow. You were patient during my lows and trusted I would overcome when I believed I would not. Suffice to say I would not have come this far without your guidance.

I would like to thank my committee members, Dr. Karpac, Dr. Menet, and Dr. Riley for their guidance and support throughout the course of this research. Despite meeting for about 7-8 times for ~2 hrs each, a total of 14-16 hours across seven years, know that I was a nervous wreck a week out before every meet. My wife and family can attest that I held your opinions highly. Your constructive criticism was always welcomed and resulted in my work benefiting.

I would like to give a special thank you to Dr. Wesley Thompson. You unknowingly gave me confidence when I needed it the most. Your kindness helped me overcome my self-doubt. Your ability to treat others in training as if they were on an equal playing field gave me room to grow and learn. You will always by one of my greatest role models.

Thanks also go to the department faculty and staff for making my time at Texas A&M University a great experience.

I would like to thank Nikita Ojha, Paola Correa, and Xiaoyan Guo for helping me connect with my now wife Oneida Ibarra. The times we shared, although brief, impacted my life in a profound way.

Finally, thanks to my family. My parents both worked and supported three children under less-than-ideal conditions. Immigrating to a new country and establishing a life through night shifts and physical labor. I hope to honor your legacy. My sisters endured alongside me and supported me through childhood's arduous moments. In adulthood they have consistently supported me during moments of doubt. And to all the family members unmentioned, I hope I made you proud.

CONTRIBUTORS AND FUNDING SOURCES

Contributors

This work was supervised by a dissertation committee consisting of Professors Dr. Garcia, Dr. Menet, and Dr. Riley of the Department of Biology and Professor Dr. Karpac of the Department of Molecular & Cellular Medicine.

The data analyzed for Chapters VI and VII was conducted in part by Jimmy Goncalves (J.G.), Yufeng Wan (Y.W.), Xiaoyan Guo (X.G.), Kyoungsun Rha (K.R.), Brigitte LeBoeuf (B.L.), Liusuo Zhang (L.Z.), Kerolayne Estler (K.E.), and L. René Garcia (L.R.G.) of the Department of Biology and were published in 2020. Specifically, conceptualization, J.G., Y.W., X.G., and L.R.G.; methodology, J.G., Y.W., X.G., K.R., and L.R.G.; formal Analysis, J.G., Y.W., X.G., K.R., and L.R.G.; investigation, J.G., Y.W., X.G., K.R., B.L., L.Z., K.E., and L.R.G.; writing – original draft, L.R.G.; writing – review and editing, J.G., Y.W., K.R., and B.L.; visualization, J.G., Y.W., K.R., and L.R.G.;

All other work conducted for the dissertation was completed by J.G. independently.

Funding Sources

This work was made possible in part by Howard Hughes Medical Institute.

NOMENCLATURE

FAT-5	C. elegans homologue of the Stearoyl-CoA 9-Desaturase
FAT-6	C. elegans homologue of the Stearoyl-CoA 9-Desaturase
FAT-7	C. elegans homologue of the Stearoyl-CoA 9-Desaturase
PCK-1	C. elegans homologue of the Phosphoenolypyruvate CarboxyKinase
PCK-2	C. elegans homologue of the Phosphoenolypyruvate CarboxyKinase
SDHA-1	C. elegans homologue of the Succinate Dehydrogenase Subunit A
UNC-103	C. elegans homologue of the ERG K^+ channel
EGL-2	C. elegans homologue of the EAG K^+ channel
CaMKII	C. elegans homologue of the Calcium/calmodulin protein kinase II
SOD-4	C. elegans homologue of Superoxide Dismutase
TCA	Tricarboxylic Acid Cycle
GCaMP	GFP calcium calmodulin permutated protein
YFP	Yellow Fluorescent Protein

TABLE OF CONTENTS

Page

ABSTRACT ii

DEDICATION iv

ACKNOWLEDGEMENTS v

CONTRIBUTORS AND FUNDING SOURCES vii

NOMENCLATURE viii

TABLE OF CONTENTS ix

LIST OF FIGURES xiii

CHAPTER I INTRODUCTION 1

- Age and Metabolism in Behavioral Decline 1
  - Age Dependent Declines in Cognition and Locomotion 1
  - Metabolism Mediated Modulation of Behavioral Decline 2
- *C. elegans* Male Mating Behavior Models Age-Dependent Behavioral Decline 4
  - Mating Behavior 4
  - Regulation of Neuromuscular Excitability in Mating Behavior 5
  - Food Deprivation Modulates Neuromuscular Excitability 7
  - Age Dependent Changes in Behavioral Decline 8
  - Lifespan and Tissue Degradation 8
  - Dysregulated Metabolic Changes in Behavioral Decline 9
- PEPCK Regulation 11
  - Differing Roles of PEPCK 11
- Stearoyl-Coa Desaturase Role in Behavioral States And Performance 12
  - Stearoyl-CoA Desaturases (SCD) Function and Regulation 13
- Role of Lipid Catabolism in Neuronal Function 14
  - β-oxidation 14
  - Electron Carriers and Superoxide Generation 15
  - The Tradeoff Between Glucose and Palmitic Acid Metabolism 17
  - Lipid Utilization 18
  - Epidermal Support Tissue for Neuronal Fat Accumulation 18
- Disrupted Lipid Metabolism Impacts Neuronal Function 19
- Dissertation Objectives 20

CHAPTER II FOOD DEPENDENT REGULATION OF FAT-6 23

Age Dependent Increases in Fatty Acid Desaturases Transcription 23
Tissue Specific Expression of FAT-6 Supports Lipid Storage 24
Male Gonad Regulates Dynamic Levels of FAT-6 29
Metabolic Characterization of FAT-6 And FAT-7 31
FAT-6 Regulates Lipid Stores Under Fed Conditions 37
Chapter II Summary 39

CHAPTER III CHANGES IN BEHAVIOR WITH AGE 40

Identification of Behavioral States in Early Aging Males 40
Markov Model State Diagrams for Early Aging Wild Type Males 44
Markov Model State Diagrams for Early Aging *fat-6(lf);fat-7(lf)* Males 47
Chapter III Summary 50

CHAPTER IV FAT SYNTHESIS ADJUSTS MATING PERFORMANCE 51

Dysregulated Fatty Acid Metabolism Results in Mating Fitness Decay 51
Epidermal Rescue Maintains Mating Endurance of Aging Wild Type Males 57
Chapter IV Summary 62

CHAPTER V FAT SYNTHESIS AND NEURON FUNCTION 63

Dysregulated Fat Synthesis Disrupts Neuronal Calcium 63
Fatty Acid Desaturase Loss Alters UNC-103 K^+ Channel Levels 68
Chapter V Summary 73

CHAPTER VI PEPCK EXPRESSION MAINTAINS MATING FITNESS 74

Tissue Specific Expression of PEPCK 74
Mating Behavior of PEPCK Mutants 77
Rescue of PEPCK Deficient Mating Behavior 80
PEPCK Bidirectional Regulation 83
Chapter VI Summary 85

CHAPTER VII SDHA-1-REGULATION OF PEPCK IN AGING MALES 86

Succinate Dehydrogenase Disruption Increases PEPCK 86
SDHA-1 Modulation of Neighboring Tissue Metabolism 88
Characterization of SDHA-1 91
PEPCK Increases Require TCA Cycle and ETF Disruption 93
Chapter VII Summary 95

CHAPTER VIII EXPERIMENTAL PROCEDURES 96

Strains 96

Feeding Exploring Mating Assay (FEM) 97
Markov Model 97
Analyzing the Raw and Modeled Data 100
Potency Assay, Copulation Fitness Assay, and Copulation Endurance Assay 101
Mating Interference (MI) Assay 103
Construction of Plasmids and Transgenic Strains 104
FAT-6 Crisper/Cas9 Plasmids, Expression Plasmids and Transgenics 104
Plasmids Used For Conducting Tissue-Specific Rescue of *fat-6(lf)* 106
CRISPR/Cas9-mediated Recombination of YFP into Genomic *fat-6* 107
CRISPR/Cas9-mediated Mutation of *him-5(e1490)* 108
Gonad Ablation 109
Quantification of Fluorescence 109
RT-qPCR 112
General Protocol 113
Nile Red Staining and Quantification 114
Oxygen Consumption Assay 115
Aldicarb Assay 115

CHAPTER IX SUMMARY OF EXPERIMENTS AND DISCUSSION 117

Summary of Experimental Results 117
Discussion 122
Transcriptional Responses in *fat-6(lf);fat-7(lf)* Males 123
Spatial Regulation of FAT-6 in Males 124
Tissue Specific Rescue's Reveal Required Metabolism in the Male Tail 124
Fuel Utilization in the Neurons and Epidermis of the Male Tail 126
Epidermal Support Tissue for Neuronal Fat Accumulation 127
Functionally Diverse Neuron and Muscles in the Male Tail 128
Neuronal Morphological Changes with Age 129
Locomotor Motor Neurons and Spicule Circuitry Connectivity 130
Future Experiments 131
Transcriptional Responses in *fat-6(lf);fat-7(lf)* Males 131
Spatial Regulation of FAT-6 in Males 132
Epidermal Support Tissue for Neuronal Fat Accumulation 133
Conclusion 134

REFERENCES 136

APPENDIX 145

Cell Excitability in *fat-6(lf)* 145
fat-6(lf);fat-7(lf) Sensitivity to ROS 146
PEPCK Expression in *fat-6(lf);fat-7(lf)* 147
Mating Latency and Disengagement of *fat-6(lf);fat-7(lf)* 148

Behavioral Switches of Starved Males.....151
Artificial Activation of LUA Interneuron 152
Ca^{2+} Imaging of the Cholinergic Ventral Cord.....154

LIST OF FIGURES

Page

Figure 1 Regulation of neuromuscular excitability with age and food deprivation. 6

Figure 2 Fold changes in metabolic gene expression in aging *C. elegans* males.....11

Figure 3 Schematic of β Oxidation contribution to proton motive force 17

Figure 4 Early aging wild type males increase fatty acid synthesis genes. 24

Figure 5 CRISPR/Cas9 YFP knock-in design and FAT-6::YFP in *C. elegans*. 25

Figure 6 Endogenous FAT-6 expression in male *C. elegans*. 26

Figure 7 FAT-6::YFP does not disrupt FAT-6 wild type function. 27

Figure 8 FAT-6::YFP remains dynamic in *fat-5(lf);fat-7(lf)* mutant males. 27

Figure 9 FAT-6::YFP in aging hermaphrodites. 28

Figure 10 FAT-6::YFP and neutral lipid stores in aging wild type males. 29

Figure 11 Gonad regulated FAT-6 expression in male *C. elegans*. 30

Figure 12 Neutral lipid stores in *fat-6(lf);fat-7(lf)* mutant male *C. elegans*. 31

Figure 13 Rescue and oxidation of lipid stores in aging *fat-6(lf);fat-7(lf)* males. 33

Figure 14 Whole worm respiration of *fat-6(lf);fat-7(lf)* males.....34

Figure 15 Metabolic gene expression of *fat-6(lf);fat-7(lf)* males. 36

Figure 16 Food deprivation decreases FAT-6::YFP in wild type *C. elegans*. 38

Figure 17 Food consumption decreases in early aging wild type males. 41

Figure 18 Illustration of the assay design and identification of behavioral states. 42

Figure 19 Visualized feeding, mating, and exploring behaviors across time. 43

Figure 20 Transition in feeding behavior in early aging wild type males. 43

Figure 21 1st Order transition matrixes for aging wild type males. 44

Figure 22 Co-localization between Raw and Modeled data. 45

Figure 23 Markov model state diagrams for early aging wild type males. 46
Figure 24 Visualized feeding, mating, and exploring behaviors across time.....48
Figure 25 Transitional behavior in early aging *fat-6(lf);fat-7(lf)* males.....49
Figure 26 Premature transition to exploring behavior for aging *fat-6(lf);fat-7(lf).*.....49
Figure 27 Mating performance of *fat-6(lf);fat-7(lf)* mutant males.....52
Figure 28 Mating fitness of *fat-6(lf);fat-7(lf)* mutant males.....53
Figure 29 Mating endurance of *fat-6(lf);fat-7(lf)* mutant males.....55
Figure 30 Day 2 *fat-6* prolongs the mating performance of wild type males. 56
Figure 31 Mating fitness of *fat-6(lf)* and *fat-7(lf)* males. 56
Figure 32 Intestinal rescue of *fat-6(lf);fat-7(lf)* lipid storage. 58
Figure 33 Hypodermal and Intestinal rescue of *fat-6(lf);fat-7(lf)* mating fitness.....58
Figure 34 Tissue specific rescue of 72 hour mating fitness of *fat-6(lf);fat-7(lf)*males. ...59
Figure 35 Overexpression of intestinal *fat-6* does not alter mating performance. 59
Figure 36 Mating disrupted due to low motivation and mail tail positioning defect. 61
Figure 37 Neuron specific deficits in *fat-6(lf);fat-7(lf)* males.....64
Figure 38 Quick repolarization of *fat-6(lf);fat-7(lf)* male cholinergic neurons.....67
Figure 39 Characterization of cholinergic neurons in *fat-6(lf);fat-7(lf)* males. 68
Figure 40 K+ channel expression and function in *fat-6(lf);fat-7(lf)* males. 70
Figure 41 Increased *egl-2* in non Prc *unc-103(lf)* and *fat-6(lf);fat-7(lf)*; *unc-103(lf)*. 71
Figure 42 PCK-1 and PCK-2 Sequence Alignment. 75
Figure 43 Expression pf *pck-1* and *pck-2* in male *C. elegans*. 76
Figure 44 *pck-1(lf);pck-2(lf)* Decline in Mating Performance. 78
Figure 45 *egl-2* K+ channel expression in PEPCK mutant males.....80
Figure 46 Neuromuscular PEPCK maintains mating potency in day 1 males. 81

Figure 47 PEPCK derived glucose prolongs mating fitness of wild type males.....83
Figure 48 PEPCK expression in *pck-1(lf)* and *pck-2(lf)* aging males. 84
Figure 49 A Mutation in SDHA-1 Increases PEPCK. 87
Figure 50 Metabolic Compensation in *sdha-1* 88
Figure 51 *sdha-1* dysfunction tissue specifically regulates PEPCK levels 89
Figure 52 PEPCK derived glycerol contributes to lipid storage in *sdha-1(lf)* 91
Figure 53 *sdha-1(lf)* mitochondria puncta morphology 92
Figure 54 *sdha-1(lf)* larval and adulthood development 92
Figure 55 *sdha-1(lf)* survives electron carrier dependent ROS death 93
Figure 56 *sdha-1(lf)* Dependent Increases in *pck-2*::YFP 94
Figure 57 Example of Behavioral State Assignment 97
Figure 58 Creating a binary sequence of events.....97
Figure 59 Calculating Frequency of Behavior 98
Figure 60 Calculations of Markov Model Proportions 99
Figure 61 Probabilistic Predictions of Behavioral States.....100
Figure 62 Excitability in *fat-6(lf)* males. 146
Figure 63 Paraquat Survival in *fat-6(lf);fat-7(lf)* males. 147
Figure 64 The expression of PEPCK in *fat* mutants. 148
Figure 65 Mating Latency of *fat-6(lf);fat-7(lf).*.....149
Figure 66 Mating Disengagement of *fat-6(lf);fat-7(lf)* males. 150
Figure 67 Competitive fitness declines in *fat-6(lf);fat-7(lf).*.....150
Figure 68 Visualized feeding, mating, and exploring behaviors in starved males.....151
Figure 69 Artificial Activation of LUA Interneuron. 153
Figure 70 Complete Cholinergic Calcium Transients in *fat-6(lf);fat-7(lf)*.....154

CHAPTER I

INTRODUCTION

Age and Metabolism in Behavioral Decline

Age is associated with inevitable cognitive and locomotive decline. Despite metabolism being implicated in exacerbating dysfunction with age, we have yet to fully understand how fuel utilization results in behavioral decline. The metabolic costs associated with aging, in part explained by the disposable soma theory, have to be balanced to the organism's needs; growth, reproduction, and maintenance (Kirkwood 1977) . As an organism ages, commitments to increased physical activity could result in premature behavior decline incurred by a high metabolic cost; increased mitochondrial ROS generation. Contrary to this, behavioral changes with age and consequently metabolic disease may instead underlie aging (Matthews, George et al. 2012, Schrack, Knuth et al. 2014, Biswas, Oh et al. 2015). Finally, behavioral decline can also be exacerbated by environmental stressors which result in metabolic switches, commonly seen in hepatic induction (Evans 1993, Maronpot, Yoshizawa et al. 2010).

Age Dependent Declines in Cognition and Locomotion

Declines in cognitive ability are often associated with neurodegenerative diseases including Alzheimer's (AD) and Parkinson's (PD) disease. AD has been characterized by extracellular amyloid plaque and intracellular tau protein build up resulting in

neuronal dysfunction and death (Mattson, Pedersen et al. 1999). PD is the result of dopaminergic neurons age dependent cell death coinciding with premature decline in dopamine production (Mattson, Pedersen et al. 1999). Furthermore, these neurodegenerative diseases are linked with age dependent metabolic changes; increases in mitochondrial ROS production.

As for declines in physical ability, in *C. elegans*, aging isogenic populations have been studied for deficits in locomotion using a touch stimulus. After characterizing touch responses, they found animals could be grouped into three categories with progressively failing locomotion responses (Herndon, Schmeissner et al. 2002). Interestingly, before muscle degradation could be observed, mid aged animals did not move unless touched (Herndon, Schmeissner et al. 2002). Furthermore, onset of age-related locomotion decline and rate of decline varied in individual animals (Herndon, Schmeissner et al. 2002). Both insulin signaling and food deprivation have been implicated in exacerbating and delaying locomotor decline respectively (Glenn, Chow et al. 2004).

Metabolism Mediated Modulation of Behavioral Decline

The age dependent decline in cognition is associated with neurodegenerative disease and correlates with metabolic impairment. For Alzheimer's disease, a mitochondrial cascade hypothesis has been suggested in which a predisposition to increased basal levels of mitochondrial respiration results in rapid plaque formation exacerbating dysfunction and removal of compromised cells (Swerdlow and Khan

2004). As for Parkinson's disease, animal models studied are created through dopaminergic cell death induced by oxidative damage. Oxidative damage is possible through complex I inhibitors of the ETC, mutants with defective mitochondria and susceptibility to ROS, and mutants for mitochondrial kinases (Beal 2005).

The metabolism underpinning increased risk of neurodegenerative diseases, such as Alzheimer's or dementia, seems to be partially caused by an abnormally high level of lipids in the blood (dyslipidemia). Diets emphasizing reduced intake of saturated fats, DASH, have been shown to decrease low density lipoprotein cholesterol and cognitive decline (Appel, Sacks et al. 2005, Tangney, Li et al. 2014). While some studies have shown low fat diets and diets high in unsaturated fats decrease the production of Alzheimer's associated plaques in the mouse brain, we are still unsure of how fuel utilization contributes to cognitive and locomotor decline (Amtul, Uhrig et al. 2011).

In *C. elegans*, locomotor decline can by modulated by mutants of *daf-2*, insulin receptor, and *daf-16*, FOXO transcription factor. Specifically, decreased insulin signaling in *daf-2* mutants prolongs body movement while mutants of *daf-16*, constitutive insulin signaling, cause premature decline in body movements (Glenn, Chow et al. 2004, Huang, Xiong et al. 2004). Feeding behavior has also been implicated in modulating behavioral decline. Specifically, mutants of *eat-2* have observable decreases in pharyngeal pumping resulting in caloric restriction and consequently prolonged body movements (Huang, Xiong et al. 2004). Altogether, previously published work across multiple model organisms has established a strong link between metabolism and age-dependent neuromuscular dysfunction.

C. elegans Male Mating Behavior Models Age-Dependent Behavioral Decline

Mating Behavior

C. elegans hermaphrodites as a model organism has been studied for its rapid generation time, ease of genetic manipulation, and small nervous system composed of 302 neurons. Contrarily, males have 385 neurons, with 170 neurons dedicated to mating through the use of a specialized tail. Male mating behavior is composed of multiple coordinated steps involving initial hermaphrodite contact, vulval searching, turning behavior, spicule insertion, and sperm transfer. In *C. elegans* males the spicule does not act as a conduit for sperm transfer but instead anchors the male tail. Therefore, spicule intromission behavior is a tightly coordinated such that the spicule movement is regulated precisely for efficient sperm transfer with a moving hermaphrodite.

The circuit responsible for spicule insertion is composed of multiple sensory-motor neurons. The neurons control complex muscles capable of fast and slow twitch like responses. For example, proprioceptive neurons, upon sensing the vulva, normally elicit a continuous high frequency spicule prodding motor response encompassing multiple muscles. Vital to the process of spicule prodding is the continuous contraction and relaxation of protractor muscles. When the spicules partially penetrate the vulval slit, the SPC proprioceptive motor neurons induce sustained spicule muscle contraction, which forces the spicules through the vulva.

The sensory-motor neurons, controlling fast and slow twitch like muscles, are also electrically and chemically connected to other tissues, e.g. necessary for sperm

release. The extensive connections between neurons and other tissues require temporal regulation of differing motor programs (LeBoeuf, Correa et al. 2014). Therefore, we can expect a high degree of complexity in regulating appropriate responses under the burden of a concurrent mating behavior. Maintaining the appropriate responses also requires energy demanding regulation of ions by leak channels. We postulate that a substantial metabolic requirement is needed for the intromission circuitry to quickly respond to the vulva and maintain extended sessions of mating. Also, the precise temporal regulation of motor programs most likely requires external metabolic support.

Regulation of Neuromuscular Excitability in Mating Behavior

Early research into the membrane excitability of the neuromuscular circuit controlling mating behavior established channels and receptors involved in regulating spicule movement. In males missing the SPC neuron, L-VGVV/*egl-19*, and Ryr/*unc-68,* the spicules protracted from the tail (Fig. 1) (Garcia, Mehta et al. 2001). In addition, drug assays, using acetylcholine agonists, validated upstream receptors involved in mediating changes in muscle contraction; nicotinic and muscarinic AChR (Fig. 1) (Garcia, Mehta et al. 2001). Finally, by inducing increases of neurotransmitter in the synaptic cleft, using aldicarb, they found males did not protract their spicules when they were collectively missing specific neurons and muscles; PCB, PCC, SPC, and anal depressor (Garcia, Mehta et al. 2001). The tissue specificity of spicule insertion regulation was later validated in K^+ channel mutants of *unc-103* which inappropriately

protract their spicules only when the SPC and anal depressor were intact (Fig. 1) (Garcia and Sternberg 2003).

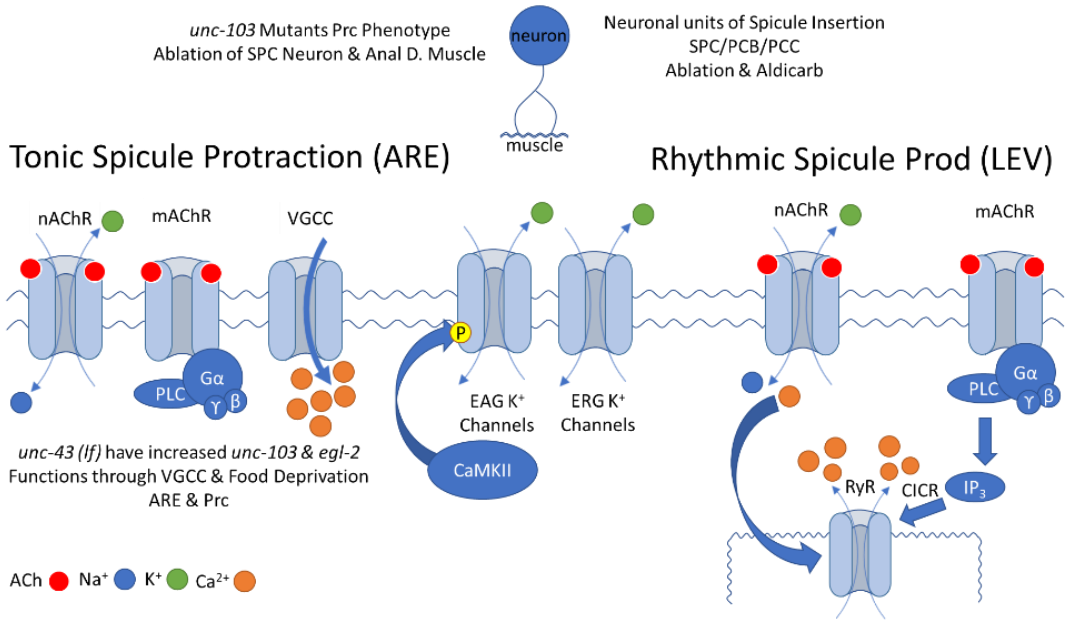

Figure 1 Regulation of neuromuscular excitability with age and food deprivation. Receptors and K^+ and Ca^{2+}Channels, regulating cell excitability, discussed throughout the introduction. Regulation of spicule movement is split between tonic and rhythmic muscle contraction. Short descriptions inform effects of mutations and methods used to validate function. ACh=acetylcholine, Na^+=sodium, K^+=potassium, Ca^{2+}=calcium, nAChR=nicotinic acetylcholine receptor, mAChR=muscarinic acetylcholine receptor, PLC=phospholipase C, IP3= inositol triphosphate, RyR=ryanodine receptor, VGCC=L-Type voltage gated calcium channel, CICR=calcium induced calcium release, CaMKII= Calcium/calmodulin-dependent protein kinase II, EAG=ether-a-go-go K^+ channel, ERG= ether-a-go-go related gene K^+ channel, $G_{alpha/beta/gamma}$= G protein coupled receptor.

Food Deprivation Modulates Neuromuscular Excitability

Variability in spicule protraction constitutive (Prc) phenotype in *unc-103(lf)* resulted in the surprising finding that transient food deprivation hyperpolarizes the neuromuscular circuitry regulating mating behavior (Gruninger, Gualberto et al. 2006). A suppressor screen of *unc-103(lf)* found a mutant of *lev-11*/Tropomyosin which caused changes in feeding behavior, muscle contraction of pharynx perturbed (Gruninger, Gualberto et al. 2006). Specifically, the loss of *lev-11* resulted in the activation of NSM neurons increasing pharynx contraction and downregulating sex neuromuscular excitability (Gruninger, Gualberto et al. 2006).

To further address how changes in feeding behavior and deprivation resulted in hyperpolarization of the sex muscle and neurons, additional mutants were characterized. Mutants of CaMKII/*unc-43* were found to show a Prc phenotype similar to ERG/*unc-103* mutants (LeBoeuf, Gruninger et al. 2007). Both channels are thought to function redundantly in muscles to regulate membrane excitability (LeBoeuf, Gruninger et al. 2007). Despite this redundancy, *unc-43(lf)* displayed Prc through L-VGCC/egl-19 and not RyR/unc-68 as seen in *unc-103(lf)* (Fig. 1) (LeBoeuf, Gruninger et al. 2007).

Interestingly under starved conditions, CaMKII was also found to modulate the function of EAG/*egl-2* K^+ channels through phosphorylation increasing *egl-2*'s function and expression (Fig. 1) (LeBoeuf, Gruninger et al. 2007, LeBoeuf, Guo et al. 2011). Furthermore, the effects of food deprivation were found to be due to chemosensory AWC neuronal activation, insulin peptide secretion, and insulin receptor, *daf-2*, activation in sex muscles (Gruninger, Gualberto et al. 2008). The *daf-2* activation and

Prc suppression was independent of FOXO/*daf-16* and required PLCγ/IP_3 calcium activation of CaMKII (Gruninger, Gualberto et al. 2008).

Age Dependent Changes in Behavioral Decline

In aging *C. elegans* males, progressive increases in cell excitability result in declines in coordination, ectopic spicules prodding, and mating behavior decay. Specifically, the copulatory neurons and muscles of 72 hr adult males are hyper-excited, showing increases in calcium transients and sensitivity to acetylcholine agonist stimulation. Interestingly, the excitability of sex muscles can be reversed by specific heterozygotes of cholinergic receptor mutants, shown by decreases in acetylcholine agonist response and increased mating potency. Similar to previously published work, behavioral decay with age can be modulated by food deprivation inducing *daf-2*-dependent CAMKII/UNC-43 phosphorylation of EAG/EGL2 K^+ channels that hyperpolarize excitable cells (LeBoeuf, Gruninger et al. 2007, LeBoeuf, Guo et al. 2011). We postulate that transient starvation also induces metabolic adaptations to overcome the behavioral decline associated with aging.

Lifespan and Tissue Degradation

Caenorhabditis elegans virgin males grown in laboratory conditions decline in mating behavior during the first 3-5 days of adulthood despite having a median lifespan of ~10 days (Gems and Riddle 2000). Rapid male mating behavior decline suggests physiological changes are taking place in which neuron and muscle function is

compromised (Guo, Navetta et al. 2012). The compromised function of neurons and muscles is most likely not due to morphological decay. For example, muscle degradation is observed by day 8 of adulthood, sperm activation is undisrupted by day 5 of adulthood, and the nervous system remains unchanged by day 4 of adulthood (Herndon, Schmeissner et al. 2002, Glenn, Chow et al. 2004, Cohn, Cebul et al. 2020).

Dysregulated Metabolic Changes in Behavioral Decline

Metabolism's role in behavioral decline has been studied in a mutant of *sirt-2.1*, a NAD-dependent deacetylase that regulates metabolic gene expression. Mutants of *sirt-2.*1 prematurely decline in mating behavior on day 2 of adulthood (Guo and García 2014). The behavioral decline was due to a hyper-excited mating circuit, showing increases in calcium transients during spicule insertion and sensitivity to acetylcholine agonist stimulation (Guo and García 2014). Given *sirt-2.1*'s role in metabolic gene expression, animals were characterized and found to have increased lipid storage in the intestine, increased ATP, and decreased survivability on ROS generators (Guo and García 2014).

In wild type males, ROS generators were found to cause premature decline in mating behavior and increase sensitivity to acetylcholine agonist stimulation (Guo and García 2014). The antioxidant N-acetyl cysteine (NAC) was found to reverse the effects of ROS generators and extend the mating behavior of Day 3 wild type males (Guo and García 2014). Altogether, metabolic overproduction of ROS was found to underpin mating behavior decline in aging wild type animals.

In order to address metabolic adaptations that counteract enhanced catabolism, metabolic gene expression was queried across aging males. Glycolytic and fat oxidation pathways were found to be upregulated (Fig. 2) (Guo and García 2014). To counteract these increases, enzymes involved in the electron transport chain were downregulated and anabolic metabolism was increased. Of the many anabolic genes upregulated, Phosphoenolpyruvate carboxykinase (PEPCK), an enzyme involved in gluco-/ glyceroneogenesis, was found to be responsible for the increased fat content in *sirt-2.1(lf)* (Guo and García 2014). PEPCK was also found to play a compensatory role in the premature mating behavioral decline seen in *sirt-2.1(lf)* (Guo and García 2014). Altogether, mutants of *sirt-2.*1 prematurely decline in mating behavior due to enhanced glycolytic and fatty acid oxidation catabolic processes. The alterations in metabolism lead to excessive production of ROS, disrupting calcium handling and damaging biomolecules, exacerbating behavioral dysfunction associated with age.

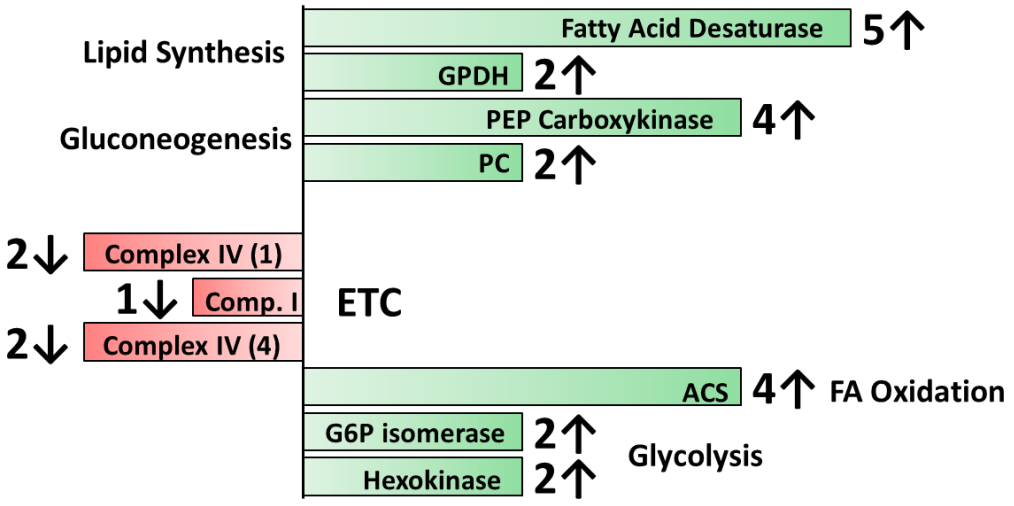

Figure 2 Fold changes in metabolic gene expression in aging *C. elegans* males. GPDH= Glycerol-3-phosphate dehydrogenase, PEP= Phosphoenolpyruvate, PC= Pyruvate carboxylase, COMP. = Complex, TCA= Tricarboxylic acid cycle, ACS= Acyl-CoA synthetase, FA= Fatty acid, and G6P= Glucose 6-phosphate.

PEPCK Regulation

Differing Roles of PEPCK

PEPCK traditionally has been shown to be cytoplasmic (PEPCK-C), where it produces PEP from mitochondrial derived OAA. However with the finding of mammalian mitochondrial PEPCK (PEPCK-M) came a new paradigm of how insulin signaling is regulated. PEPCK-M is thought to function in a sensing capacity, specifically the sensing of TCA cycle metabolites and byproducts. The flux through the TCA cycle contains mitochondrial specific reactions with specific Ca^{2+} regulation. One such specific reaction produces succinate and GTP in which GTP is bound to the mitochondria (mGTP). It's hypothesized that mGTP production is communicated to the

cytoplasm through PEPCK-M which uses mGTP to produce OAA (Stark and Kibbey 2014). How mGTP and OAA production results in increased insulin signaling is unknown but PEP introduction into the cytoplasm does result in increased insulin signaling and glucose uptake (Stark, Pasquel et al. 2009). This is of importance in understanding how varying PEPCK's may have alternate tissue specific functions. For example, neuronal PEPCK may primarily play an insulin signaling role as to increased uptake of metabolites from neighboring tissues.

In organisms lacking a mitochondrial PEPCK it remains possible that malate is transported into the cytoplasm and consequently converted into OAA. Given the need for GTP, I hypothesize that PEPCK-C function is coupled to ATP produced through glycolysis. Glycolytic reactions that produce ATP are resulting from Phosphoglycerate kinase and Pyruvate kinase which may act as mechanisms for PEPCK-C to sense glycolytic flux. The ATP produced may be easily converted into GTP through nucleoside-diphosphate kinases (NDPK). Mitochondrial GTP production may also be coupled to NDPK's resulting in increased mitochondrial specific ATP production. Altogether increased flux through glycolysis and the TCA cycle may result in cytoplasmic increases in OAA and GTP resulting in favorable conditions for PEPCK.

Stearoyl-Coa Desaturase Role in Behavioral States And Performance

Despite the correlation between increased glycolytic and fatty acid oxidation and altered behavioral decline, we do not know if metabolic changes are a cause or a

compensatory mechanism for declining behavior. To understand how fuel utilization affects neuronal activity, which determines behavioral decline, we addressed the role of increased fatty acid catabolism on behavioral states and neuromuscular system performance. Specifically, we studied mutants of Stearoyl-CoA desaturases, catalyze unsaturated fatty acid synthesis, found to increase with age within 48 hrs of adulthood in wild type males.

Stearoyl-CoA Desaturases (SCD) Function and Regulation

Stearoyl-CoA desaturases (SCD), encoded by *fat-5, fat-6,* and *fat-7,* catalyze the rate limiting step of monounsaturated fatty acid synthesis. Both *fat-6* and *fat-7* primarily desaturate stearic acid (C18:0) producing oleic acid (C18:1); *fat-5* differs in that palmitic acid (C16:0) is desaturated to palmitoleic acid (C16:1) (Watts and Browse 2000). Mutants of *fat-6* and *fat-7* are therefore suggested to be unable to synthesize triglycerides for storage and instead consumed saturated fatty acids may undergo mitochondrial β-oxidation.

SCDs in hermaphrodites are known to be genetically regulated by nuclear hormone receptors *nhr-80* and *nhr-49,* MDT-15 interacting with NHR-49, and SBREP (Van Gilst, Hadjivassiliou et al. 2005, Brock, Browse et al. 2006, Taubert, Van Gilst et al. 2006, Yang, Vought et al. 2006). Of these regulators, *nhr-49* plays the dual roles of upregulating SCDs and mitochondrial β-oxidation. This can lead to *fat-7* dependent increases in unsaturated fat synthesis and decreases in mitochondrial β-oxidation through indirect inhibition of *acs-2,* acyl-CoA synthetase, and *ech-1*, enoyl-coA hydratase (Van

Gilst, Hadjivassiliou et al. 2005). Furthermore, in hermaphrodites, the low fat phenotype of *fat-6(lf);fat-7(lf)* coupled with increased mRNA of *acs-2* and *ech-1* supports the hypothesis that mutants are unable to store triglycerides and consumed saturated fat may undergo mitochondrial β-oxidation (Brock, Browse et al. 2007).

Despite various compensatory mechanisms, including elevated *fat-5*, in the *fat-6(lf);fat-7(lf)* mutants, the low fat phenotype persists. Contrary to this finding, in the triple mutant *daf-2(lf);fat-6(lf);fat-7(lf)*, the ratio of lipids, 16;1 to 16;0, and increased fat stores suggest *fat-5* can compensate for the low fat phenotype seen in *fat-6(lf);fat-7(lf)* (Dickinson, Ward et al. 2013). This is most likely through the activation of *daf-16* which has been shown, when mutated, to reverse the *daf-2* increased levels of fat synthesis (Perez and Van Gilst 2008). The low fat phenotype of *fat-6(lf);fat-7(lf)* can also be counteracted by increased *pod-2* mRNA, which irreversibly produces malonyl-CoA, by NHR-64 depletion (Liang, Ferguson et al. 2010).

Role of Lipid Catabolism in Neuronal Function

β-oxidation

β-oxidation of short ($<C_8$), medium (C_8-C_{12}), and long chain fatty acids (C_{14}-C_{20}) predominantly occurs in the mitochondria (Reddy and Hashimoto 2001). Peroxisomes can functionally complement the mitochondria with the β-oxidation of long chain fatty acids (C_{14}-C_{20}) but given the exclusive ability to catabolize very long fatty acids ($>C_{20}$) we expect *C. elegans* to rely primarily on mitochondrial β-oxidation for bacterially

derived palmitic acid (C_{16}) (Tanaka, Ikita et al. 1996, Reddy and Hashimoto 2001). Peroxisomes can also metabolize palmitic acid into medium chain fatty acids (C_8-C_{12}) which is then transported to the mitochondria given its exclusive medium chain β-oxidation (Reddy and Hashimoto 2001).

Briefly, β-oxidation starts with fatty acid activation resulting in an acyl-CoA. Activated fatty acids are then transported into the mitochondrial matrix by the carnitine shuttle. The acyl-CoA undergoes dehydration resulting in the formation of a double bound and FADH2. After a hydration and dehydration steps a –OH functional group is converted into a double bound –O, produces NADH. This is followed by bond cleavage producing an acetyl-CoA and another shorter acyl-CoA. This process can be continued always producing a single FADH2, NADH, and acetyl-CoA. Once an acyl-CoA reaches a carbon length of four it runs through a last cycle of β-oxidation and produces a single additional acetyl-CoA.

Under conditions in which β-oxidation runs rampant, additional acetyl-CoA can be converted with oxaloacetate into citrate and transported out of the mitochondria. Once in the cytoplasm citrate is broken down into oxaloacetate and acetyl-CoA. Cytoplasmic acetyl-CoA is then made into malonyl-CoA, the first substrate of fatty acid synthesis.

Electron Carriers and Superoxide Generation

A cycle of β-oxidation produces a single $FADH_2$, NADH, and acetyl-CoA which can be used to generate ATP and accompanying ROS. The primary contribution to ATP from lipid catabolism, 75%, comes from the formation of acetyl-CoA. A single acetyl-

CoA contributes 3 NADH and 1 $FADH_2$ whose electrons pass through complex I and II respectively (Fig. 3). $FADH_2$ and NADH, which originates from β-oxidation, contribute to 25% of the total ATP generated from lipid catabolism. Specifically, the NADH is oxidized and produces a proton motive force through complex I (Fig. 3). Diverging from stereotypical electron transport, β-oxidation derived $FADH_2$ is handled by intermediate electron carrier called electron transferring flavoprotein (ETF). ETF specifically interacts with and removes the electrons from ACADs (acyl-CoA dehydrogenases), involved in the first step of β-oxidation. ETF dehydrogenase pass the electrons to coenzyme Q and consequently through complex III (Fig. 3). There is evidence to suggest that an overabundance of β-oxidation derived $FADH_2$ contributes to extensive $O_2^{\bullet -}$ production. For example, reverse electron transport (RET) at complex I, in isolated mitochondria, occurs when a high proton motive force is generated from increased electron supply to the CoQ pool from β-oxidation (Murphy 2009).

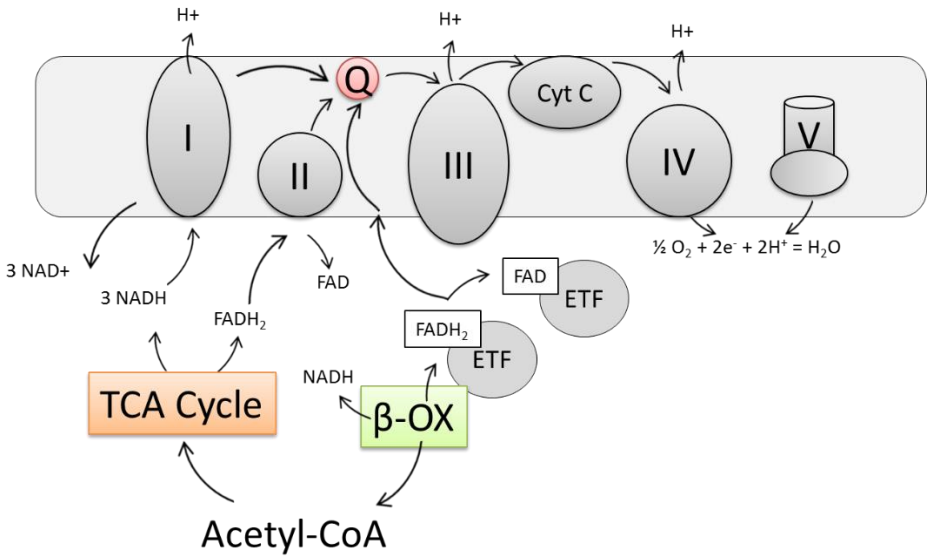

Figure 3 Schematic of β Oxidation contribution to proton motive force
For every two carbons liberated from β-oxidation of an activated fatty acid a $FADH_2$, NADH, and acetyl-CoA are produced. TCA cycle derived $FADH_2$ contributes to a proton motive force through complex II. β-oxidation derived $FADH_2$ contributes to a proton motive force through β-oxidation dependent ETF. Then ETF dehydrogenase passes electrons to coenzyme Q and consequently through complex III.

The Tradeoff Between Glucose and Palmitic Acid Metabolism

Glycolytic metabolism produces acetyl CoA which can take part in an irreversible reaction to produce malonyl CoA, the first substrate in fatty acid synthesis. In the enzyme fatty acid synthetase (FAS), a series of condensation, reduction, and dehydration steps results in short saturated fatty acids. If FAS continues for 7 cycles, palmitic acid is formed (Tracey, Steyn et al. 2018). It is generally understood that when a fatty acid undergoes B-oxidation, loss of 2 carbons, it can produce a single acetyl CoA, NADH, and $FADH_2$. For palmitic acid, 7 β-oxidation cycles produce seven NADH and FADH2. After a final processing step, 8 acetyl CoA are formed. Therefore, palmitic acid

normally results in ~106 ATP's after undergoing β-oxidation. In comparison glucose produces ~36 ATP's. The tradeoff between substrate and ATP production can ultimately be summed by the 5 fold increase of oxygen consumption through palmitic acid catabolism (Tracey, Steyn et al. 2018).

Lipid Utilization

Previously published work has shown that medium chain fatty acids contribute ~20% to the neuronal acetyl-CoA pool (Ebert, Haller et al. 2003). Labeling of octanoate (C_8) and glutamine isotopomer analysis, glutamine synthetase is astrocyte-specific, revealed that a majority of medium chain fatty acids are metabolized in astrocytes (Ebert, Haller et al. 2003). Glutamine is indirectly made in astrocytes from the catalysis of a TCA cycle metabolite, alpha ketoglutarate, to glutamate. Given this information we hypothesize that in wild type males the epidermis may act similarly to astrocytes resulting in a significant contribution of neuronal acetyl CoA.

Epidermal Support Tissue for Neuronal Fat Accumulation

Previously published work has shown that neurons secrete fatty acids for processing in astrocytes, avoiding activity dependent dysfunction (Ioannou, Jackson et al. 2019). The authors induced neuronal excitotoxicity and measured increases in lipid peroxidation, oxidative radicals reacting with unsaturated fatty acids (Ioannou, Jackson et al. 2019). Subsequently, neuronal lipoproteins then traffic free fatty acids to astrocytes (Ioannou, Jackson et al. 2019). In turn, astrocytes increase cytoplasmic lipolysis during

enhanced neuronal activity by sensing glutamate NMDA, glutamate receptor, binding (Ioannou, Jackson et al. 2019). Astrocytic mitochondria are also found with increased loads of saturated fat following enhanced neuronal activity (Ioannou, Jackson et al. 2019).

Disrupted Lipid Metabolism Impacts Neuronal Function

The neurons and muscles responsible for performing behavior are known to be modulated by lipid metabolism. Specifically, neuronal function can be affected by lipid based oxidative stress. Previous work has shown that increased levels of triglycerides in the blood correlate with higher rates of respiration, producing ROS, causing enhanced ATP sensitive K+ channels which alongside K+/H+ exchanger results in higher metabolic rates. This is expected to induce a hypermetabolic state to compensate for the high circulating lipids (Alberici, Oliveira et al. 2006). ATP sensitive K+ channels are not the only known channels to change under disrupted lipid metabolism. Hydrogen peroxide, a byproduct of increase lipid oxidation, has been shown to change the conformation of K^+ channels (Jabr and Cole 1993). In some cases, inward rectifying K+ channels could no longer maintain resting K^+ levels, opening probability decreased, resulting in a premature activation (depolarization) (Jabr and Cole 1993). In other cases, hyperpolarization was induced by ATP sensitive K^+ channels (Jabr and Cole 1993). The change in K+ conformations was thought to be caused by oxidation of phospholipid

membranes and Ca^{2+} mishandling and secretion form the sarcoplasmic reticulum (Jabr and Cole 1993).

Lipid metabolism can also affect neuronal mitochondrial behavior and energy dynamics. Specifically, palmitate supplementation in sensory neurons, dorsal root ganglia, has been shown to decrease mitochondrial motility due to depolarization (Rumora, Lentz et al. 2018). Supplemented neurons were characterized as having increased respiration, ATP turnover, and proton leak (Rumora, Lentz et al. 2018). As a result, mitochondria could longer provide ATP to subcellular locations in need (Rumora, Lentz et al. 2018). Dyslipidemia, high fat diets in mice, has also been shown to decrease neuronal function associated with limb movement. High fat diets lead to increased oxidized low-density lipoproteins that specifically cause DRG, dorsal root ganglia, neuron injury via oxLDL receptors (Vincent, Hayes et al. 2009). The activation of oxLDL receptors results in intracellular oxidative stress through activation of NADH oxidase in dendrites (Vincent, Hayes et al. 2009). Altogether, dysfunctional lipid metabolism leads to systemic changes in K^+ channel conformation, mitochondrial function, and ROS generation across neuronal processes.

Dissertation Objectives

In Chapter II, I address a *C. elegans* male age dependent shift in metabolic gene transcription of *fat-5*, *fat-6*, and *fat-7*. Despite the increases in transcription of *fat-6*, FAT-6 protein levels decline in various parts of the intestine with age. The anterior

intestine maintains FAT-6 protein levels into day 2 of adulthood consistent with increased lipid storage in the intestine with age. I characterize various metabolic perturbations in *fat-6(lf);fat-7(lf)* consistent with increased catabolism of saturated fat. Consistent with the role of FAT-6, under fed conditions creating lipid stores, we found food deprivation results in FAT-6 degradation.

In Chapter III, I address behavioral state changes in aging wild type male *C. elegans*. Using a 2nd order Markov Model, we concluded that aging wild type males increase recurrent exploring and decrease recurrent feeding behavior. We validated changes in feeding behavior, by measuring *E. coli* consumption during early aging. Furthermore, *fat-6(lf);fat-7(lf)*, a model of increased saturated fat oxidation, showed premature, day 1, increases in recurrent behaviors seen in day 2 wild type males. Altogether this suggests that decreases in feeding result in physiological changes that result in increased fat oxidation and increased mating.

In Chapter IV, I address *fat-6*'s role in maintaining mating fitness during early adulthood. Specifically, epidermal *fat-6* is sufficient to maintain mating fitness. In males lacking Stearoyl CoA desaturases we found defective spicule intromission dysfunction results in premature decline in mating fitness. Specifically *fat-6(lf);fat-7(lf)* mutants cannot stabilize male tail position over the vulva hinting at a lack of cholinergic motor control of muscles involved in both body posture and spicule motion.

In Chapter V, I addressed the neuronal activity of the cholinergic ventral cord in *fat-6(lf);fat-7(lf)* males. Mutants showed exaggerated responses and shortened duration. This defect could account for the uncoordinated behavior displayed during the male's

spicule insertion attempts. Due to the heightened neural excitation and transmitter release we found muscle-expressed *unc-103* isoform A was upregulated to mitigate possible downstream muscle spasms from the altered neural activity.

In Chapter VI we addressed the role of PEPCK in mating behavior. Males lacking functional PEPCK, *pck-1(lf);pck-2(lf)*, were found to prematurely decline in mating performance on day 1 of adulthood. We also found epidermal *pck-2* provides glycolytic metabolites to *pck-1*-deficient neurons and muscles. Interestingly, we found *pck-1*-deficient neurons and muscles adjust neighboring tissues PEPCK levels to match disrupted gluco-glyceroneogenesis metabolism.

In Chapter VII we continued to address PEPCK regulation. A EMS mutagenesis screen on PCK-2::YFP animals resulted in a missense mutation in succinate dehydrogenase subunit A, encoded by *sdha-1*, increasing *pck-2*::YFP. We suggested that metabolites were being rerouted out of the mitochondrial TCA cycle in *sdha-1(lf)*. This shift in metabolism resulted in PEPCK produced glycerol contributing to intestinal lipid stores, delayed development, puncta-like mitochondrial morphology, and resistance to electron carrier dependent ROS induced death.

In Chapter VIII I summarize Chapters II-VII, discuss the implications of fuel utilization in the male tail, and outline potential future experiments.

CHAPTER II

FOOD DEPENDENT REGULATION OF FAT-6

Age Dependent Increases in Fatty Acid Desaturases Transcription

In an earlier study, metabolic changes in the male *C. elegans* were found to sustain copulation behavior during the first two days of adulthood (Guo, Navetta et al. 2012, Guo and García 2014). RT-qPCR analysis of male metabolic gene expression was conducted on day 1 and day 2 of adulthood (Guo and García 2014). Of the genes queried, the fatty acid desaturases genes *fat-5/6/7*, involved in lipid synthesis, showed a 3-9 fold increase in expression. It was hypothesized that between days 1-2, adult males increased their fatty acid synthesis as a compensatory response to continued fatty acid breakdown for energy and biomass (i.e. gamete) production. Here, we validated the changes in fatty acid desaturase gene expression by doing RT-qPCR analysis on eight to fifteen independent biological replicates, each replicate containing pooled transcripts of three males across the first two days of adulthood. Both *fat-5* and *fat-6* RNA significantly increased from day 1 to day 2 of adulthood; *fat-7* RNA is elevated on day 2 but not with statistical significance (Fig. 4). The slight change in *fat-7* levels may be explained by its redundant function with *fat-6* (Watts and Browse 2000).

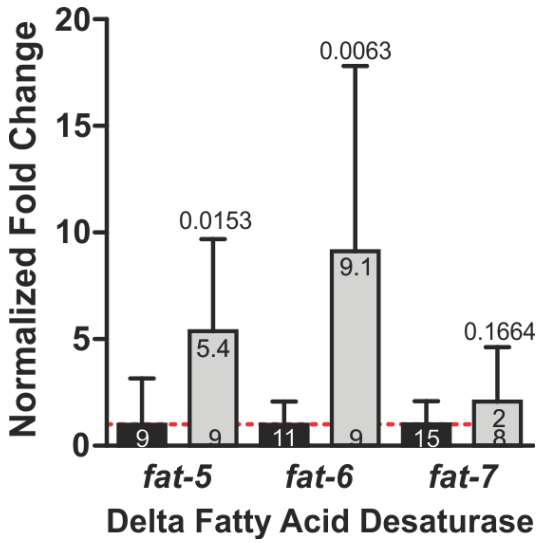

Figure 4 Early aging wild type males increase fatty acid synthesis genes.
Relative mRNA expression level of delta fatty acid desaturases *fat-5*, *fat-6*, and *fat-7* in 1-day-old wild type and 2-day-old wild type males (unpaired t-test). Each individual gene was normalized to the wild type equivalent. Numbers of animals assayed are listed at the bottom. Bars and whiskers represent mean and standard deviation.

Tissue Specific Expression of FAT-6 Supports Lipid Storage

Since fatty acid desaturase gene expression increases in aging males, we asked how the protein levels correlated with mRNA amounts. FAT-6 protein was visualized using a CRISPR/Cas9 generated YFP and Cre/loxp flanked knock-in (see methods) (Fig. 5). We observed FAT-6::YFP expression in the epidermis and intestine throughout larval development and into adulthood in hermaphrodites and males (Fig. 6). However, head and tail epidermal expression was diminished by day 1 of adulthood. FAT-6::YFP epidermal signal in the hermaphrodite head and male was 10% of that seen in the intestine. On day 2 and day 3 of male adulthood, the epidermal expression drops to 1%

of the intestinal signal. This observation differed from previously published work in which a *fat-6*::GFP transgene displayed strong expression in the epidermis throughout development (Brock, Browse et al. 2006). To validate the FAT-6::YFP CRISPR/Cas9 allele was functioning similar to wild-type FAT-6, we introduced the knock-in into a *fat-7(lf)* mutant and measured intestinal neutral lipids. If FAT-6 was compromised by the YFP, then the *fat-7(lf)* mutant would have a low fat phenotype, similar to the published *fat-6(lf);fat-7(lf)* mutant (Brock, Browse et al. 2007). We measured an increase in intestinal neutral lipids and whole intestine FAT-6::YFP levels in *fat-7(lf) and fat-5(lf);fat-7(lf)* males (Fig. 7), suggesting FAT-6 function was not compromised.

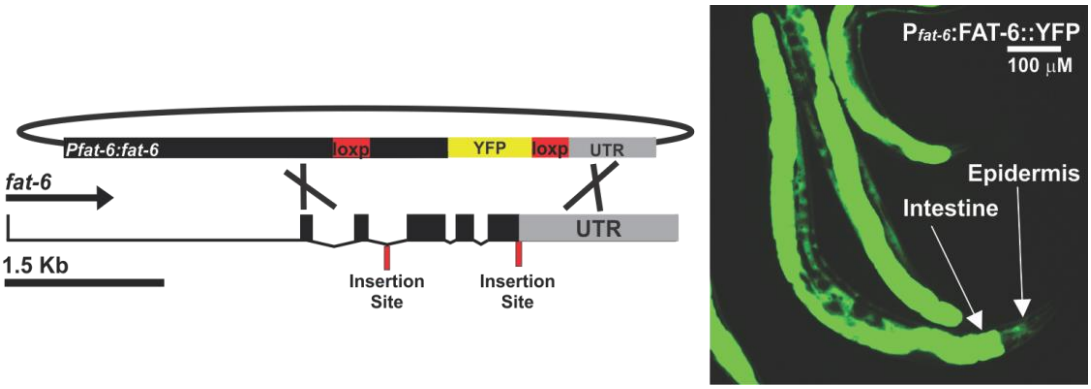

Figure 5 CRISPR/Cas9 YFP knock-in design and FAT-6::YFP in *C. elegans*.
Cartoon of CRISPR/Cas9 FAT-6::YFP knock-in design and confocal images of FAT-6::YFP expression in adult hermaphrodites; contrast was increased to see low expressing hypodermal expression.

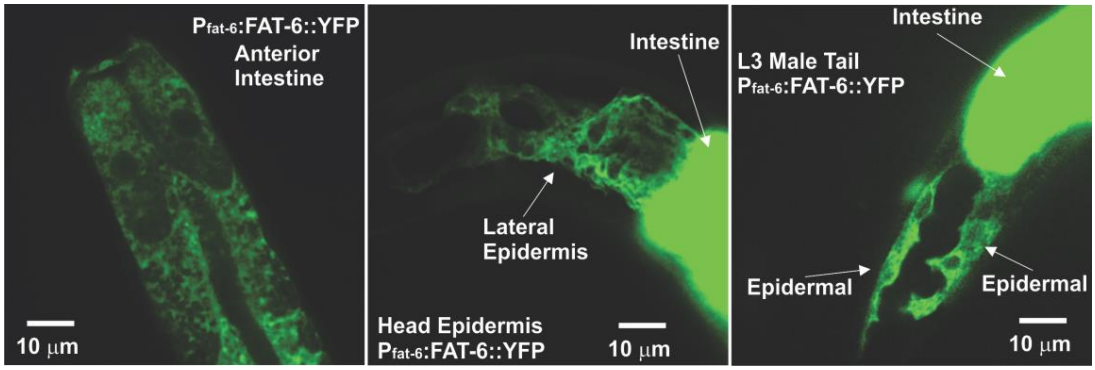

Figure 6 Endogenous FAT-6 expression in male *C. elegans*.
(Left Panel) FAT-6::YFP in the intestine, (Middle Panel) head epidermis, and (Right Panel) epidermis of the male tail.

To validate that the FAT-6::YFP CRISPR/Cas9 allele was functioning similar to wild-type FAT-6, we introduced the knock-in into a *fat-7(lf)* mutant and measured intestinal neutral lipids. If FAT-6 was compromised by the YFP, then the *fat-7(lf)* mutant would have a low fat phenotype, similar to the published *fat-6(lf);fat-7(lf)*mutant (Brock, Browse et al. 2007). We measured an increase in intestinal neutral lipids and whole intestine FAT-6::YFP levels in *fat-7(lf)* and *fat-5(lf);fat-7(lf)* males (Fig. 7 and 8), suggesting that FAT-6 function was not compromised.

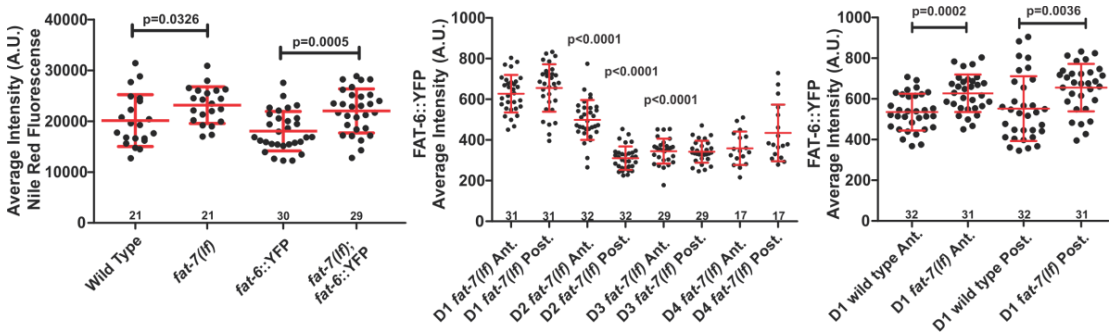

Figure 7 FAT-6::YFP does not disrupt FAT-6 wild type function.
FAT-6::YFP expression and Nile Red staining quantified by a series of rectangular ROI's drawn over the intestine (unpaired t-test).

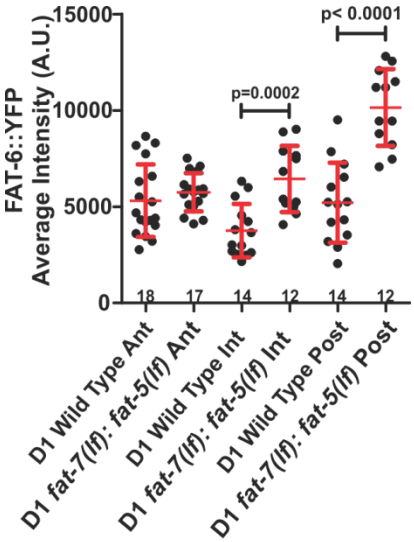

Figure 8 FAT-6::YFP remains dynamic in *fat-5(lf);fat-7(lf)* mutant males.
FAT-6::YFP expression quantified by a series of rectangular ROI's drawn over the intestine (unpaired t-test).

Contrary to the increased transcription of *fat-6* in aging males, FAT-6::YFP levels decreased with age in specific segments of the intestine in hermaphrodites and males (Fig. 9 and 10B). In aging males, the anterior-most intestine remained unchanged

until day 3 of adulthood (60 hrs) (Fig. 10A and 10B). The posterior intestine, adjacent to the gonadal seminal vesicle (spermatid storage) decreased from day 1 to day 2 of adulthood (36 hrs) (Fig. 10B). Attenuation of posterior intestinal FAT-6 might suggest a need for supporting reproductive functions. As FAT-6::YFP intensity decreased in both the intestine and epidermis with age, we observed a concomitant increase in neutral lipids in the intestine, validating its minimal presence was still functional in increasing lipid stores (Fig. 10A and 10C). Also consistent with the anterior intestines maintenance of FAT-6::YFP into day 2 of adulthood, the largest increase in neutral lipids were seen in the anterior intestine on day 3. This suggests, during days 1 and 2 of adulthood, *fat-6* transcription augments FAT-6 function in the anterior intestine.

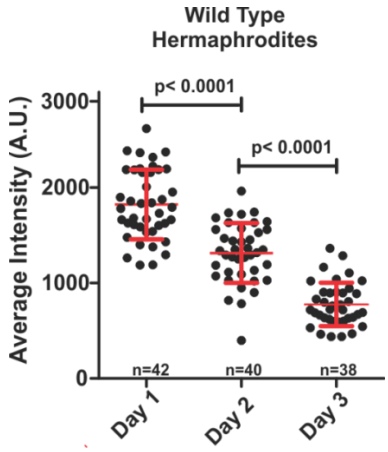

Figure 9 FAT-6::YFP in aging hermaphrodites.
Yellow emission fluorescence intensity of aging hermaphrodites in a region of interest (ROI) encompassing the intestine (unpaired t-test). Fluorescence values are in arbitrary units (A.U). Each dot represents the ROI of a single hermaphrodite. Numbers of animals assayed are listed at the bottom. Bars and whiskers represent mean and standard deviation.

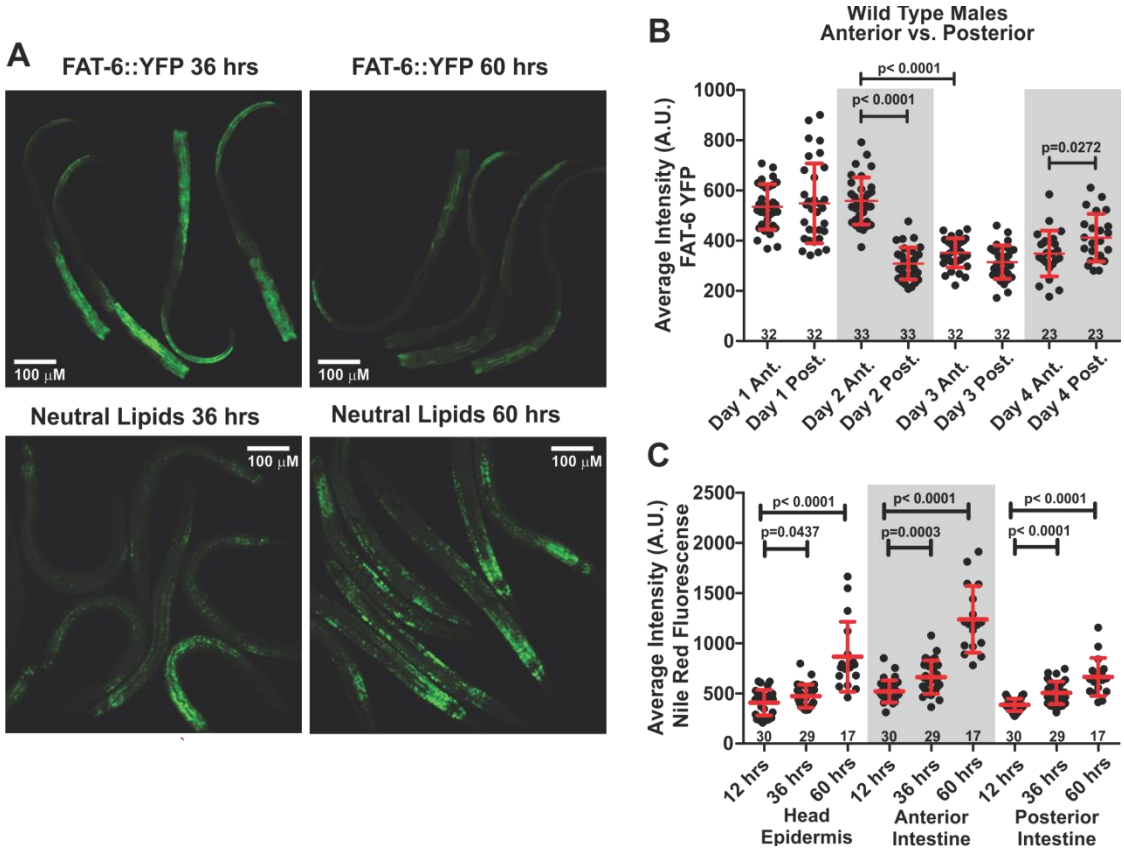

Figure 10 FAT-6::YFP and neutral lipid stores in aging wild type males.
(A) Confocal images of FAT-6::YFP expression and Nile Red staining in aging adult males. (B) FAT-6::YFP expression in aging males was quantified by a series of rectangular ROI's drawn over the intestine (unpaired t-test).The series of ROI's corresponding to the first half of the intestine were designated anterior. The posterior was composed of the second half of the intestine reaching to the end of the intestine. (C) Nile Red staining in aging adult males was quantified by a series of rectangular ROI's drawn over the head epidermis and intestine (unpaired t-test). (A, B, and C) Numbers of animals assayed are listed at the bottom. Bars and whiskers represent mean and standard deviation.

Male Gonad Regulates Dynamic Levels of FAT-6

Since the region of the intestine adjacent to the somatic gonad showed decreased FAT-6::YFP fluorescence with age, we asked if intestinal FAT-6 is responsive to the

reproductive system. To determine the gonad's role in the regulation of intestinal FAT-6, the somatic and germline gonad of L1 males were laser-ablated, and FAT-6::YFP was quantified in day 1 adults (Fig. 11). While the mean average intensity was unaffected, virgin and mock-ablated males both showed high variance in FAT-6::YFP levels in the intermediate and posterior intestine, adjacent to the gonad. However in animals where the gonad was ablated, the variance was significantly lowered, indicating idiosyncratic levels of intestinal FAT-6::YFP is modulated by the gonad.

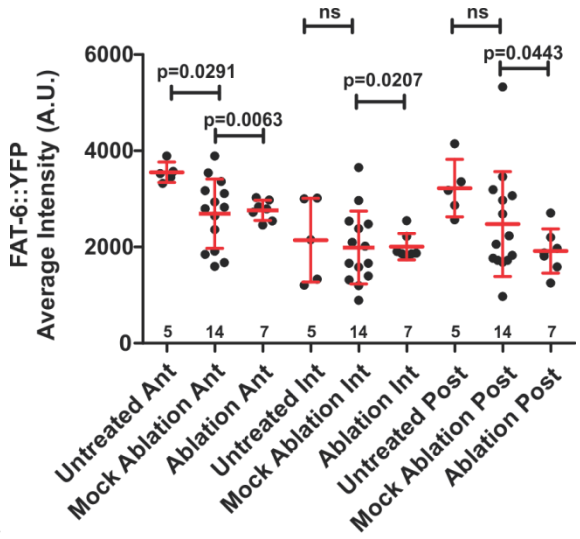

Figure 11 Gonad regulated FAT-6 expression in male *C. elegans*.
Laser-ablated the gonad precursor cells and quantified FAT-6::YFP fluorescence in day 1 adults. All mock ablated and ablated animals were subjected to 5% Noble agar and immobilized with 10mM azide for no more than 10 minutes.

Metabolic Characterization of FAT-6 And FAT-7

To quantify FAT-6's activity in generating intestinal triglycerides, we stained neutral lipid droplets using Nile Red. We hypothesized that elevated *fat-6* transcription on day 2 occurs to increase intestinal triglyceride stores in the anterior intestine, to offset concurring fat catabolism in other tissues. In contrast to wild type, we observed *fat-6(lf);fat-7(lf)* males, similar to published results in hermaphrodites, display a low-fat phenotype with a 68% decrease in neutral lipids (Brock, Browse et al. 2007) (Fig. 12). We therefore suggest that in mutants, bacterial-ingested saturated fat is not efficiently converted into neutral lipids in the intestine and instead catabolized or excreted (Tanaka, Ikita et al. 1996).

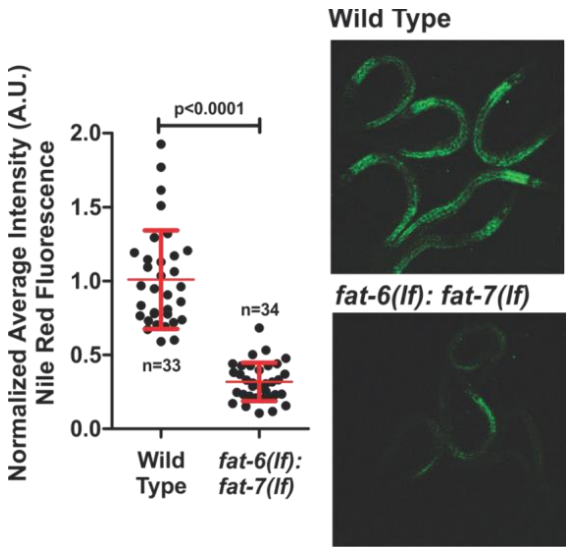

Figure 12 Neutral lipid stores in *fat-6(lf);fat-7(lf)* mutant male *C. elegans*.
Nile Red staining of day 1 adult males. Top panel represents a group of wild type males. Bottom panel displays a group of desaturase mutants.

We next investigated the accumulation and catabolism of neutral lipids during the first three days of adulthood. Stearoyl-CoA desaturases, *fat-6* and *fat-7*, catalyze the rate limiting step of unsaturated fatty acid synthesis by converting stearic acid to the unsaturated fat oleic acid. We postulated oleic acid supplementation (via the OP50, see methods) on *fat-6(lf);fat-7(lf)* mutants could restore intestinal neutral lipids stores (Brock, Browse et al. 2007, Shi, Li et al. 2013). Conversely if we removed oleic acid from the mutant's diet, we could use Nile Red staining to measure how fast the males mobilized their neutral lipid stores. Mutants and wild type were fed oleic acid-containing bacteria throughout development up to day 1 of adulthood, after which they were transferred to non-oleic acid supplemented plates. We hypothesized that after oleic acid feeding, mutant and wild type males would have similar amounts of intestinal triglyceride stores; after removal from oleic acid supplementation, the mutants should deplete their intestinal fat stores. As expected, oleic acid supplementation increased the neutral lipids in wild type and mutant similarly (Fig. 13). However, after removing mutant males from oleic acid-containing food, we unexpectedly observed an initial increase in neutral lipids within 24 hours, challenging our expectation of immediate lipid catabolism. But by the 3rd day of adulthood neutral lipids stores decreased, indicating a temporary delay in fat utilization. In contrast, wild type males increase neutral lipid stores across all three days of adulthood, suggesting fat oxidation and fatty acid synthesis occur concurrently in adult wild type males. The kinetics of oleic acid metabolism in *fat-6(lf);fat-7(lf)* males suggest that if there is an interruption in unsaturated fat synthesis, either through mutation or dietary stress, lipids are temporary

trafficked from other regions of the worm to the intestine, followed by lipid redistribution and usage.

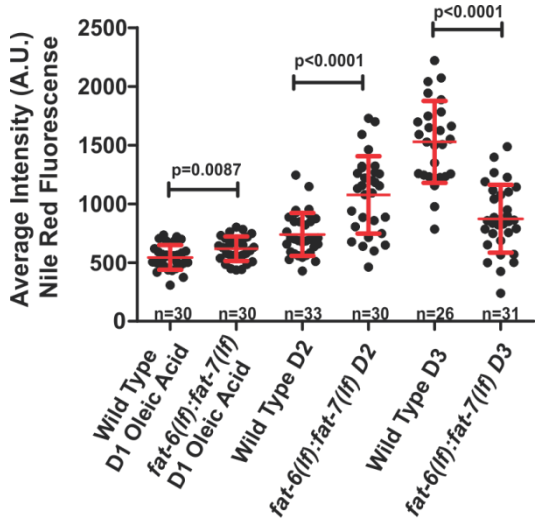

Figure 13 Rescue and oxidation of lipid stores in aging *fat-6(lf);fat-7(lf)* males. Nile Red staining of day 1-3 males with and without oleic acid. Desaturase mutants were under continuous oleic acid supplementation until day 1 of adulthood. Day 2 males were therefore off oleic acid for 24 hrs. Day 3 males were off oleic acid for 48 hrs.

Given that *fat-6(lf);fat-7(lf)* mutants are defective for storing intestinal lipids, we assayed respiration to determine if unresolved fat was over catabolized. If the mutants continually ingest bacterial-derived saturated fat (C_{16}) and circumvent lipid synthesis, the intestine may uptake and transport free fatty acids or their byproducts, to other tissues in the worm (Tanaka, Ikita et al. 1996). β-oxidation of short($<C_8$), medium (C_8-C_{12}), and long chain fatty acids (C_{14}-C_{20}) predominantly occurs in the mitochondria (Reddy and Hashimoto 2001). Peroxisomes can functionally complement the mitochondria with the β-oxidation of long chain fatty acids (C_{14}-C_{20}) but given the

exclusive ability to catabolize very long fatty acids (>C_{20}) we expect mutants to rely primarily on mitochondrial β-oxidation for bacterially derived palmitic acid (C_{16}) (Tanaka, Ikita et al. 1996, Reddy and Hashimoto 2001). Peroxisomes can also metabolize palmitic acid into medium chain fatty acids (C_8-C_{12}) which is then transported to the mitochondria given its exclusive medium chain β-oxidation (Reddy and Hashimoto 2001). Therefore, β-oxidation byproducts of free fatty acids are expected to increase mitochondrial respiration. To quantify respiration, we recorded voltage changes in 1.5 ml tubes populated with well-fed day 1 adult males in S-basal solution, a common buffer used for growing worms in culture. The voltage changes approximate changes in oxygen. Indeed, we observed an increase in respiration, validating an increase in saturated fat catabolism (Fig. 14).

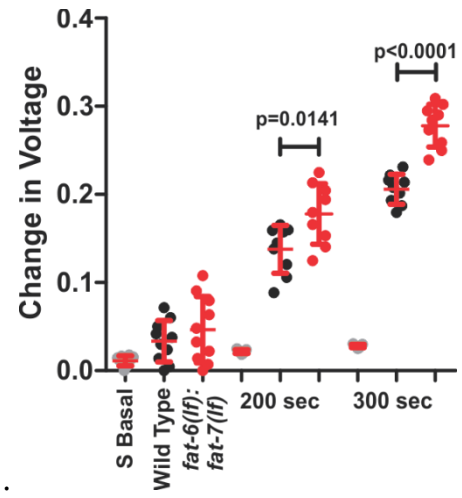

Figure 14 Whole worm respiration of *fat-6(lf);fat-7(lf)* males.
The respiration of 50 males was measured by change in voltage. Bars and whiskers represent mean and standard deviation.

Since *fat-6(lf);fat-7(lf)*mutants showed increased respiration, we performed single worm RT-qPCR to query potential expression changes in other metabolic genes. Because there are three stearoyl-CoA genes, *fat-5*, *fat-6*, and *fat-7,* we expect that the last remaining desaturase gene, *fat-5,* should be upregulated to provide some unsaturated fat in *fat-6(lf);fat-7(lf)*mutants. In addition, if the *fat-6(lf);fat-7(lf)*mutants over-catabolize saturated fat and respiration increases as a result, then we might also expect expression changes in genes such as *ctl-1* (catalase, which coverts H_2O_2 to water and oxygen), *sod-4* (superoxide dismutase, which coverts O_2^- and O_2 into H_2O_2), t20h4.5 (NADH dehydrogenase, which is part of the electron transport complex), *cco-1* (cytochrome-c oxidase) and *ech-2*(enoyl-CoA hydratase, which is involved in β-oxidation). Not surprisingly, we measured significant increases in *fat-5* by ~4 fold, which is similar to previous reports for hermaphrodites (Fig. 15) (Brock, Browse et al. 2007).

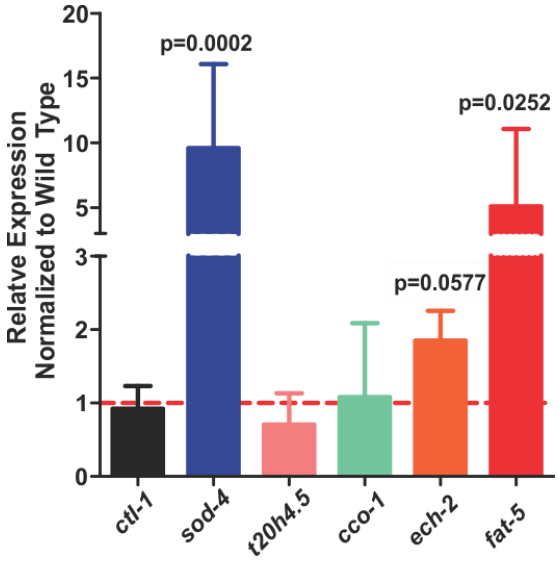

Figure 15 Metabolic gene expression of *fat-6(lf);fat-7(lf)* males.
Relative mRNA expression level of metabolic genes *sod-4, ctl-1, t20h4.5, cco-1, ech-2, and fat-5* in 1-day-old *fat-6(lf);fat-7(lf)* males (unpaired t-test). Each individual gene was normalized to the wild type equivalent. Numbers of animals assayed are listed at the bottom. Bars and whiskers represent mean and standard deviation.

We measured significant increases in *sod-4* by ~10 fold (Fig. 15). The extracellular and membrane bound superoxide, *sod-4*, has been implicated in creating H_2O_2 that inhibits PTP, protein tyrosine phosphatases, dependent inhibition of insulin signaling (Goldstein, Mahadev et al. 2005, Doonan, McElwee et al. 2008, Gems and Doonan 2009) . If insulin signaling is activated, we expect increases in metabolic processes, glycogen and lipid synthesis, as well as decreases in lipolysis and gluconeogenesis (De Meyts 2000). However, we did not measure significant increases in most of the other genes involved in fatty acid oxidation, indicating that not all facets of metabolism transcriptionally adjusted to over-oxidation of ingested fat.

FAT-6 Regulates Lipid Stores Under Fed Conditions

Since day 2 adult male FAT-6 protein levels decreased in different tissues, we asked what other condition could alter the enzyme's stability. During adulthood, FAT-6 balances the storage of unsaturated fat with saturated fat oxidation; however, during bouts of food deprivation, ingestion of saturated fat decreases and catabolism of stored fuel occurs. Under this condition, we expect fatty acid desaturases to play a minimal role. Thus, we asked how changes in feeding affect FAT-6 in wild type and the *fat-7(lf)* mutant. We found 2 hrs of starvation induces FAT-6::YFP degradation in both wild type and mutants (Fig. 16A). Wild-type hermaphrodites showed similar degradation 4 hrs after food removal (Fig. 16B). The dimorphic difference is likely due to hermaphrodites having a 3 times larger FAT-6::YFP pool during day 1 of adulthood. Interestingly, 12 hrs of refeeding after 5 hr of starvation induced FAT-6::YFP level to rebound higher than the well fed cohorts (Fig. 16A), suggesting that male's physiology might be adapting to a potential future food stress.

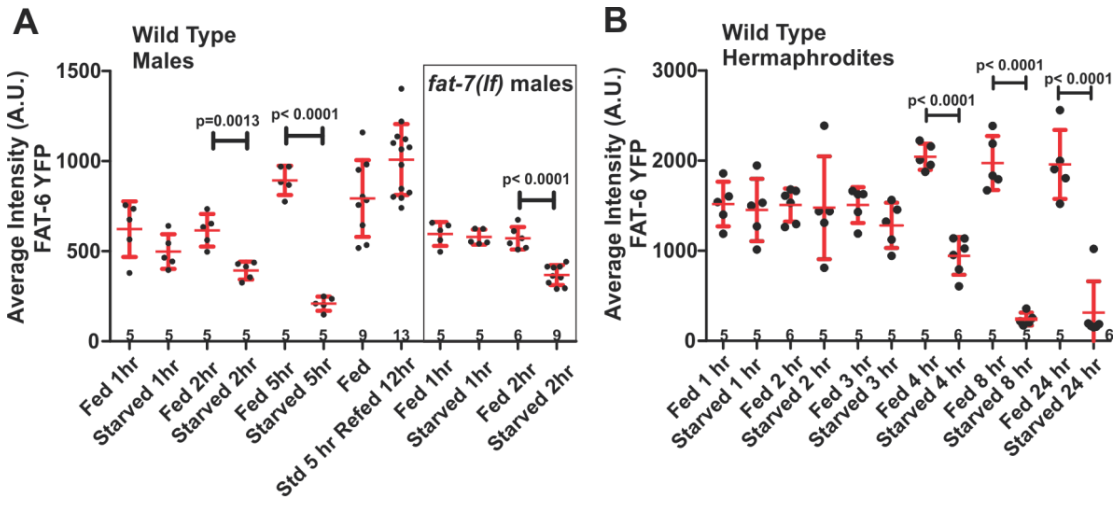

Figure 16 Food deprivation decreases FAT-6::YFP in wild type *C. elegans*.
FAT-6::YFP expression quantified by a series of rectangular ROI's drawn over the intestine (unpaired t-test). Starved animals were grown on NGM plates lacking OP50 and a glycerol ring was used to contain males on plate.

Chapter II Summary

C. elegans males were found to undergo an age dependent shift in metabolic gene transcription. The transcription of *fat-5*, *fat-6*, and *fat-7* all showed increases on day 2 of adulthood compared to day 1 of adulthood. Despite the increases in transcription of *fat-6*, FAT-6 protein levels decline in various parts of the intestine with age. The anterior intestine maintains FAT-6 protein levels into day 2 of adulthood consistent with increased lipid storage in the intestine with age. Maintaining the lipid stores in wild type males required *fat-6* and *fat-7*. In *fat-6(lf);fat-7(lf)* mutant males the lack of intestinal lipid storage results in increased mitochondrial respiration and suboptimal compensatory mechanisms; *fat-5* and *sod-4* involved in lipid synthesis and ROS scavenging respectively. Consistent with the role of FAT-6, under fed conditions creating lipid stores, we found food deprivation results in FAT-6 degradation. After a refeeding, FAT-6 protein levels remained dynamic in wild type and mutant backgrounds. Specifically the FAT-6 protein levels in *fat-7(lf)* and *fat-5(lf);fat-7(lf)* mutants increased as a potential compensatory mechanism.

CHAPTER III

CHANGES IN BEHAVIOR WITH AGE

Identification of Behavioral States in Early Aging Males

Lower FAT-6 protein levels after acute food deprivation made us ask if the FAT-6 reduction in a normally well-fed day 2 wild type males is also correlated with changes in feeding behavior. To assay feeding, we introduced well-fed day 1 and day 2 males to a lawn of *E. coli* expressing a red fluorescent protein and measured how fast ingested fluorescent bacteria accumulated in the intestine (Fig. 17). Surprisingly, we found bacterial consumption was decreased in day 2 males relative to day 1 males (Fig. 17). Presumably, *ad libitum* feeding during the first 24 hours of adulthood is sufficient to attenuate food intake in the older males; as a result, lower ingested saturated fat could account for reduced need for fatty acid desaturase function.

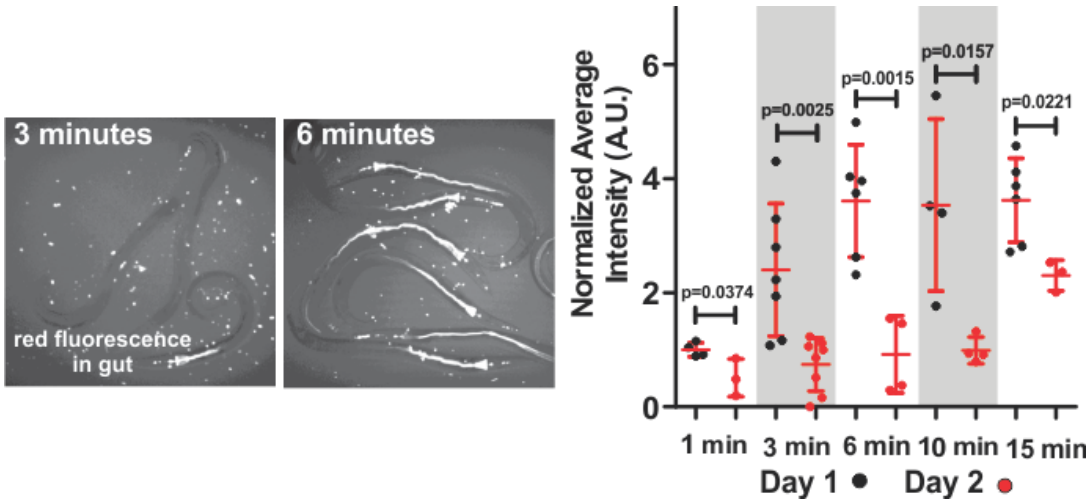

Figure 17 Food consumption decreases in early aging wild type males.
OP50 expressing pTimer was used to measure food consumption of day 1 and day 2 wild type males. Males were allowed to be incubated on fluorescent OP50 at varying time points. We quantified the fluorescence within the intestinal lumen at specific time points.

The day 2 wild type male's reduction in food ingestion prompt us to measure behavioral alterations to their food-seeking and copulation preference. We designed mating arenas to monitor a day 1 or day 2 male's choice to feed, mate, or explore its environment (See Methods). The ~6 mm X 6 mm square NGM agar mating arena contained three paralyzed hermaphrodites (lying on no food), ~4 mm diagonally opposite a ~2 mm diameter bacterial lawn (Fig. 18). After an hour, to allow hermaphrodite and bacterial secreted cues to permeate the arena, a single day 1 male (~ 12 hrs post L4 molt) or day 2 male (~36 hrs post L4 molt) was added to the arena and behavior was digitally recorded at 15 frames per second for one hour. Males in each frame of the one-hour video were given a different arbitrary value if they were feeding, mating or exploring. These values were color-coded and plotted across time per male

(Fig. 19). To analyze the data, we quantified the proportion of time spent on each behavior within the one-hour recording. These proportions were then plotted on a ternary plot (Fig. 20). As a data point, defined as a single male worm, moves towards any of the vertices, the proportion of time spent on a behavioral state increases to a proportion of 1.0 or 100%. From first approximation, day 1 males spent more time eating than mating, whereas the day 2 male spent more time mating than eating (Fig. 20).

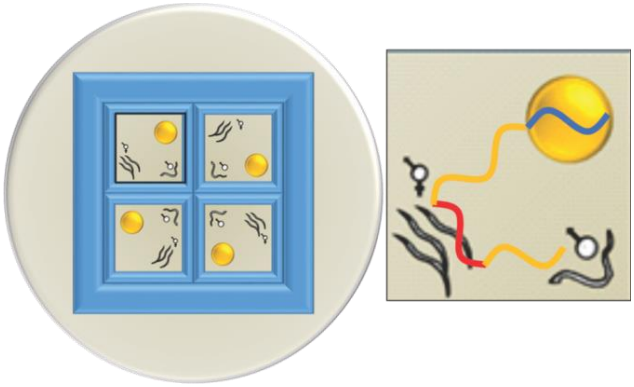

Figure 18 Illustration of the assay design and identification of behavioral states. Four separate mating arenas each contained three paralyzed hermaphrodites opposite a bacterial lawn. After one-hour incubation, four wild type males were added, one per arena, and behavioral choices were digitally recorded at 15 frames per second for one hour.

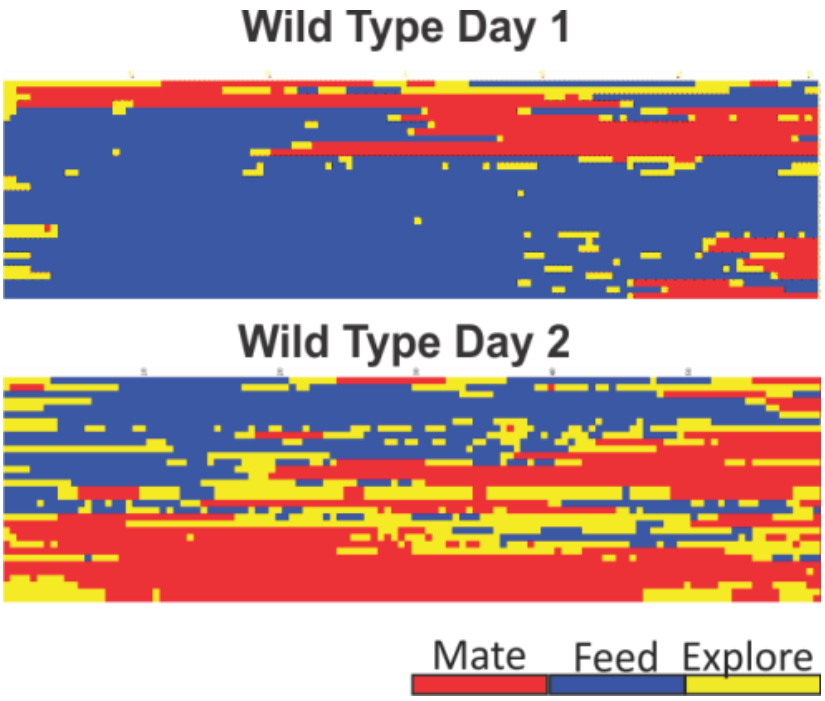

Figure 19 Visualized feeding, mating, and exploring behaviors across time.
Raw data colorized in blue, yellow, and red for feeding, exploring, and mating behaviors respectively. The vertical axis corresponds to individual males. The horizontal axis corresponds to time in minutes.

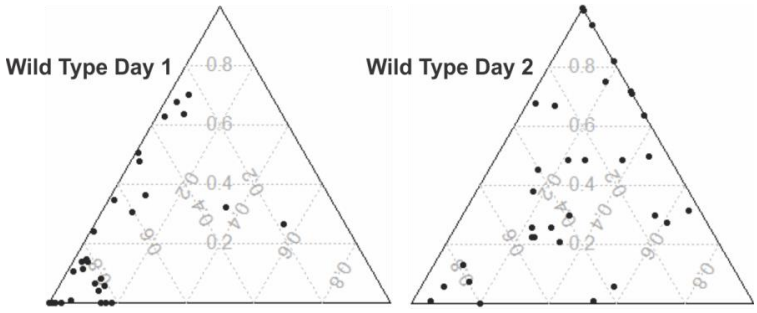

Figure 20 Transition in feeding behavior in early aging wild type males.
Raw data plotted in a ternary graph. In this graph each vertices of the triangle represents a 100% proportion of a certain behavioral state. Each point is an individual male plotted according to the proportion of time spent feeding (Left Corner), exploring (Top Corner), or mating (Right Corner).

Markov Model State Diagrams for Early Aging Wild Type Males

Previous research showed that hidden Markov models can be used in *C. elegans* hermaphrodites to analyze behavioral states, such as roaming, dwelling and quiescence (Gallagher, Bjorness et al. 2013). Here, we used similar Markov modeling to make probabilistic predictions in the male's feeding, exploring and mating behavioral states (See Methods). We attempted multiple models to find parameters that produced simulations approximating observed behaviors. First order models, which attempt to simulate what the male will do in the future, based on its current activity were not predictive (Fig. 21) (Powell). However, a second order model, which incorporates what the male was doing 15 seconds in the past with its current behavior, best simulated the observed data (Fig. 22).

Transition Matric D1 Wild Type 1st Order
[[0.98,0.02,0],[0.18,0.71,0.11],[0,0.025,0.975]]

	A_{feed}	$B_{Explore}$	C_{mate}
A_{feed}	0.98	0.02	0.00
$B_{Explore}$	0.18	0.71	0.11
C_{mate}	0.00	0.025	0.975

Transition Matric D2 Wild Type 1st Order
[[0.91,0.09,0],[0.10,0.82,0.08],[0,0.04,0.96]]

	A_{feed}	$B_{Explore}$	C_{mate}
A_{feed}	0.91	0.09	0.00
$B_{Explore}$	0.10	0.82	0.08
C_{mate}	0.00	0.04	0.96

Figure 21 1st Order transition matrixes for aging wild type males.
We used a first order Markov model to describe behavior in day 1 and day 2 wild type males. It did not recapitulate the behaviors as well as a second order Markov model. We show the simple transition matrix for aging wild type males.

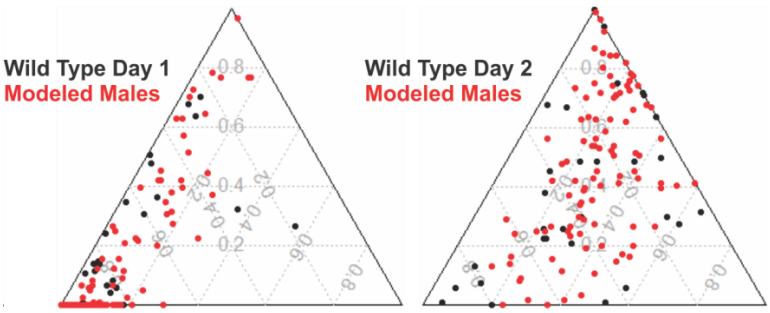

Figure 22 Co-localization between Raw and Modeled data.
Raw data, in black, was plotted in a ternary graph. In this graph each vertices of the triangle represents a 100% proportion of a certain behavioral state. Each point is an individual male plotted according to the proportion of time spent feeding (Left Corner), exploring (Top Corner), or mating (Right Corner). Markov modeled data is depicted in red and co-localizes with the raw data in black.

Markov model probabilities can be displayed as a state diagram or as a transition matrix (Fig. 21 and 23). We designed a state diagram to predict the male's future behavioral state based on its current and past states. In our state diagram, the male's current state can be feeding, exploring, or copulating; denoted by the three circles. The color of the circle or arrow (see figure legend) identifies the males behavioral state 15 seconds in the past (see figure legend). The value, within a circle or arrow, refers to the probability of transitioning to a future state, given the previous and current behavioral state. The direction of the arrow refers to the future state. For example, in wild type day 1 panel E, a yellow arrow emanating from the feeding circle and pointing to the exploring circle indicates that an exploring male has a 64% probability of continuing to explore, if it was previously eating 15 seconds in the past. A red arrow emanating from the exploring circle and pointing back to the exploring circle means a copulating male, that was previously exploring 15 seconds in the past will have a 6% probability of

disengaging with its mate and returning to exploratory behavior. The colored circles also represent a continuous behavioral state. For example, the value within a blue circle indicates the probability that a currently feeding male that was feeding, will continue to feed.

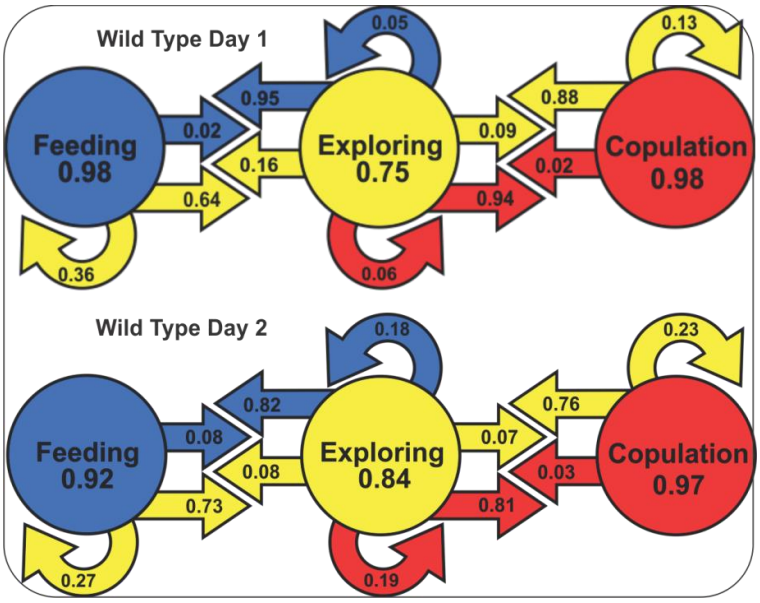

Figure 23 Markov model state diagrams for early aging wild type males.
Show the proportions governing behavioral states of aging wild type males. The color identifies the previous behavioral state. The probability, within a circle or arrow, refers to transition between two states given a known starting behavioral state.

From the modeling data, the day 2 males show increased probability of recurrent exploring behavior and decreased probability of recurrent feeding behavior. Interestingly, although older males appear to spend more time mating (Fig. 20 and 22), the modeling probability values suggest the male's mating drive between the two days are unchanged (probability values in the red circles, Fig. 23). The data suggests wild-

type male's reduced feeding state, coupled with its increased exploratory behavior; indirectly promote the frequency and duration of a day 2 male's mating incidence.

Markov Model State Diagrams for Early Aging *fat-6(lf);fat-7(lf)* Males

We then asked if over-catabolizing and not storing lipids alter the male's feeding, mating and exploring states (Fig. 24 and 25). Similar to wild type, the recorded behavioral choices of *fat-6(lf); fat-7(lf)* males showed increases in mating from day 1 to day 2 (Fig. 22 and 25). Like wild type, the modeling values indicate that between these two days, the probability of sustaining copulation is maintained, and the exploring state probability increases (Fig. 25 and 26). However, where the *fat-6(lf);fat-7(lf)* mutant males differ from wild type is their exploring state probabilities are higher on day 1, and their feeding state probabilities do not decrease on day 2 (Fig. 26). These differences are not unexpected since catabolizing fat could be correlated with sustaining exploring behavior, a state normally occurring when a starving animal searches for food (Sawin, Ranganathan et al. 2000, Hills, Brockie et al. 2004, Gray, Hill et al. 2005, Van Gilst, Hadjivassiliou et al. 2005, Ben Arous, Laffont et al. 2009, Calhoun, Tong et al. 2015, Pradhan, Quilez et al. 2019). Additionally, not storing fat also could be correlated with sustaining feeding behavior, since the males might not be producing food satiety signals (Avery and Horvitz 1990, Sawin, Ranganathan et al. 2000, Lipton, Kleemann et al. 2004, You, Kim et al. 2008, Lemieux, Cunningham et al. 2015, Ryu, Cheon et al. 2018). Taken together, the *fat-6(lf);fat-7(lf)* male's behavior hint that for wild type, changes in

feeding and exploring behavior might account for the changes in day 1 and day 2 fat metabolism.

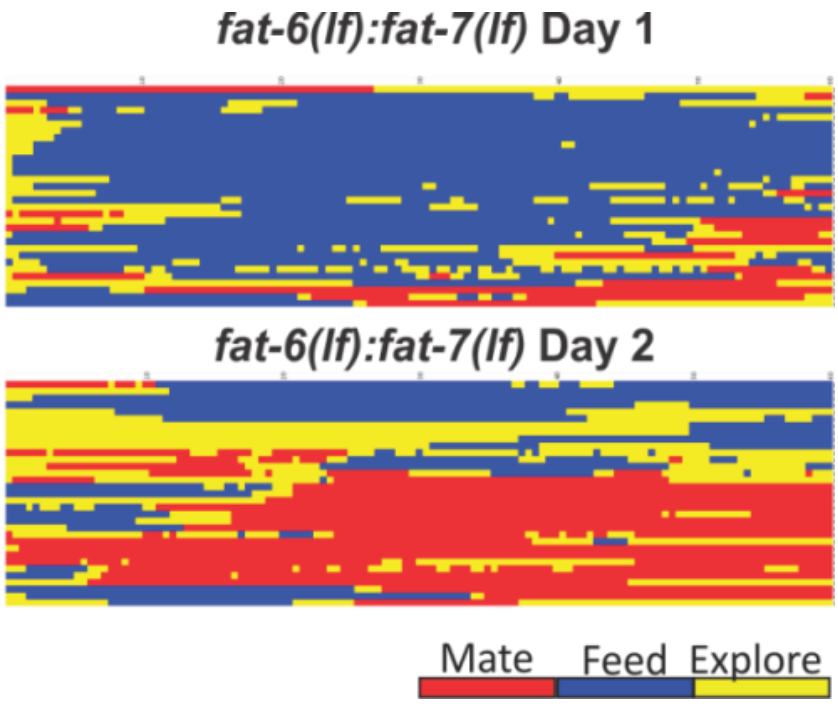

Figure 24 Visualized feeding, mating, and exploring behaviors across time.
Raw data colorized in blue, yellow, and red for feeding, exploring, and mating behaviors respectively. The vertical axis corresponds to individual males. The horizontal axis corresponds to time in minutes.

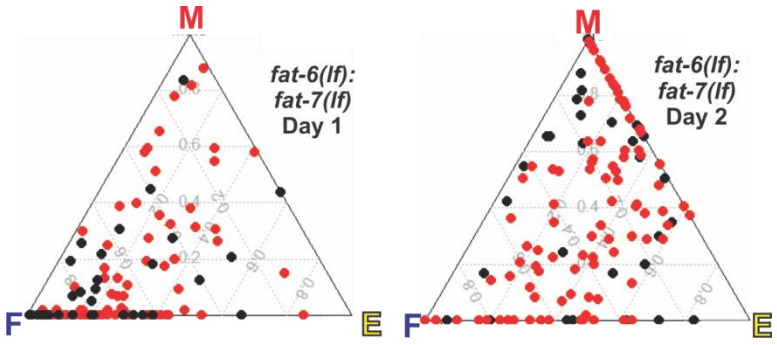

Figure 25 Transitional behavior in early aging *fat-6(lf);fat-7(lf)* males.
Raw data, in black, was plotted in a ternary graph. In this graph each vertices of the triangle represents a 100% proportion of a certain behavioral state. Each point is an individual male plotted according to the proportion of time spent feeding (F), exploring (E), or mating (M). Markov modeled data is depicted in red and co-localizes with the raw data in black.

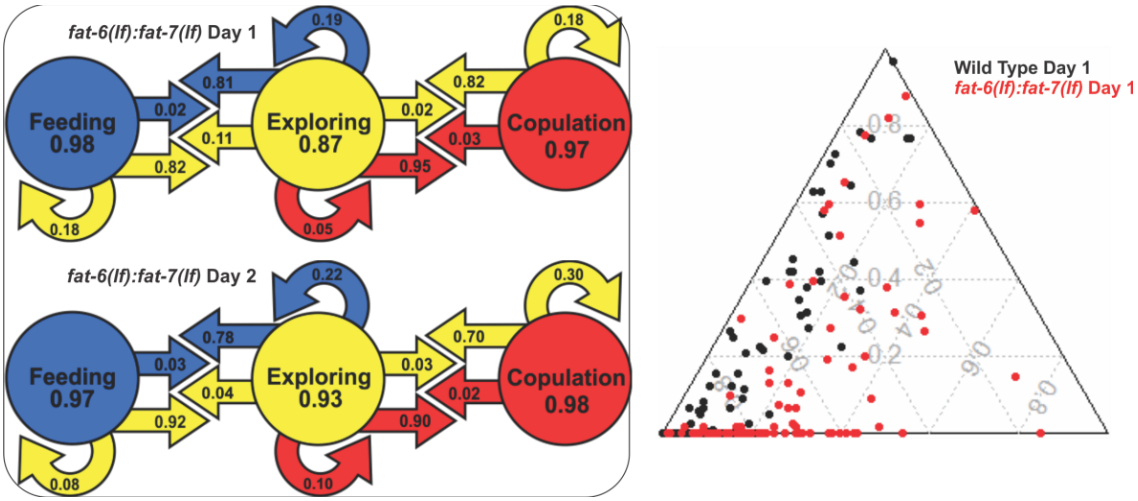

Figure 26 Premature transition to exploring behavior for aging *fat-6(lf);fat-7(lf)*.
Show the proportions governing behavioral states of aging mutant males. The color identifies the previous behavioral state. The probability, within a circle or arrow, refers to transition between two states given a known starting behavioral state. 2nd order Markov modeled data for wild type and *fat-6(lf);fat-7(lf)* day 1 adults superimposed on the same ternary plot. Feeding (Left Corner), exploring (Top Corner), or mating (Right Corner).

Chapter III Summary

A 2nd order Markov Model was created to understand how behavioral states change in aging wild type male *C. elegans*. The model used previous behavioral states as a starting point for probabilistic predictions. We concluded that aging wild type males increase recurrent exploring and decrease recurrent feeding behavior. We validated changes in feeding behavior, by measuring *E. coli* consumption during early aging. Furthermore, *fat-6(lf);fat-7(lf)*, a model of increased saturated fat oxidation, showed premature, day 1, increases in recurrent behaviors seen in day 2 wild type males. Altogether this suggests that decreases in feeding result in physiological changes that result in increased fat oxidation and increased mating.

CHAPTER IV

FAT SYNTHESIS ADJUSTS MATING PERFORMANCE

Dysregulated Fatty Acid Metabolism Results in Mating Fitness Decay

The behavioral choice assay indicated fat metabolism disruption does not alter male reproductive drive between days 1-2; however, we did not know how copulation ability or performance was affected. Excessive fuel, provided by *fat-6(lf); fat-7(lf)*-induced over-catabolism of fat, could enhance copulation performance. Alternatively, dysregulated fat oxidation, coupled with reduced lipid storage could disrupt neural muscular processes tuned to glycolytic-mediated fuel. We used a potency assay to determine if the *fat-6(lf);fat-7(lf)* mutations disrupted copulation performance. A single day 1 to day 5 male is paired with a moving *pha-1(lf)* hermaphrodite, whose self-progeny normally die at room temperatures. After a week of co-incubation, if the hermaphrodite produced at least one viable cross-progeny at room temperature, then the male is scored as potent. Surprisingly during day 1- 5 of adulthood, the kinetics of *fat-6(lf);fat-7(lf)* males mating potency is similar to wild type males; although day 2 mutant males were slightly more potent than wild type (Fig. 27).

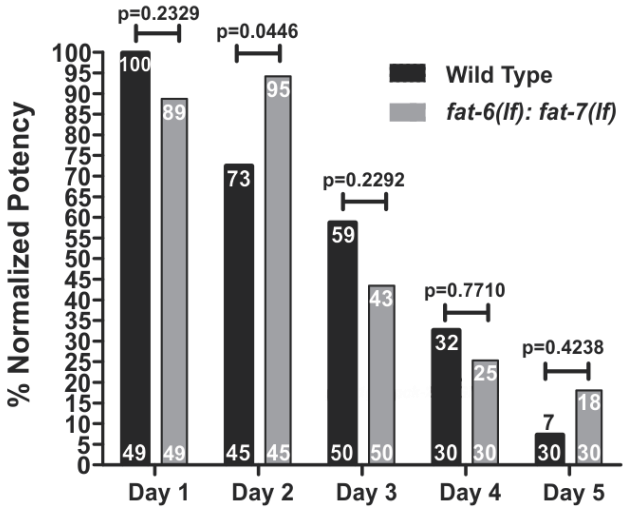

Figure 27 Mating performance of *fat-6(lf);fat-7(lf)* mutant males.
The mating potency of wild type and *fat-6(lf);fat-7(lf)* males. The percentage of successful mating's listed at the top of the bars. P values were determined using Fisher's exact test.

The wild type-like decay profile of *fat-6(lf);fat-7(lf)* mating potency is different from other previously studied mutants. For example, metabolic mutants of *sir-2.1(lf),* a NAD-dependent deacetylase metabolic gene regulator, and *pck-2(lf),* which encodes the gluco-/glyceroneogenesis enzyme phosphoenolpyruvate carboxykinase, display premature decline in mating performance (Guo and García 2014, Goncalves, Wan et al. 2020). Since copulation potency was not changed, we asked if the *fat-6(lf);fat-7(lf)* mutations affect mating fitness, which can be assessed by both the ability to out-compete other males for mates and to impregnate multiple mates. Mating fitness was first examined by competing a single wild type and *fat-6(lf);fat-7(lf)* male on a 5 cm bacterial lawn, containing a single moving *fog-2* female. The first male to impregnate the female within 3 hours was deemed successful. To validate paternity, the wild-type males (and

the cross-progeny) contained the PCK-2::YFP marker (Goncalves, Wan et al. 2020). In the control experiment, the YFP marker did not interfere with copulation (Fig. 28). When we addressed the fitness of day 1 and day 3 *fat-6(lf);fat-7(lf)* males, we found that for both days, 75-85% of *fat-6(lf);fat-7(lf)* mutants lost to wild-type males (Fig. 28) indicating they were competitively less fit.

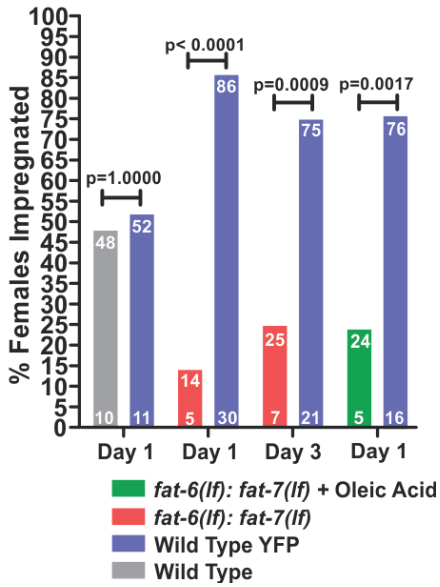

Figure 28 Mating fitness of *fat-6(lf);fat-7(lf)* mutant males.
The mating fitness of competing wild type and *fat-6(lf);fat-7(lf)* males. Wild type males carrying a fluorescent protein were tested against wild type males lacking a fluorescent protein. Once both strains were found to be equivalent, only wild type males carrying a fluorescent protein were used in competition assays against *fat-6(lf);fat-7(lf)* males. Numbers of animals assayed are listed at the bottom. P values were determined using Fisher's exact test.

One complication with the *fat-6(lf);fat-7(lf)* mutants is their slowed development, by 24 hrs, compared to wild type; the limited production of unsaturated fat likely delays

growth and alters cell lipid membrane composition. To address the possibility that failure to produce unsaturated lipids indirectly affects behavioral performance, we uncoupled unsaturated lipid storage and unregulated saturated lipid catabolism by feeding *fat-6(lf);fat-7(lf)* males oleic acid. Stearoyl-CoA desaturases, *fat-6/7*, catalyze the rate limiting step of unsaturated fatty acid synthesis producing oleic acid. The oleic acid feeding results in faster development and lipid storage, but the deficiency in fatty acid desaturases should still cause mutants to over-catabolize ingested saturated lipids (Brock, Browse et al. 2007). We observed males, fed oleic acid, were still uncompetitive against wild type for copulation (Fig. 28), indicating that despite copulation competency under non-competitive conditions, over-catabolizing saturated fat reduces mating performance.

The reduction in mating competitiveness then led us to ask if disrupting fat metabolism also alters the male's fitness to impregnate multiple mates over time. To assay the mating endurance of aging males, a single 12 hour adult (day 1) wild type, *fat-6(lf)* single mutant, *fat-7(lf)* single mutant or oleic acid-fed *fat-6(lf);fat-7(lf)* double mutant male was placed with ten day 1 virgin *fog-1* females on a 5 mm diameter bacterial lawn. Every 12 hrs, impregnated females were counted, removed, and replaced with similarly aged virgin females; the male and virgin females were moved to a fresh lawn (Goncalves, Wan et al. 2020). After quantifying 72 hours of serial mating, wild-type males mated with 4 to 18 females, with a mean of 9 females per male (Fig. 29). Furthermore, wild type males were able to serially copulate without decline up to 36 hrs of adulthood (Fig. 30). In regards to *fat-6(lf)* or *fat-7(lf)* single mutants, their mating

profiles were not substantially different from wild type (Fig. 31), confirming that the fatty acid desaturase genes can compensate mutually. Contrary to wild type and single mutants, oleic acid-fed double mutant males significantly mated into fewer females after 24 hrs (Fig. 29). The double mutant's ability to continually mate decreases after 36 hours (Fig. 30). Also, on day 1-2 of adulthood, double mutants impregnate fewer females than wild type (Fig. 30). The period of time between 36 and 48 hrs is noteworthy, as it coincides with the *fat-6* RNA increases seen in wild type males. These observations suggest that *fat-6* expression in one or more tissues maintains serial mating robustness.

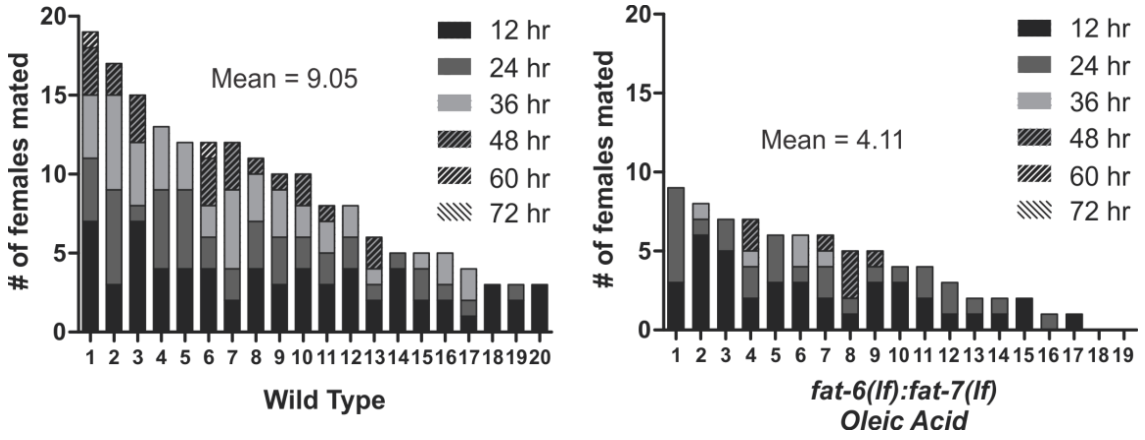

Figure 29 Mating endurance of *fat-6(lf);fat-7(lf)* mutant males.
The serial mating assay of wild type and L1-Day 1 Oleic acid supplemented *fat-6(lf);fat-7(lf)* males. The number of females impregnated is seen from 12 hrs, bottom black rectangle, to 72 hrs in rectangular subdivisions. Each column of rectangles represents a single male across 72 hours. Males are organized, from left to right, by the total sum of females impregnated.

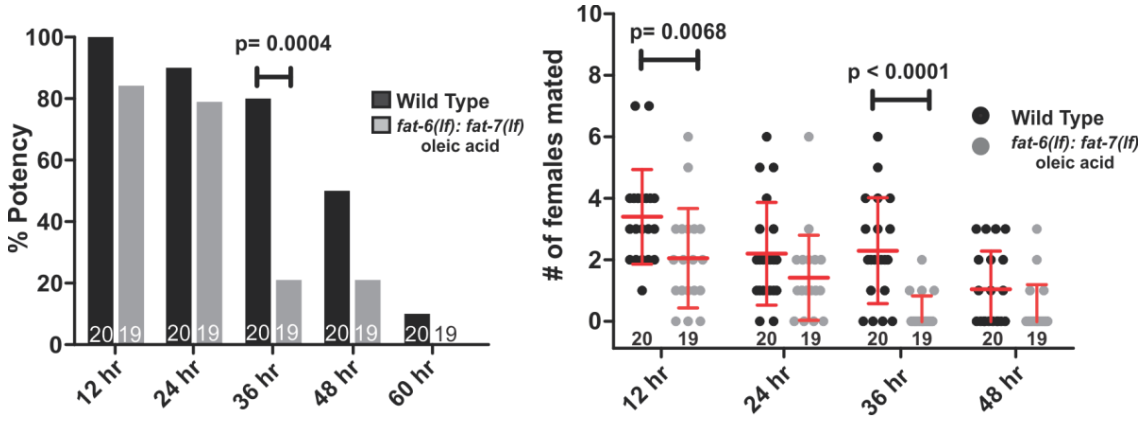

Figure 30 Day 2 *fat-6* prolongs the mating performance of wild type males.
The serial mating assay of wild type and L1-Day 1 Oleic acid supplemented *fat-6(lf);fat-7(lf)* males was analyzed. P values were determined using Fisher's exact test.

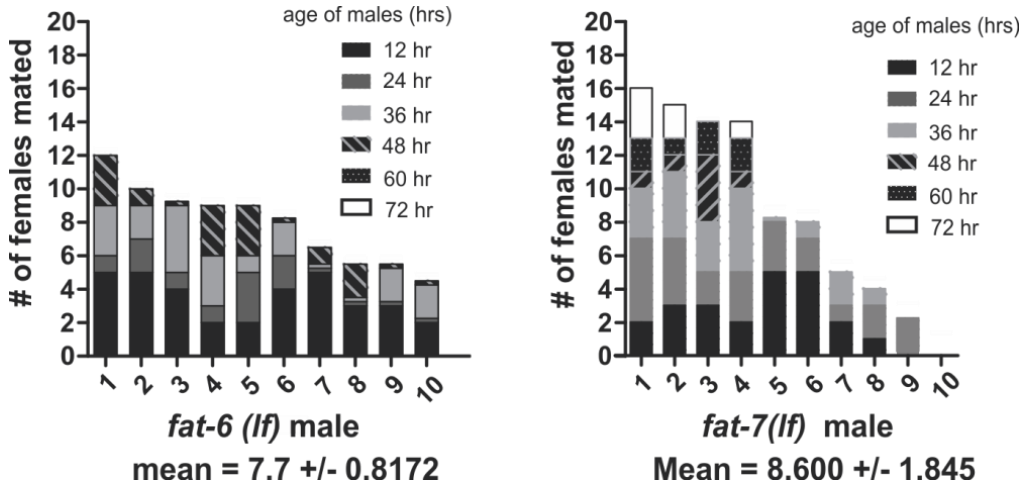

Figure 31 Mating fitness of *fat-6(lf)* and *fat-7(lf)* males.
Serial mating assays were conducted with *fat-6(lf)* and *fat-7(lf)* males. The number of females impregnated is seen from 12 hrs, bottom black rectangle, to 72 hrs in rectangular subdivisions. Each column of rectangles represents a single male across 72 hours. Males are organized, from left to right, by the total sum of females impregnated.

Epidermal Rescue Maintains Mating Endurance of Aging Wild Type Males

To address where *fat-6* functions for copulation, we drove the expression of FAT-6::YFP in *fat-6(lf);fat-7(lf)* males' intestine (using the *gtl-1* promoter) and/or epidermis (using the *dpy-7* promoter)(Johnstone and Barry 1996, Teramoto, Lambie et al. 2005). We then asked if the transgenic *fat-6* expression increases the number of serial impregnations after 72 hrs of mating. Intestinal FAT-6::YFP expression rescued intestinal neutral lipid storage (Figure 32), but did not improve the total number of impregnations (Fig. 33B and 34). We also address whether overexpressing intestinal *fat-6* disrupts wild type behavior. We found no significant alteration in mating potency on day 2 of adulthood (Fig. 35). Surprisingly, epidermal FAT-6::YFP expression in *fat-6(lf);fat-7(lf)* males did increase the number of females that males serially mated into (Fig. 33C and 34). Expression of FAT-6::YFP in both intestine and epidermis also improved the *fat-6(lf);fat-7(lf)*males' mating endurance, but not substantially better than just epidermal expression (Fig. 33D and 34). Since wild type adult FAT-6 enzyme accumulation in the epidermis peaks at day 1, either low enzyme levels and/or persistence of its products must be vital to sustain reproductive fitness through adulthood.

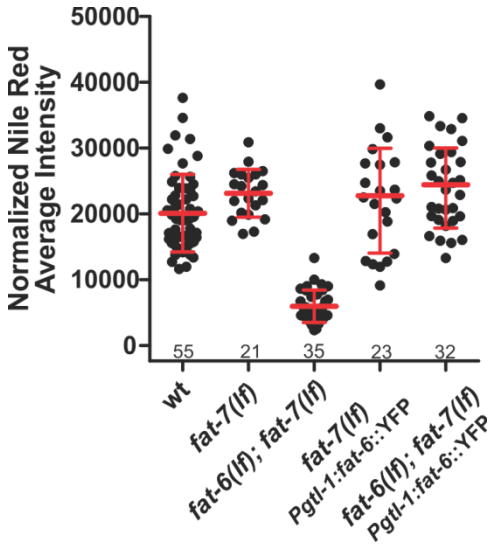

Figure 32 Intestinal rescue of *fat-6(lf);fat-7(lf)* lipid storage.
Nile Red staining of day 1 adults with intestinal FAT-6::YFP in *fat-7(lf)* and *fat-7(lf);fat-6(lf)* males. Numbers of males assayed for each strain are listed below data. Bars and whiskers represent mean and standard deviation. P values were determined using unpaired t-test.

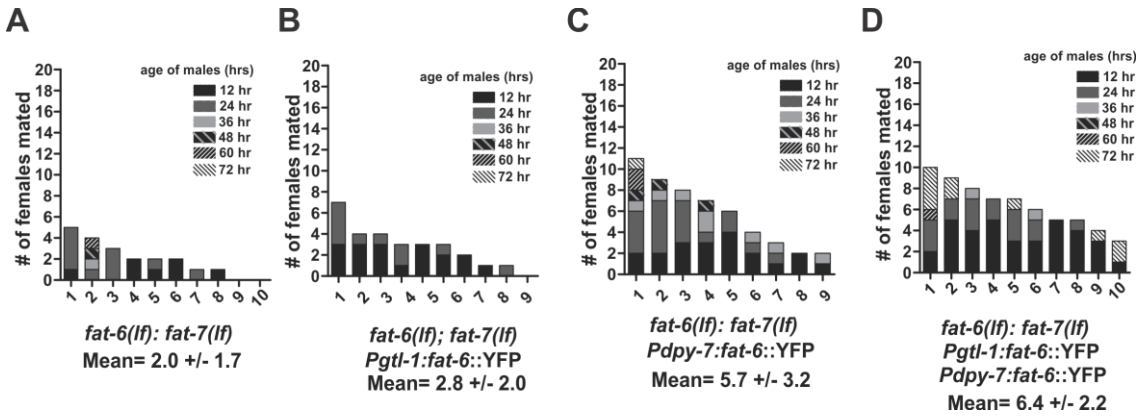

Figure 33 Hypodermal and Intestinal rescue of *fat-6(lf);fat-7(lf)* mating fitness.
The serial mating assay of wild type and tissue specific rescued *fat-6(lf);fat-7(lf)* males. The number of females impregnated is seen from 12 hrs, bottom black rectangle, to 72 hrs in rectangular subdivisions. Each column of rectangles represents a single male across 72 hours. Males are organized, from left to right, by the total sum of females impregnated. A total of 9-10 males were analyzed.

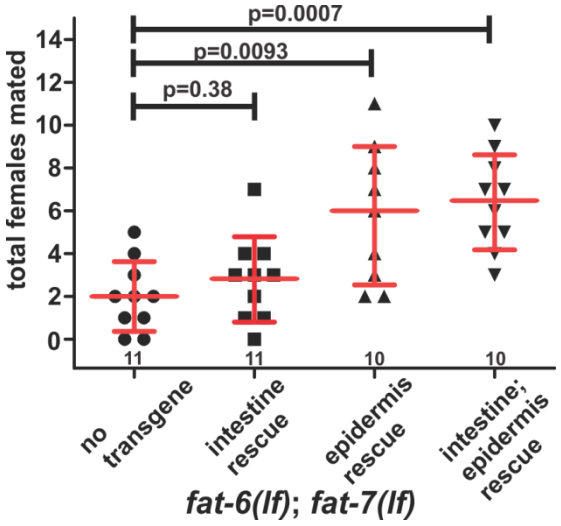

Figure 34 Tissue specific rescue of 72 hour mating fitness of *fat-6(lf);fat-7(lf)*males. The quantification of mating endurance across all tissue rescues. The total number of females mated per male was quantified. Each data point represents a single male and all its mating's across 72 hours. Mutant and rescue monikers refer to *fat-6(lf);fat-7(lf)* males. P values were determined using Man Whitney t-test.

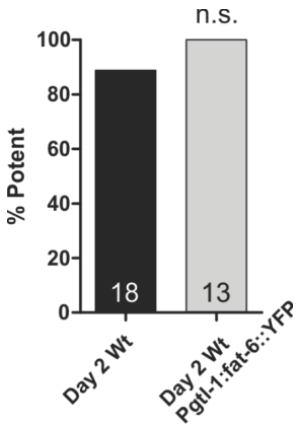

Figure 35 Overexpression of intestinal *fat-6* does not alter mating performance. The mating potency of wild type males with and without intestinal *fat-6* overexpression is shown. Numbers of animals assayed are listed at the bottom. P values were determined using Fisher's exact test.

Finally, we asked how reducing fatty acid desaturases affects motor steps of copulation. We digitally recorded the mating attempts of day 1 wild type and *fat-6(lf);fat-7(lf)* males with locomotion defects, easy to penetrate hermaphrodites. Within a 10-minute observation window, the most obvious motor defect of the double mutants is their ability to insert their spicules into their mates. Wild type males were able to insert immediately into hermaphrodites within one or two attempts of contacting the vulva (Fig. 36A). In contrast, double mutant males can recognize their mate's vulva and initiate repetitive high frequency spicule thrusts, but have difficulty in maintaining their position over the vulval slit. The males would slip off the vulva and then reattempt to insert their spicules between 2 to >15 times before they would insert and ejaculate (Fig. 36A). This defect increased the time males spent attempting to breach the vulva (Fig. 36B). Since spicule intromission requires the male to stabilize its position over the vulva while contracting its protractor muscles, the double mutant's deficit could be due to a defect in cholinergic motor control of muscles involved in both body posture and spicule motion (Gao and Zhen 2011, Kawano, Po et al. 2011, Liu, Ge et al. 2011, Wen, Po et al. 2012, Gao, Guan et al. 2018).

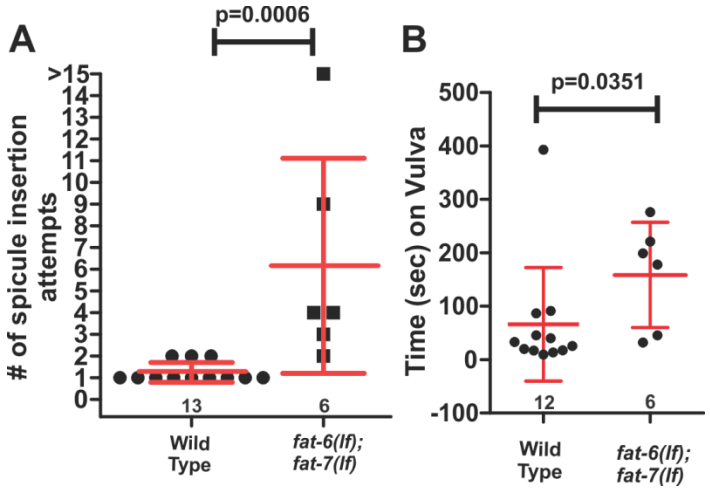

Figure 36 Mating disrupted due to low motivation and mail tail positioning defect. Males were video recorded during the act of mating for day 1 wild type and *fat-6(lf);fat-7(lf)* males. Recordings were stopped after 10 min and the number of males having mated was counted. Recordings were analyzed by measuring the time spent on various steps of mating behavior. P values were determined using unpaired t-test (spicule attempts) and Man Whitney t-test (Time on Vulva).

Chapter IV Summary

The increased transcription of *fat-6* and anterior intestinal FAT-6 protein levels was found to maintain mating fitness during early adulthood. During early adulthood epidermal *fat-6* is sufficient to maintain mating fitness. We suggest, in aging wild type males, a multi-tissue coordinated mobilization of internally stored fat maintains mating fitness. In males lacking Stearoyl CoA desaturases we expect defective spicule intromission is responsible for premature decline in mating fitness. Specifically *fat-6(lf);fat-7(lf)* mutants cannot stabilize male tail position over the vulva hinting at a lack of cholinergic motor control of muscles involved in both body posture and spicule motion.

CHAPTER V

FAT SYNTHESIS AND NEURON FUNCTION

Dysregulated Fat Synthesis Disrupts Neuronal Calcium

The *fat-6(lf);fat-7(lf)* male's difficulty to insert their spicules during mating prompted us to first determine if cholinergic stimulation of spicule protractor muscle contraction was defective. We introduced wild type and double mutant males to baths containing increasing concentrations of the non-specific cholinergic agonist arecoline to ask if receptors on the spicule neurons and protractor muscles can promote spicule protraction (Correa, LeBoeuf et al. 2012). We found the double mutant's response to exogenously applied arecoline was similar to wild-type, indicating that cholinergic signal transduction and muscle contraction are functional (Fig. 37A).

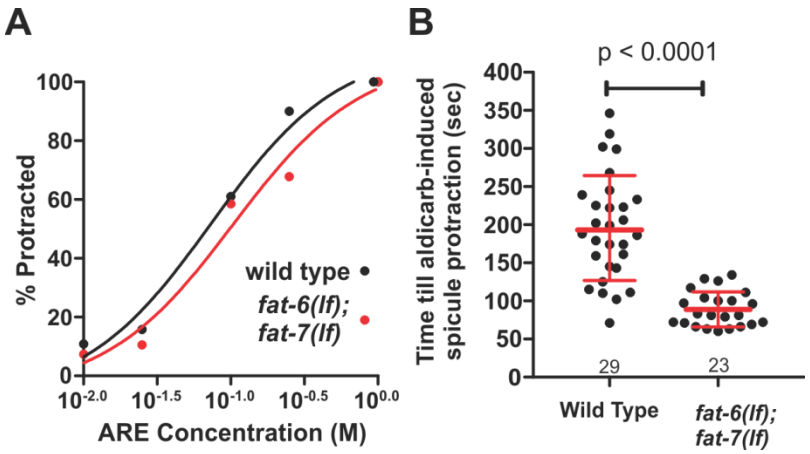

Figure 37 Neuron specific deficits in *fat-6(lf);fat-7(lf)* males.
Wild type and *fat-6(lf);fat-7(lf)* day 1 males were incubated in increasing arecoline and aldicarb concentration. We quantified the protraction of the spicule as a proxy for muscle contraction. Bars and whiskers represent mean and standard deviation. P values were determined using Mann Whitney t-test.

We then used the drug aldicarb to ask if cholinergic secretion from the SPC, PCB or PCC copulation neurons was altered in the double mutant. Aldicarb inhibits acetylcholine esterase, an enzyme responsible for degrading acetylcholine at the synaptic cleft (Rand and Russell 1985, Nguyen, Alfonso et al. 1995, Miller, Alfonso et al. 1996). Under inhibition, spontaneous release from cholinergic neurons leads to acetylcholine buildup and can result in sex muscle contraction and spicule protraction. If cholinergic transmission is attenuated in the double mutant, then longer exposure or higher concentration of the drug might be required to induce muscle contraction. If cholinergic transmission is hyperactive, then less exposure or less concentration of the drug would be needed. We placed wild type and mutant males on agar pads infused with 5, 10 or 15mM aldicarb. On 5 and 10mM aldicarb, neither male responded after 1 minute exposure. However, at 15mM aldicarb, *fat-6(lf);fat-7(lf)* males responded faster than the

wild type (Fig. 37B). This indicated that a deficiency in fatty acid desaturases leads to increased spontaneous cholinergic release in the spicule protraction circuitry. However, the increased synaptic transmission does not account for why the mutants do not stabilize their posture over the vulva during spicule insertion attempts.

Given the cholinergic spicule neurons may be spontaneously releasing more acetylcholine, we asked if cholinergic motor neurons in the male posterior ventral cord might also have heightened activity. We used the promoter of a vesicular acetylcholine transporter *unc-17* to drive the expression of the G-CaMP6 fluorescent calcium sensor in these neurons (Fig. 38) (Alfonso, Grundahl et al. 1993, Alfonso, Grundahl et al. 1994, Alfonso, Grundahl et al. 1994, Chen, Wardill et al. 2013). Calcium plays many roles in neuromuscular circuitry including neurotransmitter release, postsynaptic control of gene expression, metabolic enzyme activation, and activation of muscle contraction. Since recording these neurons' activity during mutant's copulation is challenging, we restrained wild type and *fat-6(lf);fat-7(lf)* males under a coverslip using with 10% noble agar and Polybead polystyrene 0.1 um microspheres (Kim, Sun et al. 2013). As the males struggle under the coverslip, we were able to record changes in the neuronal calcium transients. From the digital recordings, ROI's were drawn over neurons and calcium responses were measured for ~40 seconds (Fig. 38 and 39). The double mutant showed higher calcium transients in posterior cholinergic ventral cord neurons DA8, VA12, CA9, DA7, AS10 and a neuron we could not definitively identify (Fig. 38B); the other neurons, VA11, DB7, VB11, CA8 VA10, and an additional ventral cord neuron we could not identify, produced average calcium transients similar to wild type (Appendix).

Additionally, for some neurons in the double mutant, such as VA12, VA11, DA7 and VB11, the average signal duration was also shorter (Fig. 38C), suggesting faster repolarization. These observations indicate that with reduced fatty acid desaturases, enhanced lipid catabolism and/or lipid membrane deficits can exaggerate the intensity and shorten the duration of cholinergic neural activity in some cells. This defect could account for the uncoordinated behavior displayed during the male's spicule insertion attempts.

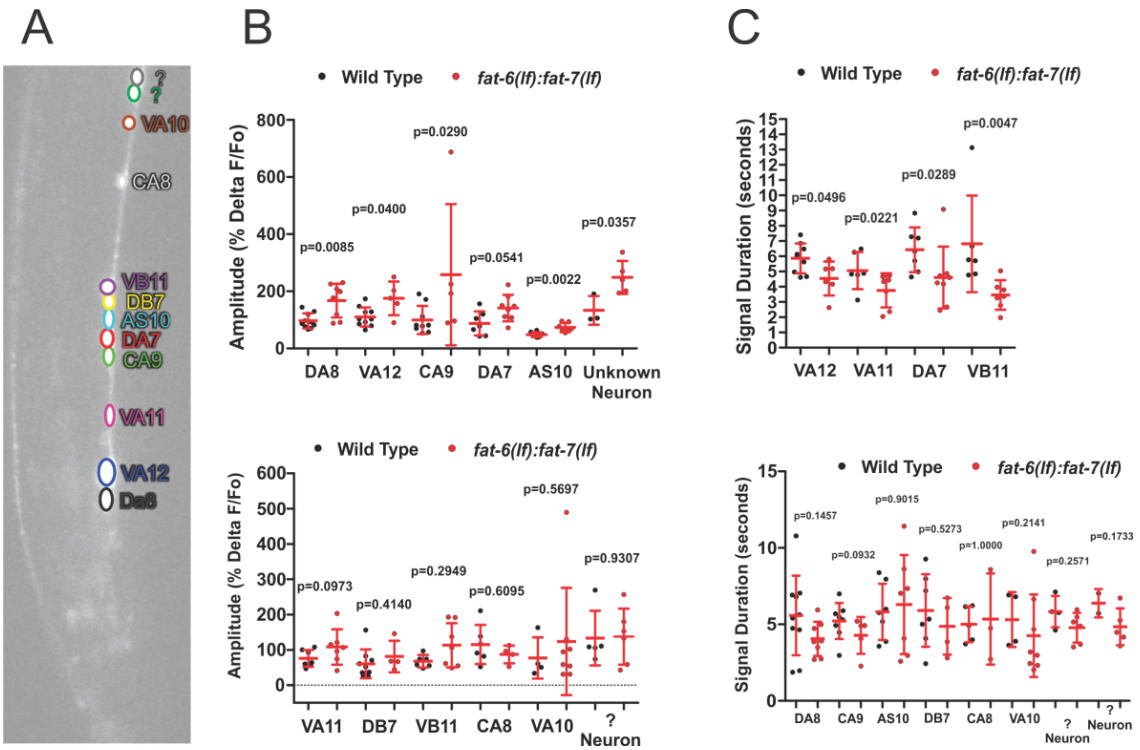

Figure 38 Quick repolarization of *fat-6(lf);fat-7(lf)* male cholinergic neurons.
(A)ROI's were drawn for 12 cholinergic neurons (10 identified in this figure) and fluorescence calcium waves were recorded across time. (B) Every peak for an individual specific neuron was quantified in every male across both wild type and *fat-6(lf);fat-7(lf)* day 1 males. Every peaks local max and local min was determined and the difference calculated. (C) For every peak the amplitude was halved and used as a threshold. We then measured the distance between both sides of a single peak where the threshold and the peaks side intercepted.

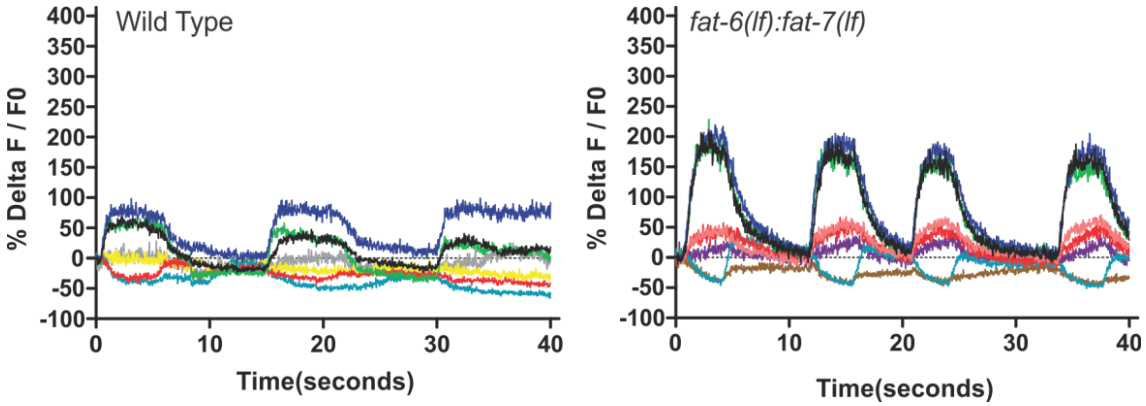

Figure 39 Characterization of cholinergic neurons in *fat-6(lf);fat-7(lf)* males. GCAMP, calcium sensor, fluorescence was video recorded in wild type and *fat-6(lf);fat-7(lf)* day 1 males mounted on 10% noble agar and Polybead polystyrene 0.1 um microspheres. ROI's were drawn for 12 cholinergic neurons and fluorescence calcium waves were plotted across time. We were able to draw matching ROI's for every neuron and in both strains.

Fatty Acid Desaturase Loss Alters UNC-103 K^+ Channel Levels

The increase in spontaneous cholinergic neurotransmitter release and altered calcium transients suggest membrane threshold and repolarization regulation are perturbed. These processes can be regulated by K+ channel activity (Wang, Saifee et al. 2001, Liu, Chen et al. 2007, Collins and Koelle 2013, Liu, Chen et al. 2014, Steciuk, Cheong et al. 2014, Alqadah, Hsieh et al. 2016). Previous research has identified ERG (*ether-ago-go-related gene*)-like/UNC-103, EAG (*ether-a-go-go*)/EGL-2, and BK (*big potassium*)/SLO-1 K^+ channels participate in regulating the excitability of the spicule protraction circuit. Defects in these channels will induce spontaneous sex muscles contraction, causing the spicules to protract out of the tail (the Protraction constitutive, Prc phenotype). However, in the absence of any one of these K^+ channels, a

compensatory upregulation of the remaining K^+ channels can ameliorate spicule protraction defects, reducing the probability of sex muscle spasms (LeBoeuf and Garcia 2012). Interestingly food-deprivation stress, which leads to catabolism of internal lipid stores, can further boost the compensatory increase in K+ channel expression (Gruninger, Gualberto et al. 2006, LeBoeuf, Gruninger et al. 2007, Gruninger, Gualberto et al. 2008, LeBoeuf, Guo et al. 2011). Thus, we asked if the male alters K+ channel expression as a consequence of *fat-6* and *fat-7* deficiency.

To address this question, we performed single worm RT-qPCR analysis of ERG-like/*unc-103*, EAG/*egl-2*, and BK/*slo-1* K^+ channels on wild type and *fat-6(lf);fat-7(lf)* males. We surveyed different K+ channel alternative splice forms using shared exon regions. We found that only *unc-103* channel expression was significantly down-regulated (Fig. 40A). This result was surprising since *fat-6(lf);fat-7(lf)* males do not display the abnormal Prc phenotype like the *unc-103(lf)* males (Fig. 40B).

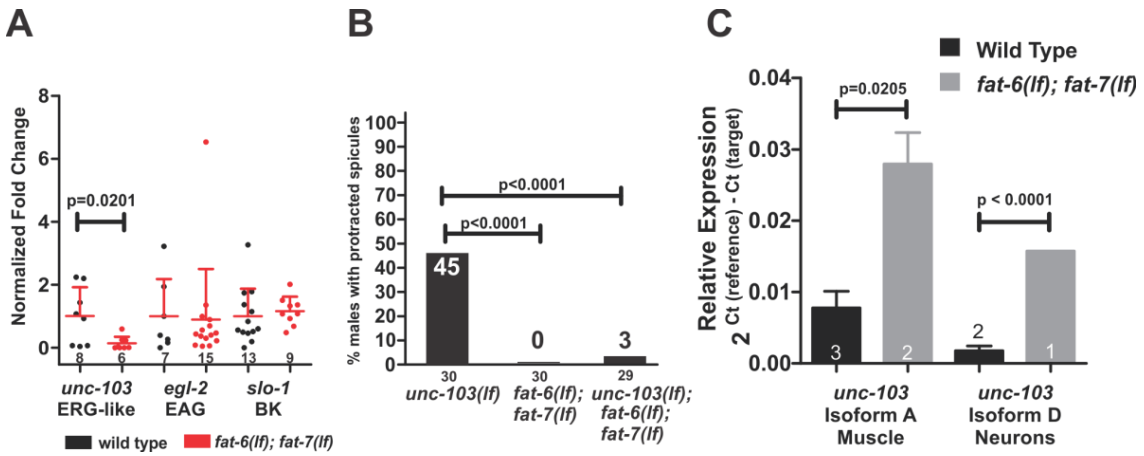

Figure 40 K+ channel expression and function in *fat-6(lf);fat-7(lf)* males.
(A) Relative mRNA expression level of K+ channel genes ERG-like/UNC-103, EAG/EGL-2, and BK/SLO-1 K+ channels in wild type and *fat-6*(lf;*fat-7(lf)* males (unpaired t-test). Each individual gene was normalized to the wild type equivalent. Numbers of animals assayed are listed at the bottom. Bars and whiskers represent mean and standard deviation. (B) Spicule protraction of *unc-103(lf)*, *fat-6(lf);fat-7(lf)*, and *fat-6(lf);fat-7(lf);unc-103(lf)*. L4 males were separated and assayed under no treatment after reaching adulthood. (C) Relative mRNA expression level of isoforms A and D of ERG-like/UNC-103 K+ channels in wild type and *fat-6*(lf;*fat-7(lf)* males (unpaired t-test). Attempts were made to measure all isoforms of ERG-like/UNC-103 K+ channels but we could not reach comparable levels in mutants.

unc-103 is broadly expressed in neurons and muscles, thus we examined ten *unc-103* isoforms to determine if all or some of the tissue specific isoform were down-regulated (Reiner, Weinshenker et al. 2006). We found all but two isoforms were below detection in the *fat-6(lf);fat-7(lf)* males; surprisingly, the two isoforms detected, *unc-103*A and D isoforms, were both upregulated (Fig. 40C). Likely, these two isoforms account for most of the signal in the previous *unc-103* RT-qPCR assay (Fig. 40A). Isoform A is expressed in all body wall and sex muscles, including 4 neurons in the head. Isoform D is expressed in neurons URA, PVM, and 1 neuron in all each of the male's 9 pairs of copulatory sensory rays. The down-regulation of neuronal *unc-103*

isoforms could account for the heightened neural excitation and transmitter release, and the upregulation of the muscle-expressed isoform A could mitigate possible downstream muscle spasms from the altered neural activity.

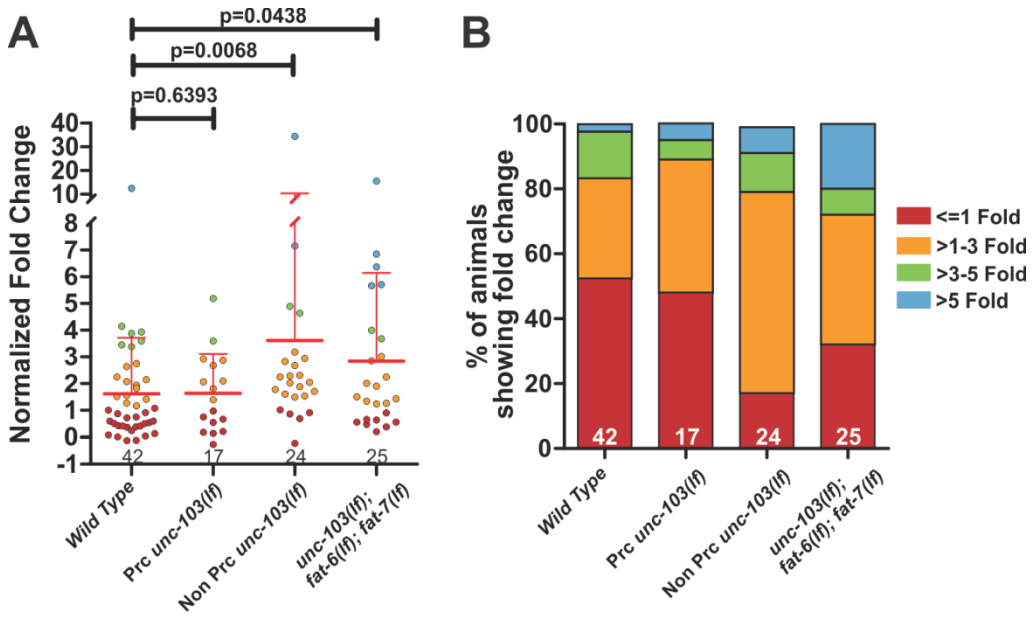

Figure 41 Increased *egl-2* in non Prc *unc-103(lf)* and *fat-6(lf);fat-7(lf); unc-103(lf)*. (A) Relative mRNA expression level of EAG/EGL-2 K+ channels in wild type, Prc *unc-103(lf)*, Non-Prc *unc-103(lf)*, and Non-Prc *fat-6(lf);fat-7(lf)* males. Data was normalized to the median of wild type data set. (B) The proportion of males showing a specific fold change was graphed based on data from (A). *fat-6(lf);fat-7(lf) egl-2* levels are biased to larger fold changes (>5 fold) versus *unc-103(lf)* (1.0-3.0). No P value was provided as this serves only as a different visual representation of data seen in (A).

To test the idea that muscle-enriched UNC-103 K+ channels can modulate muscle function in the absence of fatty acid desaturases, we created triple mutant *unc-103(lf); fat-6(lf);fat-7(lf)* males. We asked if the fatty acid desaturase mutations could increase the penetrance of the Prc phenotype. Surprisingly, *unc-103(lf); fat-6(lf);fat-7(lf)*

males were suppressed for the *unc-103(lf)*-induced Prc phenotype (Fig. 40B). This result prompted us to consider earlier work indicating transient starvation, induces lipolysis, can increase EAG/EGL-2 K+ channel expression. Since we established earlier that *fat-6(lf);fat-7(lf)* double mutants abnormally catabolize ingested lipids, we asked if the *fat* mutations interacted with *unc-103(lf)* to alter EAG/*egl-2* expression. A quadruple *unc-103(lf);egl-2(lf);fat-6(lf);fat-7(lf)* mutant was too sick to generate and maintain, so we performed single worm RT-qPCR analysis of *egl-2* on *unc-103(lf);fat-6(lf);fat-7(lf)* males; 0/25 showed the Prc phenotype (Fig. 41A). We compared their expression with wild type and *unc-103(lf)* single mutant animals, where we separated males displaying a Prc phenotype (17/41 males) or a non-Prc phenotype (24/41 males) (Fig. 41A). We found that for Prc-displaying *unc-103(lf)* mutant males, *egl-2* expression levels were not significantly different from wild-type males (Fig. 41A). However, for both the sub-population of non-Prc *unc-103(lf)* single mutant males and the *unc-103(lf);fat-6(lf);fat-7(lf)* triple mutant, *egl-2* expression was significantly elevated (Fig. 41A). We analyzed the distribution of *egl-2* expression and a significant proportion of triple mutant males showed greater 5-fold increases in *egl-2*, which differed from the response of other assayed males (Fig. 41B). Altogether, we suggest the levels of unsaturated lipid synthesis and lipid catabolism can alter K^+ channel expression, resulting in differential excitation activity used for spicule insertion behavior. Furthermore given that we know spicule muscle spasms can be reduced by food deprivation through *egl-2* expression, we suggest the metabolic state of *fat-6(lf);fat-7(lf)* males might share signaling commonalities occurring during food deprivation.

Chapter V Summary

The loss of stearoyl CoA desaturases resulted in a premature decline in mating fitness due to deficits in body posture and spicule insertion. We addressed the functionality of the *fat-6(lf);fat-7(lf)* sex muscles responsible for spicule insertion and found wild type responses to exogenous applied arecoline, an acetylcholine receptor agonist. We also observed the neuronal activity of the cholinergic ventral cord responsible for locomotion during mating. We found *fat-6(lf);fat-7(lf)* neurons showed exaggerated responses and shortened duration. This defect could account for the uncoordinated behavior displayed during the male's spicule insertion attempts. Due to the heightened neural excitation and transmitter release we found muscle-expressed *unc-103* isoform A was upregulated to mitigate possible downstream muscle spasms from the altered neural activity. Finally, we showed disruption of lipid catabolism can sensitize males lacking functional *unc-103* by increasing *egl-2* K+ channel expression, resulting in differential excitation activity used for spicule insertion behavior.

CHAPTER VI

PEPCK EXPRESSION MAINTAINS MATING FITNESS[*]

Tissue Specific Expression of PEPCK

In an earlier study, metabolic changes in the male *C. elegans* were found to sustain copulation behavior during the first two days of adulthood (Guo, Navetta et al. 2012, Guo and García 2014). RT-qPCR analysis of male metabolic gene expression was conducted on day 1 and day 2 of adulthood (Guo and García 2014). Of the genes queried, the PEPCK genes *pck-1/2*, involved in gluco-glyceroneogenesis, showed a ~2 fold increase in expression. It was hypothesized that between days 1-2, adult males increased their gluco-glyceroneogenesis as a compensatory response to continued mitochondrial oxidative metabolism. Previous research, using an antibody, had shown that *pck-1* was expressed in hermaphrodite muscle, intestine and pharynx (Ballard and Hanson 1969, Yuan, Kadiyala et al. 2012, Yuan, Hakimi et al. 2016). But given the similarity, 71% in amino acid identity, between *pck-1* and *pck-2* and potential antibody

[*] Figures reprinted from "Succinate Dehydrogenase-Regulated Phosphoenolpyruvate Carboxykinase Sustains Copulation Fitness in Aging C. elegans Males." by Goncalves J, Wan Y, Guo X, Rha K, LeBoeuf B, Zhang L, Estler K, Garcia LR., 2020. *iScience*, 23, Copyright 2020 by Elsevier. Material is from an open access article distributed under the terms of the Creative Commons CC-BY license. Go to https://www.sciencedirect.com/science/article/pii/S2589004220301747 for published material. Go to https://creativecommons.org/licenses/by/4.0/legalcode for full license details.

cross reactivity we wanted to observe in further detail where PEPCK was expressed in hermaphrodites and males (Fig. 42).

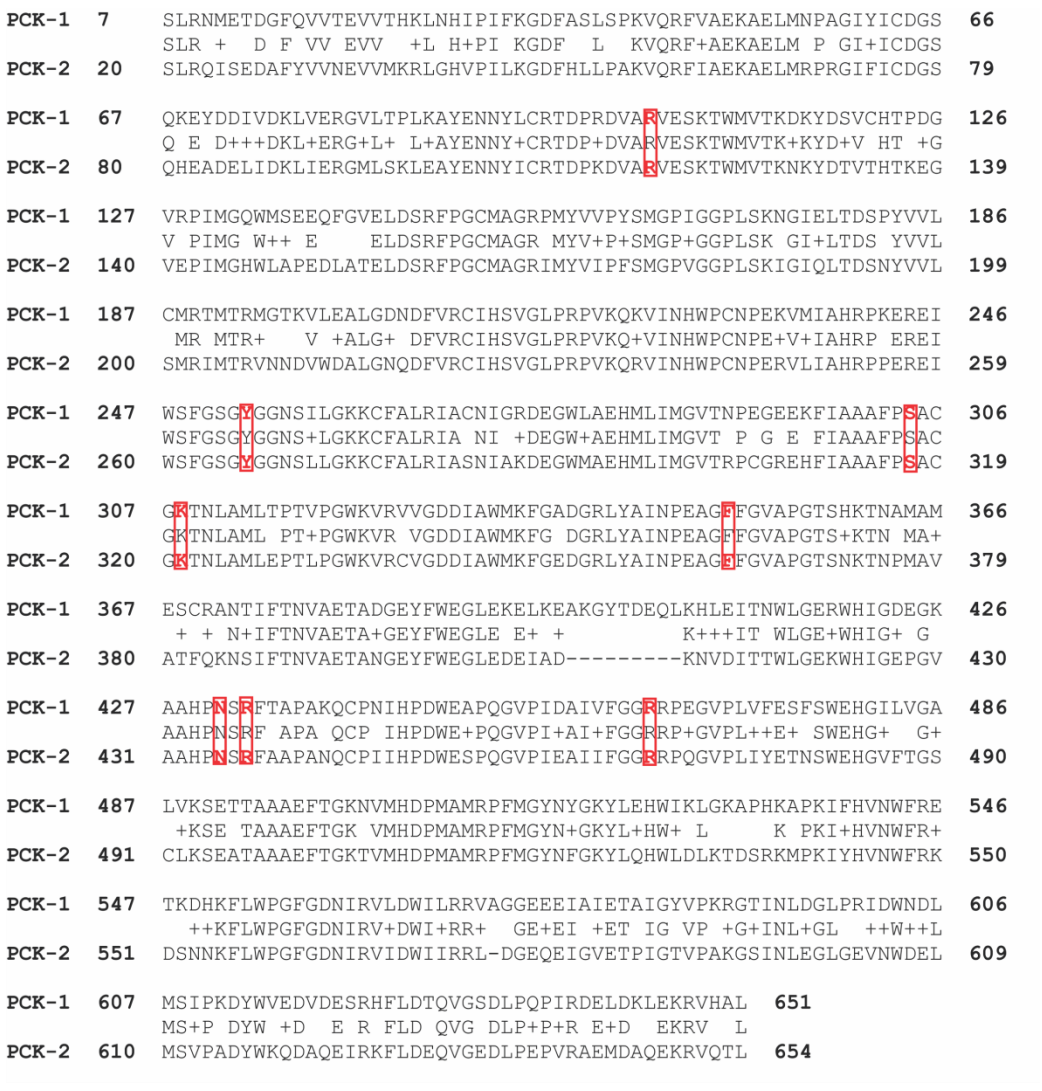

Figure 42 PCK-1 and PCK-2 Sequence Alignment.
The alignment of amino acid sequences for *pck-1* and *pck-2* show ~70% similarity. Red higlights represent regions involved in oxaloacetate and GTP binding and phosphoenolpyruvate formation.

We observed *pck-1* gene expression by YFP and Timer 2.8-kb promoter fusions. Differing from previous research, we found the expression pattern of males was limited to neurons and post synaptic muscles (Fig. 43A). A *pck-1* promoter driving the expression of cDNA confirmed cytoplasmic localization. To observe the expression of *pck-2* we used the CRISPR/Cas9 technique to replace the stop codon with YFP. We found the endogenous expression of *pck-2* overlaps with *pck-1* in the muscles but also were expressed in the intestine and epidermis (Fig. 43B and C).

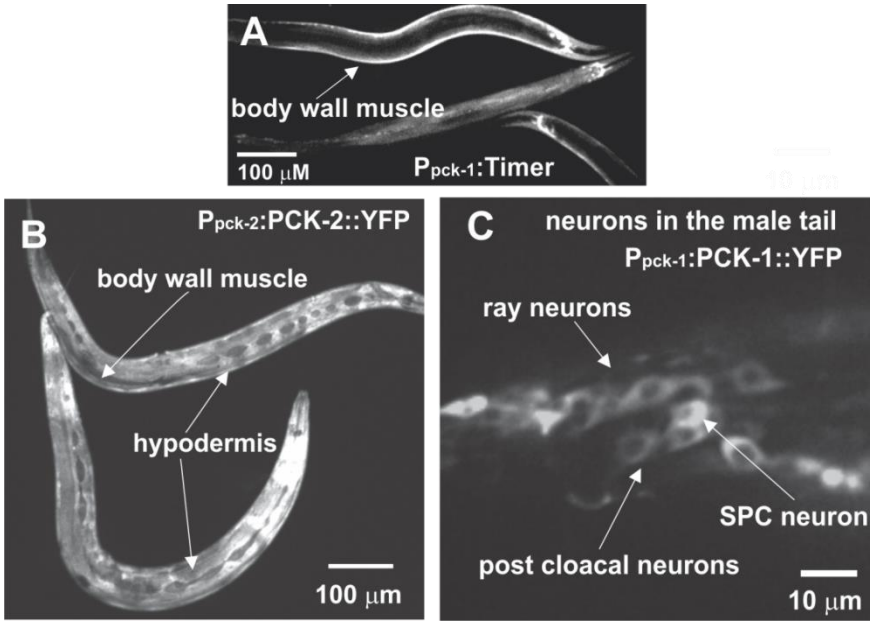

Figure 43 Expression pf *pck-1* and *pck-2* in male *C. elegans*.
(A/C) *Ppck-1*::Timer in the body wall muscle and neurons of the mail tail. (B) CRISPR/Cas9 knock-in of YFP into *pck-2* expression in the body wall muscle and epidermis.

Mating Behavior of PEPCK Mutants

The expression pattern of *pck-1/2* indicated that gluco-glyceroneogenesis disruption may alter the neuromuscular circuitry of male mating behavior between days 1-2; however, we did not know how copulation ability or performance was affected. Excessive glucose, provided by PEPCK could enhance copulation performance or damage neural muscular processes. We used a potency assay to determine if the *pck-1(lf), pck-2(lf),* and *pck-1(lf);pck-2(lf)* mutations disrupted copulation performance. A single day 1 to day 2 male is paired with a moving *pha-1(lf)* hermaphrodite, whose self-progeny normally die at room temperatures. After a week of co-incubation, if the hermaphrodite produced at least one viable cross-progeny at room temperature, then the male is scored as potent. During day 1 of adulthood, the kinetics of *pck-1(lf)* and *pck-2(lf)* males mating potency was similar to wild type males; although day 2 *pck-2(lf)* males were less potent than wild type (Fig. 44). The double mutant *pck-1(lf);pck-2(lf)* mating kinetics declined on day 1 of adulthood and continued to decline with age (Fig. 44). Altogether the PEPCK genes can compensate for each other's loss during day 1 of adulthood. On day 2 neuromuscular PEPCK could not compensate for the loss of *pck-2* suggesting a tissue specific need for gluco-glyceroneogenesis.

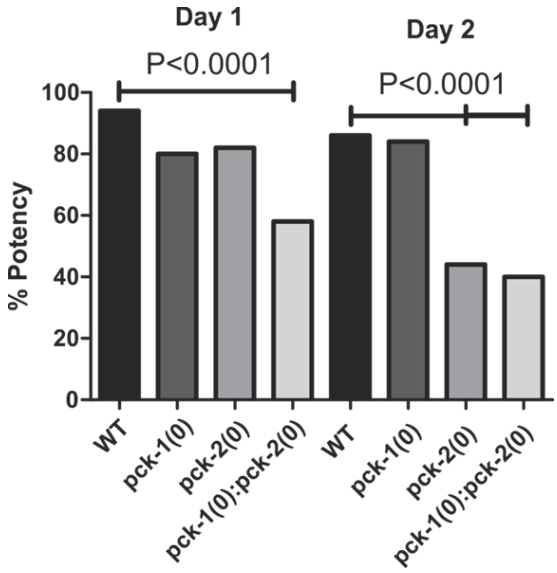

Figure 44 *pck-1(lf);pck-2(lf)* Decline in Mating Performance.
The mating potency of wild type, *pck-1(lf), pck-2(lf),* and *pck-1(lf);pck-2(lf)*males. P values were determined using Fisher's exact test.

Casual observation of mating behavior did not inform the deficits in mating had by PEPCK mutant males. But on incubation of males with large groups of hermaphrodites *pck-2(0)* and *pck-1(lf); pck-2(0)* males displayed muscle spasms similar to aging wild type male's defective in regulating membrane excitability. Previous research has identified EAG (*ether-a-go-go*)/EGL-2 K^+ channels participate in regulating the excitability of the spicule protraction circuit. Defects in this channel will result in mating potency decline with age. Interestingly food-deprivation stress, which leads to catabolism of internal sugar and lipid stores, can result in a compensatory increase in *egl-2* K+ channel expression (Gruninger, Gualberto et al. 2006, LeBoeuf, Gruninger et al. 2007, Gruninger, Gualberto et al. 2008, LeBoeuf, Guo et al. 2011).

To address if neuromuscular K+ channel dysregulation is the cause of PEPCK mutant copulation defects we used a CRISPR/Cas9 YFP knock-in of *egl-2* K+ channel to observe expression in the male's protractor muscles and SPC, SPD, and SPV neurons. Among the few cholinergic neurons involved in regulating intromission behavior the bilateral cholinergic SPC motor neurons are the only ones to chemically synapse to the bilateral dorsal/ventral protractor muscles physically associated with the spicules. The SPC is thought to function by releasing acetylcholine to switch from periodic to prolonged spicule protraction by; a) inducing repetitive spicule muscle contractions and b) sustaining muscle contraction upon breaching the vulva. The SPD and SPV sensory neurons have ciliated endings at the tip of the spicules that sense complete spicule insertion and consequently help regulate sperm transfer. The expression of *egl-2* was found to be significantly lower in *pck-1(lf);pck-2(lf)* mutants on day 1 of adulthood (Fig. 45). We suggest that *egl*-2 K+ channel expression decreases may be responsible for a premature in mating potency seen in day 1 *pck-1(lf);pck-2(lf)*. Altogether, day 1 PCK-1 and PCK-2 function promotes EGL-2 levels in the copulatory circuit.

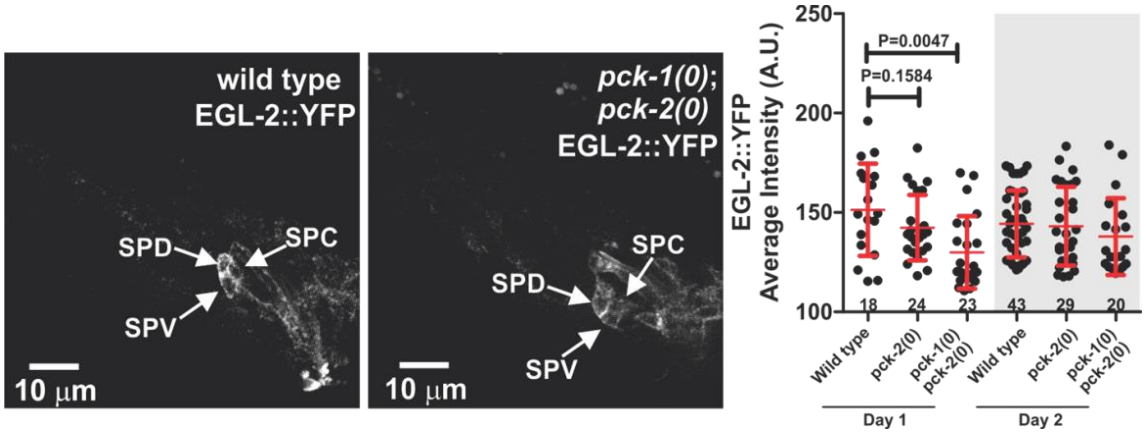

Figure 45 *egl-2* K+ channel expression in PEPCK mutant males.
CRISPR/Cas9 knock-in of YFP into *egl-2* shows expression in the sex muscles and SPC/SPD/SPV neurons. On the right we quantified the expression level of EAG/EGL-2 K+ channels in wild type and PEPCK mutant males (unpaired t-test). Numbers of animals assayed are listed at the bottom. Bars and whiskers represent mean and standard deviation.

Rescue of PEPCK Deficient Mating Behavior

To address where PEPCK functions for copulation, we drove the expression of PCK-1::YFP in *pck-1(lf);pck-2(lf)* males' neurons and muscles (using native promoter), all muscles (pan muscle *unc-103A* promoter), and all cholinergic neurons (using a acetylcholine vesicular transporter *unc-17* promoter). We then asked if the transgenic *pck-1* expression increases the mating potency of day 1 *pck-1(lf);pck-2(lf)* mating defective males. The native and cholinergic neuronal promoters PCK-1::YFP expression rescued mating potency (Fig. 46). We also drove the expression of PCK-2::YFP in *pck-1(lf);pck-2(lf)* males' epidermis (using a *dpy-7* promoter), all muscles (pan muscle *unc-103A* promoter), intestine (using a *gtl-1* promoter), and sex muscles and a few head

neurons (using *unc-103E* promoter). The epidermal and pan muscle promoters PCK-2::YFP expression rescued mating potency (Fig. 46). Altogether, *pck-1(lf)* epidermis requires PEPCK to provide metabolites to *pck-1*-deficient neurons and muscles. This suggests neurons and muscle require gluco-glyceroneogenesis on day 1 of adulthood in wild type males. Furthermore, as males age neuromuscular PEPCK function alone cannot maintain wild type mating behavior as seen in day 2 mating defective *pck-2(lf)* mutant males.

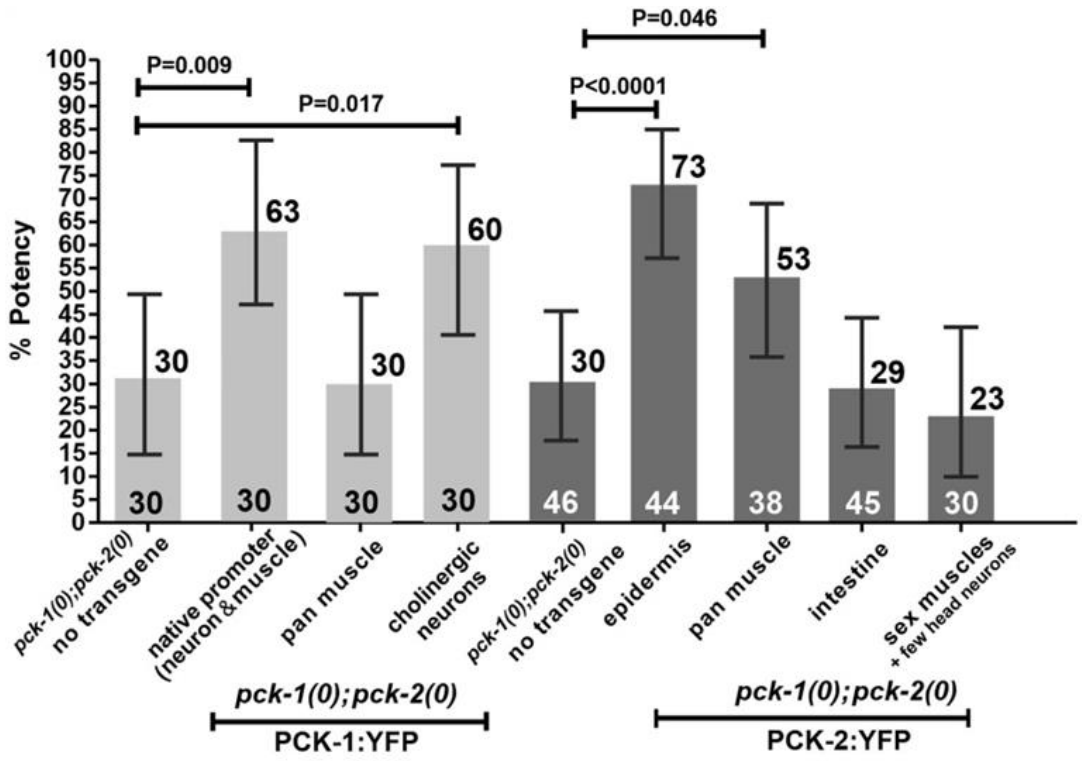

Figure 46 Neuromuscular PEPCK maintains mating potency in day 1 males.
The mating potency of wild type and tissue specific rescue of *pck-1(lf);pck-2(lf)* males. The percentage of successful mating's listed at the top of the bars. P values were determined using Fisher's exact test. Numbers of animals assayed are listed at the bottom. Bars and whiskers represent mean and standard deviation.

PEPCK enzymatically produces the glycolytic metabolite PEP from the TCA cycle metabolite OAA. We expect that if PEPCK expression increases with age that it may decrease ROS production by removing excess substrates from the TCA cycle or produce glucose and glycerol for stored sugar and triglyceride synthesis. To address how neuromuscular PEPCK functions during day 1-2, we quantified mating endurance with age. To assay the mating endurance of aging males, a single 12 hour adult (day 1) wild type, *pck-1(lf)* single mutant, *pck-2(lf)* single mutant or *pck-1(lf);pck-2(lf)*double mutant male was placed with ten day 1 virgin *fog-1* females on a 5 mm diameter bacterial lawn. Every 12 hrs, impregnated females were counted, removed, and replaced with similarly aged virgin females; the male and virgin females were moved to a fresh lawn (Goncalves, Wan et al. 2020). After quantifying 24 hours of serial mating, wild-type males mated with 0 to 6 females, with a mean of 3 females per male (Fig. 47). In regards to *pck-1(lf)* or *pck-2(lf)* single mutants, their mating profiles were not substantially different from wild type on day 1 (Fig. 47), confirming that the PEPCK genes can compensate mutually. Contrary to wild type and single mutants, PEPCK double mutant males significantly mated into fewer females during the first 24 hrs (Fig. 47). Given *pck-1(lf)* single mutants wild type mating profiles, we postulate that epidermal PEPCK can compensate for the loss of *pck-1(lf)*.

To address the function of PEPCK in the epidermis, neurons, and muscles we supplemented *pck-1(lf);pck-2(lf)* males with D-glucose. We found that D-glucose supplementation could only rescue mating endurance of day 1 *pck-1(lf);pck-2(lf)* males suggesting that neurons and muscles are fed glycolytic products from the epidermis. The

period of time between 24 and 48 hrs is noteworthy, as it coincides with the PEPCK RNA increases seen in wild type males. These observations suggest that a metabolic shift, during day 1-2, from glycolysis to potentially glyceroneogenesis and triglyceride synthesis maintains mating performance and fitness.

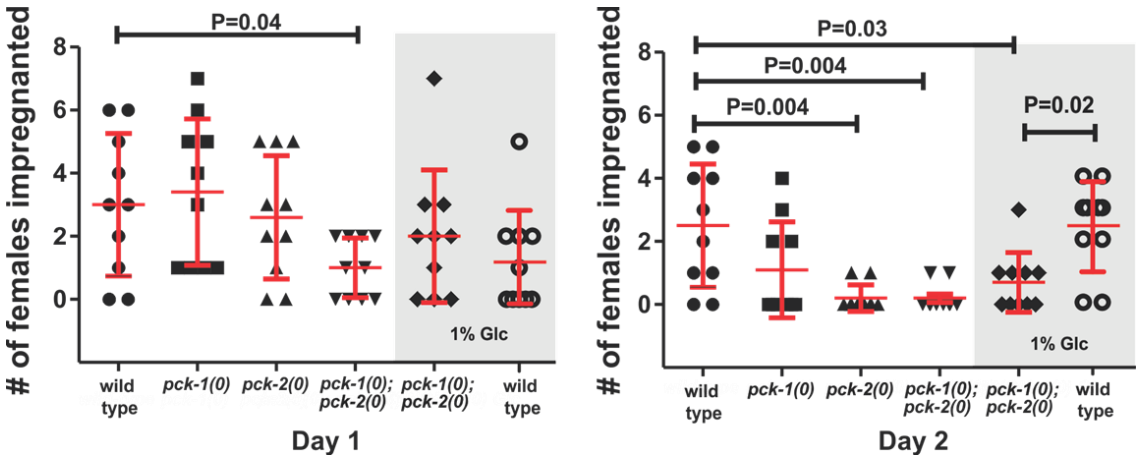

Figure 47 PEPCK derived glucose prolongs mating fitness of wild type males. The serial mating assay of wild type, *pck-1(lf)*, *pck-2(lf)*, *pck-1(lf);pck-2(lf)* males was analyzed. P values were determined using Fisher's exact test.

PEPCK Bidirectional Regulation

pck-1(lf) mutant males were found to have wild type mating performance presumably due to functional epidermal *pck-2* providing glycolytic metabolites to *pck-1*-deficient neurons and muscles. To address how PEPCK genes compensate for each other's loss we observed *pck-2* and *pck-1* expression in *pck-1(lf)* and *pck-2(lf)* mutants respectively. We used CRISPR/Cas9 induced YFP knock-in of *pck-2* and Timer 2.8-kb

pck-1 promoter fusion to quantify expression changes across adulthood. We found that PCK-2 levels decrease to better match the levels in *pck-1*-lacking tissues (Fig. 48). We suggest the metabolism of *pck-1*-deficient neurons and muscles has become overly dependent on mitochondrial respiration resulting in neighboring tissues downregulating gluco-glyceroneogenesis.

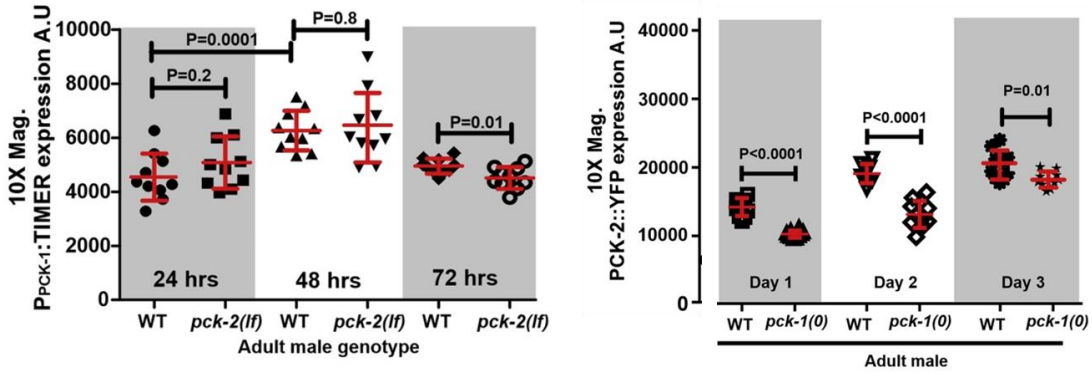

Figure 48 PEPCK expression in *pck-1(lf)* and *pck-2(lf)* aging males.
Expression was quantified by a series of rectangular ROI's drawn over the intestine (unpaired t-test). Bars and whiskers represent mean and standard deviation.

Chapter VI Summary

Males lacking functional PEPCK, *pck-1(lf);pck-2(lf),* were found to prematurely decline in mating performance on day 1 of adulthood. More so, *pck-1(lf)* mutant males were found to have wild type mating performance presumably due to the remaining PEPCK, *pck-2*. We found that epidermal *pck-2* provides glycolytic metabolites to *pck-1*-deficient neurons and muscles. Interestingly, we found *pck-1*-deficient neurons and muscles adjust neighboring tissues PEPCK levels to match disrupted gluco-glyceroneogenesis metabolism.

CHAPTER VII

SDHA-1-REGULATION OF PEPCK IN AGING MALES [*]

Succinate Dehydrogenase Disruption Increases PEPCK

We suggested that the metabolism of day 1 *pck-1*-deficient neurons and muscles had switched from glycolysis to mitochondrial respiration and neighboring tissues compensated by downregulating *pck*-2 dependent gluco-glyceroneogenesis. To address what metabolic alterations would result in PEPCK increases we performed an ethyl methanesulfonate (EMS) mutagenesis screen on PCK-1::YFP animals. We found a missense mutation in succinate dehydrogenase subunit A, encoded by *sdha-1*, increased PCK-1::YFP (Fig. 49). SDHA-1 is a part of the multi-subunit mitochondrial respiratory Complex II. Under aerobic conditions it catalyzes the conversion of succinate to fumarate in the TCA cycle and contributes to the proton motive force through complex II (Fig. 49). We suggest that disrupted complex II requires PEPCK to shunt metabolites from the TCA cycle and the ETC.

---

[*] Figures reprinted from "Succinate Dehydrogenase-Regulated Phosphoenolpyruvate Carboxykinase Sustains Copulation Fitness in Aging C. elegans Males." by Goncalves J, Wan Y, Guo X, Rha K, LeBoeuf B, Zhang L, Estler K, Garcia LR., 2020. *iScience*, 23, Copyright 2020 by Elsevier. Material is from an open access article distributed under the terms of the Creative Commons CC-BY license. Go to https://www.sciencedirect.com/science/article/pii/S2589004220301747 for published material. Go to https://creativecommons.org/licenses/by/4.0/legalcode for full license details.

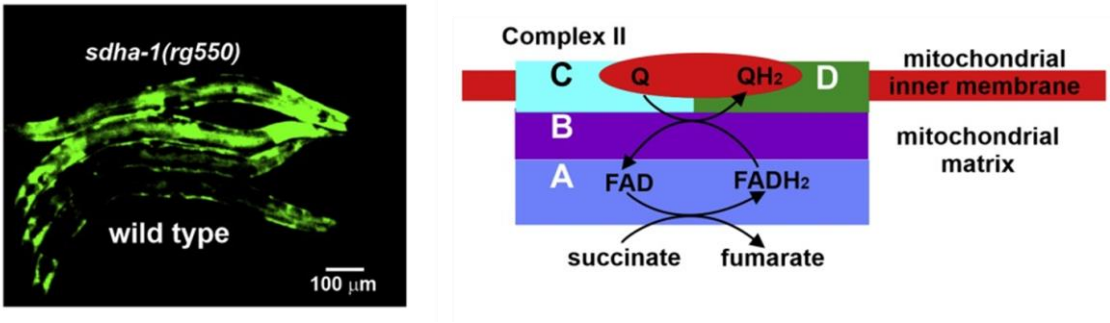

Figure 49 A Mutation in SDHA-1 Increases PEPCK.
An EMS mutagenesis screen on PCK-2::YFP animals was performed and a missense mutation in *sdha-1* was found. Also shown is a depiction of *sdha-1* function in both the TCA cycle and Complex II of the ETC.

To address the metabolism of *sdha-1(lf)* males we performed RT-qPCR analysis on three biological replicates, each replicate containing pooled transcripts of ~500 males. Because PCK-1::YFP increased in *sdha-1(lf)* we expected that the transcripts of *pck-2* and the remaining PEPCK gene, *pck-1*, should be upregulated to shunt metabolites away from the TCA cycle in *sdha-1(lf)* mutants. We might also expect expression changes in other genes involved in shunting metabolites away from the TCA cycle such as *icl-1*(isocitrate lyase) and *pyc-1*(pyruvate carboxylase). *icl-1* enzyme produces succinate and malate from isocitrate thereby avoiding a majority of the TCA cycle. *pyc-1* converts pyruvate to oxaloacetate thereby avoiding the entire TCA cycle. Not surprisingly, we measured significant increases in *pck-2*, *icl-1*, and *pyc-1* by ~4-64 fold (Fig. 50). Despite an increasing trend for *pck-1*, results were not significantly different. To further probe *pck-1* expression in *sdha-1(lf)* we used a Timer promoter fusion of *pck-1*. We found *sdha-1(lf)* aging males displayed increased *pck-1* promoter activity.

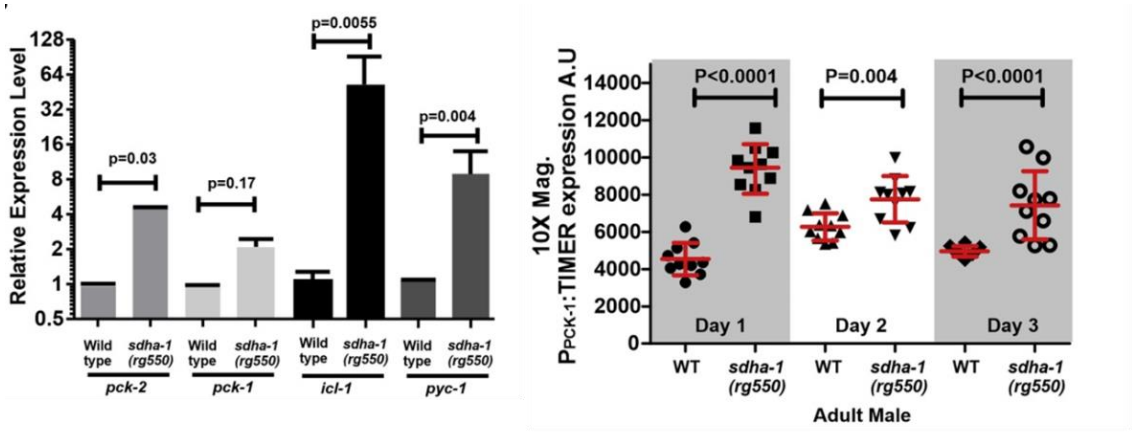

Figure 50 Metabolic Compensation in *sdha-1*
RT-qPCR analyses of *pck-2*, *pck-1*, *icl-1*, and *pyc-1* in 12- to 24-h wild-type and *sdha-1(lf)* males. Columns and whiskers show mean and standard error of the mean (paired t-test). *Ppck-1*::Timer in wild type and *sdha-1(lf)* males (Mann-Whitney t-test). 10 Animals quantified per strain. Each symbol represents a single male of the specified age. Bars and whiskers represent mean and standard deviation.

SDHA-1 Modulation of Neighboring Tissue Metabolism

In order to address whether the *pck-2* increases in transcripts were elevated specifically due to *sdha-1(lf)* dysfunction we used a rescue construct driving *sdha-1* and monitored PCK-1::YFP levels. The shortened 500 bp endogenous *sdha-1* promoter expressed in the epidermis, intestine, and body wall muscles (Fig. 51). As expected, we measured an increase in PCK-1::YFP levels in *sdha-1(lf)* when compared to wild type (Fig. 51). Reintroducing *sdha-1(lf)* using the endogenous promoter decreased PCK-1::YFP to wild type levels, suggesting that *sdha-1* dysfunction is responsible for the metabolic shift.

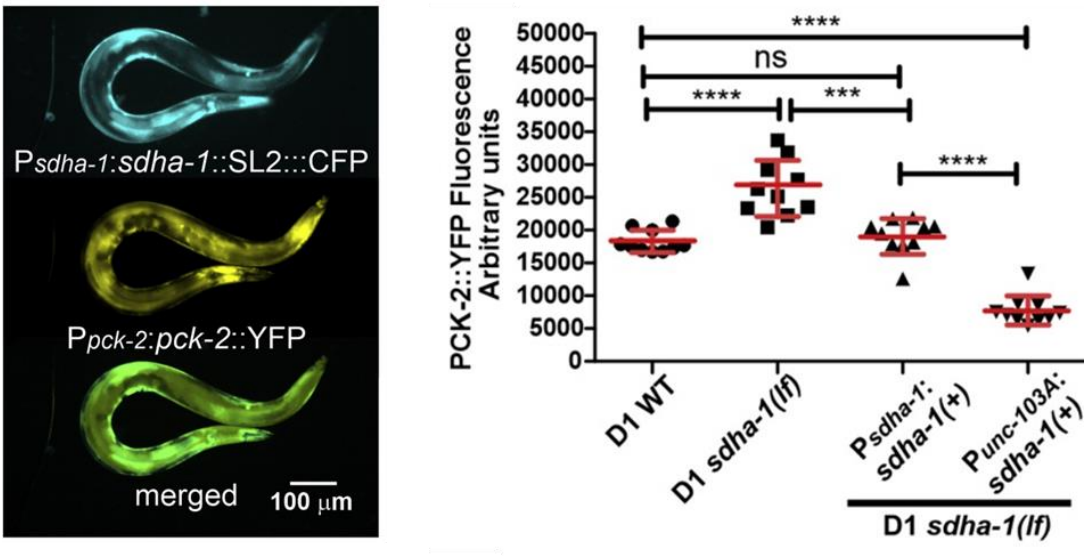

Figure 51 *sdha-1* dysfunction tissue specifically regulates PEPCK levels
The expression of *sdha-1* driven from its endogenous promoter and PCK-1::YFP shown on the left. On the right the symbols represent individual wild-type, *sdha-1(lf),* and *sdha-1(lf)* males expressing *sdha-1* from its endogenous promotor (500 bp) or a muscle promoter (*unc-103A* promoter). The number of animals quantified is 10 per strain. Bars and whiskers represent mean and standard deviation (Mann-Whitney t-test).

We previously showed that PCK-2 levels decrease in neighboring tissues to better match the levels in *pck-1*-lacking tissues (Fig. 48). To further address whether the metabolism of neighboring tissues affects PEPCK levels we expressed *sdha-1* only in the body wall and sex muscles using an *unc-103A* promoter. We found similar to the *sdha-1* endogenous promoter, epidermis and intestine decreased PCK-1::YFP levels when *sdha-1* was expressed in neighboring muscles (Fig. 51).

Given the elevated transcripts of *pck*-2 and PCK-1::YFP in *sdha-1(lf)* males, we asked whether gluco-glyceroneogenic metabolites were being created and stored. In the case of glycerol, it can contribute to the production of intestinal triglycerides. We stained neutral lipid droplets using Nile Red. We hypothesized that elevated *pck-2* transcription

occurs to increase intestinal triglyceride stores, offsetting the buildup of TCA byproducts due to decreased mitochondrial respiration. In contrast to wild type, we observed that *pck-2(lf)*, *sdha-1(lf),* and *sdha-1(lf);pck-2(lf)* males display a low-fat phenotype (Fig. 52). Despite *sdha-1(lf)* having decreased lipid stores compared to wild type, *sdha-1(lf);pck-2(lf)* males had significantly lower lipid stores than *sdha-1(lf)* single mutants. This suggested the minimal fat present in *sdha-1(lf)* was provided by PEPCK derived glycerol. To address whether *sdha-1(lf)* had a decreased rate of lipid oxidation we starved males and measured lipid stores in the intestine. We found that starved *sdha-1(lf)* males were able to reserve lipid stores in the intestine when compared to wild type, *pck-2(lf),* and *shda-1(lf);pck-2(lf)*. Altogether PEPCK produced glycerol contributes to intestinal lipid stores and with *sdha-1(lf)'s* lower mitochondrial respiration there's an adaptable rationing under food-limiting conditions.

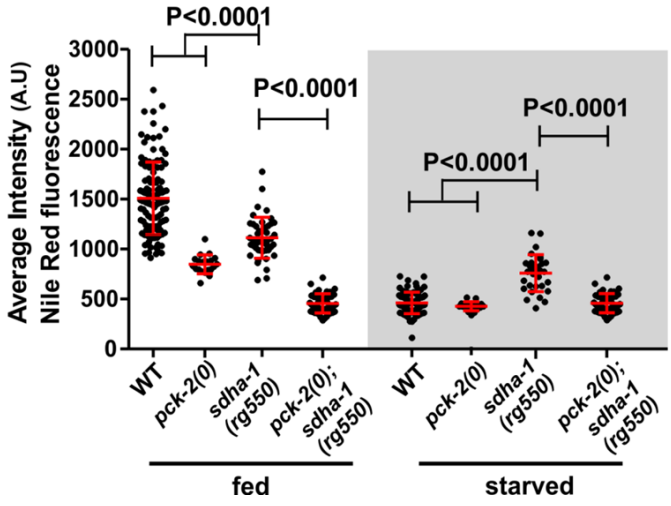

Figure 52 PEPCK derived glycerol contributes to lipid storage in *sdha-1(lf)*
Nile Red staining in aging adult males was quantified by a series of rectangular ROI's drawn over the intestine (unpaired t-test). Bars and whiskers represent mean and standard deviation.

Characterization of SDHA-1

Further casual observations of *sdha-1(lf)* showed deficits in development. We proceeded by quantifying all expected deficiencies in males lacking a functioning mitochondrion. We used a mitochondrial marker (*pdha-1*::YFP) to quantify mitochondria morphology, measured time to various larval stages and adulthood, and quantified death following paraquat (ROS generator) treatment. We found *sdha-1(lf)* mitochondria were no longer networked (Fig. 53), larval developmental was delayed (Fig. 54), and males were resistant to death by electron carrier dependent ROS generation (Fig. 55).

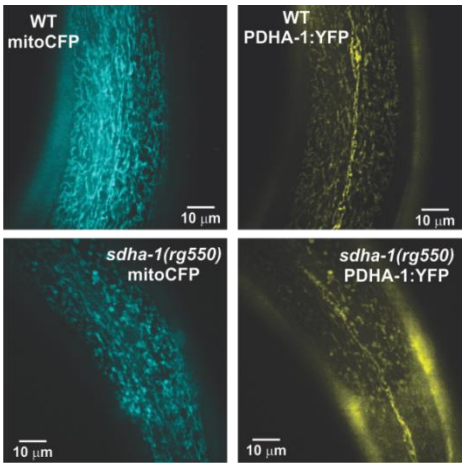

Figure 53 *sdha-1(lf)* mitochondria puncta morphology
Two mitochondrial markers were used to monitor mitochondrial networked morphology. *pdha-1*::YFP encodes pyruvate dehydrogenase which catalyzes pyruvate into acetyl-CoA.

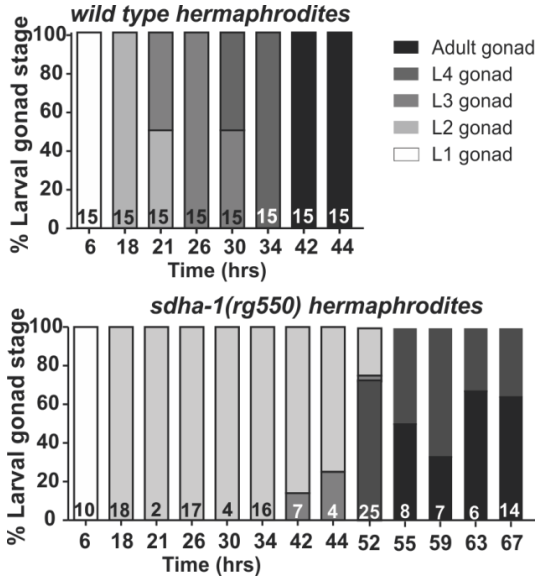

Figure 54 *sdha-1(lf)* larval and adulthood development
Gonad development was used as a proxy for larval development in wild type and *sdha-1(lf)*. After synchronizing animals in the first larval stage, specific time points were used to quantify the number of animals having reached a specific stage of gonad development.

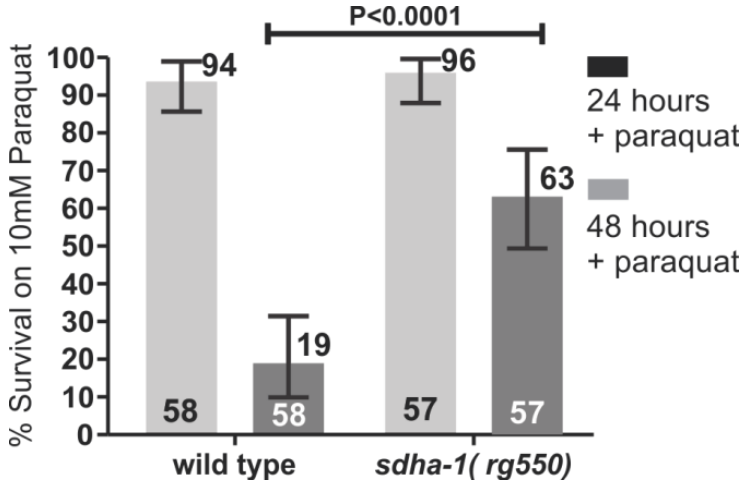

Figure 55 *sdha-1(lf)* survives electron carrier dependent ROS death
Wild type and *sdha-1(lf)* day 1 males were added to Paraquat supplemented plates. The percent of survived males was quantified (unpaired t-test). Bars and whiskers represent mean and standard deviation. The percent of survived and number of animals are found at the top and bottom of the bars respectively.

PEPCK Increases Require TCA Cycle and ETF Disruption

Despite the mitochondrial morphology and lack of electron carriers in *sdha-1(lf),* we did not know what was the cause of *pck*-2 transcript and PCK-2::YFP increases. In *sdha-1(lf)* mutants PCK-2::YFP may increase due to succinate dehydrogenase decreased function in the TCA cycle or the ETC. In order to address which aspects of *sdha-1* function results in PCK-2::YFP increases we used a mitochondrial poison rotenone (blocks electron transfer between complex I and ubiquinone), a loss of function mutant of subunit C of complex II (*mev-1*), and a competitor malonate.

Rotenone treatment addressed general ETC dysfunctions. The *mev-1(lf)* mutant addressed the sole dysfunction of the electron transport through complex II in *sdha-1(lf)*. Finally, the malonate treatment addressed *sdha-1(lf)*'s dysfunction in catalyzing succinate to fumarate. We found the treatments and genetic mutants showed variable minor decreases and increases in PCK-2::YFP which did not recapitulate the effects seen in *sdha-1(lf)*(Fig. 56). Altogether, *sdha-1(lf)* dependent increases in PCK-2::YFP are due to deficits in both the TCA cycles and ETC.

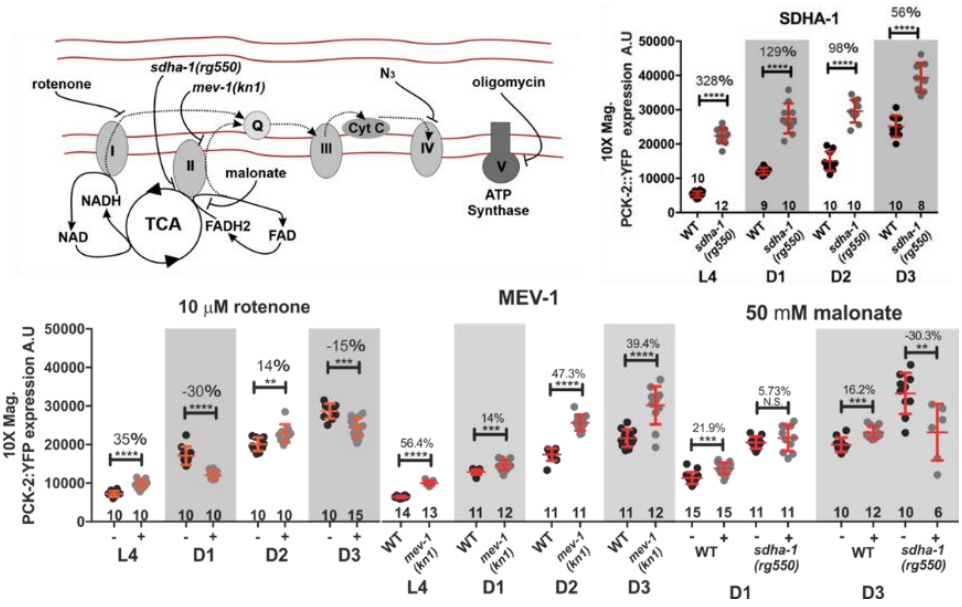

Figure 56 *sdha-1(lf)* Dependent Increases in *pck-2*::YFP
Illustrated is a cartoon of the mitochondrial electron transport system, site of action for mutations, and electron transport chain toxins. PCK-2::YFP levels in L4 and day 1 (D1) through day 3 (D3) hermaphrodites grown in the absence (-) or presence (+) of rotenone, malonate, or containing *mev-1(lf)* mutation.

Chapter VII Summary

In order to understand what metabolic alterations result in PEPCK increases we performed an EMS mutagenesis screen on PCK-1::YFP animals. We found a missense mutation in succinate dehydrogenase subunit A, encoded by *sdha-1*, increased *pck-2*::YFP. We also validated changes in *pck-2*, *icl-1*, and *pyc-1* through RT-qPCR. Altogether we suggested that metabolites were being rerouted out of the mitochondrial TCA cycle. This shift in metabolism resulted in PEPCK produced glycerol contributing to intestinal lipid stores, delayed development, puncta-like mitochondrial morphology, and resistance to electron carrier dependent ROS induced death. We also validated PEPCK expressional changes were dependent on neighboring tissue metabolism. Specifically when *sdha-1* was expressed in muscles neighboring epidermis and intestine decreased PCK-2::YFP levels.

CHAPTER VIII

EXPERIMENTAL PROCEDURES

Strains

All animals, including the wild type, contain the *him-5(e1490)* allele (Hodgkin, Horvitz et al. 1979) and were grown at 20°C on NGM agar plates containing *E. coli* OP50 (Brenner 1974). Additional strains used in the study contained the following alleles; *fat-6::YFP*(*rg802*), *him-5(e1490);fat-7(wa36);fat-6::YFP(rg802), fat-6(tm331), fat-7(wa36), fat-6(tm331);fat-7(wa36), fat-5(tm420);fat-7(wa36), fat-6(tm331);fat-7(wa36);him-5(e1490); rgIS48[*P_{gtl-1}*;fat-6::YFP], fat-5(tm420);fat-7(wa36) rgIS48 [*P_{gtl-1}*;fat-6::YFP], fat-7(wa36);him-5(e1490); rgIS48[*P_{gtl-1}*;fat-6::YFP], fat-6(tm331);fat-7(wa36);him-5(e1490); rgIS50[*P_{gtl-1}*;fat-6::YFP, *P_{dpy-7}*;fat-6::YFP], fat-5(tm420);fat-7(wa36) rgIS50 [*P_{gtl-1}*;fat-6::YFP, *P_{dpy-7}*;fat-6::YFP], fat-5(tm420);fat-7(wa36) rgEX874 [*$P_{unc-17FL}$*;G-CAMP6V;SL2;RFP], fat-5(tm420);fat-7(wa36) rgIS49 [*$P_{unc-17FL}$*;G-CAMP6V;SL2;RFP], fog-2(q71)* (Schedl and Kimble 1988).

Feeding Exploring Mating Assay (FEM)

Markov Model

Video recordings from the FEM Assay were analyzed on a frame per frame basis. Each frame was taken 15 seconds apart for one hour. Each frame was used as a data point and assigned a behavioral state based on position in the FEM assay (Fig. 57). The sequences of assigned values (A/B/C) were then transformed into three new separate binary sequences based on individual behavior (Fig. 58). The three binary sequences were then used to calculate the frequency of sustained behaviors and shifts in behavior. In order to calculate the frequency of behaviors each frame was compared to its previous frame (Fig. 59).

Time (seconds)	0	15	30	45	60	75	90	105	120	135
Him-5 Worm	B	B	C	C	C	C	B	B	A	A

Figure 57 Example of Behavioral State Assignment
Representation of workflow in which behavioral states were assigned as A= Feeding, B= Exploring, and C= Mating.

Time (seconds)	0	15	30	45	60	75	90	105	120	135
Him-5 Worm	B	B	C	C	C	C	B	B	A	A
Feeding	0	0	0	0	0	0	0	0	1	1
Exploring	1	1	0	0	0	0	1	1	0	0
Mating	0	0	1	1	1	1	0	0	0	0

Figure 58 Creating a binary sequence of events
The number one signifies that during a specific frame the *C. elegans* male was performing the corresponding behavior.

Time (seconds)	0	15	30	45	60	75	90	105	120	135
Feeding	0	0	0	0	0	0	0	0	1	1
Exploring	1	1	0	0	0	0	1	1	0	0
Mating	0	0	1	1	1	1	0	0	0	0

FF	0	0	0	0	0	0	0	0	1	
FE	0	0	0	0	0	0	0	0	0	
EE	1	0	0	0	0	0	1	0	0	
EF	0	0	0	0	0	0	0	1	0	
EM	0	1	0	0	0	0	0	0	0	
MM	0	0	1	1	1	0	0	0	0	
ME	0	0	0	0	0	1	0	0	0	

Figure 59 Calculating Frequency of Behavior
Bolded cells were compared by multiplying the values and assigning the product in a new table. This new value is also bolded below and is labeled in EM to signify a behavioral transition of exploring to mating. Sustained behaviors were classified as Feeding-Feeding (FF), Exploring-Exploring (EE), and Mating-Mating (MM). Behavioral Shifts were classified as Feeding-Exploring (FE), Exploring-Feeding (EF), Exploring-Mating (EM), and Mating-Exploring (ME). A behavioral shift of Feeding-Mating and Mating-Feeding was omitted because assay design restricted such a transition.

The final step for calculating the frequency of behavioral states was to sum all rows and divide each by the sum of all the possible behavioral states. This provided the proportion entered into the Markov Model as seen in the example below in row B (Fig. 60).

											A	B	
											Sum	Model	Calculation
1	FF	0	0	0	0	0	0	0	0	1	1	1	A1/(A1+A2)
2	FE	0	0	0	0	0	0	0	0	0	0	0	A2/(A1+A2)
3	EE	1	0	0	0	0	0	1	0	0	2	0.5	A3/(A3+A4+A5)
4	EF	0	0	0	0	0	0	0	1	0	1	0.25	A4/(A3+A4+A5)
5	EM	0	1	0	0	0	0	0	0	0	1	0.25	A5/(A3+A4+A5)
6	MM	0	0	1	1	1	0	0	0	0	3	0.75	A6/(A6+A7)
7	ME	0	0	0	0	0	1	0	0	0	1	0.25	A7/(A6+A7)

Figure 60 Calculations of Markov Model Proportions
All rows were summed and divided by the sum of all the possible behavioral states. Mathematical representations of proportion calculations located in right hand column.

In order to verify the Markov Model was acceptably similar to the raw data collected, the model was run 100 times. In order to run the model an excel script was written. The script generated a random number from 0-100. It then compared the randomly generated number to the model proportions. The comparison was used to assign a behavioral state to a single frame constituting a 15 seconds time lapse.

For example, the first behavioral state was assigned the number 0 to signify exploring. This assignment is only done for the first frame in every model. If then the random number generator is a value > 90 we assign the next behavioral state to -1, signifying mating behavior. Alternatively, if the random number generator is a value > 75 we assign the next behavioral state to 1, signifying feeding behavior, and any other value results in a 0, signifying an exploring state (Fig. 61). After establishing two behavioral states a new set of proportions is required given that the Markov Model is of a second order; uses behavioral history and present state to predict future behaviors (Fig. 61).

A	B
Random #	State
85	0
	1

A	B
Random #	State
21	0
	1
	1

Figure 61 Probabilistic Predictions of Behavioral States
After a random generator produces 85 the second behavioral state is set to 1, feeding. Now that two behavioral states have been established a new second order set of probabilities are used to establish a third state. In this example, a random number of 21 results in a third state equal to 1, feeding.

The script was repeated for 121 frames constituting a one-hour time lapse similar to FEM recordings. Each model data set was composed of 100 runs and 121 frames each. The model data set was then used to create heat maps of behavioral states. The model data set was also used to create new model proportions. These model-based proportions were compared by chi square statistical analysis to the raw data-based model proportions.

Analyzing the Raw and Modeled Data

We used a Ternary Diagram to show the proportion of worms in 3 different behavioral states. A data matrix containing total time spent on feeding, mating, and exploring per worm was used to calculate the proportion of time spent on behaviors. These proportions are then plotted in a diagram shaped as a triangle. As a data point

(worm) moves towards any of the vertices the proportion of the behavioral state increases. This allows for the comparison of aged and metabolic mutants using a distribution of total time spent on behaviors.

Potency Assay, Copulation Fitness Assay, and Copulation Endurance Assay

The potency assay was conducted as previously described (Guo, Navetta et al. 2012). L4 males from non-crowded OP50 spotted NGM plates were separated, 15 males per plate, and allowed to reach adulthood. For assays in which various ages were tested males were transferred onto new plates on a daily basis. There is evidence to suggest male pheromone secretion can kill siblings (Shi, Runnels et al. 2017). The mating partners of collected males were *pha-1(e2123)* hermaphrodites who were propagated at 15°C (permissive temperature)(Schnabel and Schnabel 1990). Upon transferring L4 hermaphrodites, 24 hrs before assay conducted, to 20°C (non-permissive temperature) all progeny can be identified as coming from successful mating's. To conduct the potency assay, at 20°C, one male was paired with one 24 hr adult *pha-1* hermaphrodite on a NGM plate containing a 5 mm diameter lawn of OP50. The age of the male could vary depending on the experiment but the *pha-1* hermaphrodite used was always a 24 hr adult. Approximately a week later, the mating was scored successful if the plate contained at least 10 cross-progeny. *pha-1* embryos and L1 larva die at 20°C, but cross-progeny, which are heterozygous for *pha-1*, are viable and reproductive.

The copulation fitness assay was conducted as previously described (LeBoeuf, Guo et al. 2011). L4 males from non-crowded OP50 spotted NGM plates were separated, 15 males per plate, and allowed to reach adulthood. For assays in which various ages were tested males were transferred onto new plates on a daily basis. L4 *fog-2(q71)* females, do not make sperm therefore cross progeny belong to mating partner, were picked 24 hrs before conducting the assay despite the age of the male (Schedl and Kimble 1988). On the day of the assay a 24hr adult male containing a CRISPR/Cas9 YFP knock in of *pck-2* and one unmarked 24 hrs adult male were paired with a virgin - *fog-2(q71)* female on a 5 mm diameter OP50 lawn. A PCK-1::YFP adult male was paired with a *him-5(e1490)* adult male to test for wild type mating fitness. Afterwards only PCK-1::YFP adult males were used against mutants. The paired males were allowed to mate for 3 hrs before being removed. The following days the female's progeny were screened for either the presence or lack of YFP to determine paternity. Plates containing progeny with YFP and lack of YFP were not counted as paternity was shared between competing males.

The copulation endurance assay, modified from previous work, measures the kinetics of male mating, number of females impregnated, across the first 3 days of adulthood (Hodgkin and Doniach 1997). L4 males from non-crowded OP50 spotted NGM plates were separated, 15 males per plate, and allowed to reach adulthood. L4 *fog-2(q71)* females were picked 24 hrs before conducting the assay. On the day of the assay one day 1 adult male was paired with 10-day 1 adult females. Every 12 hrs impregnated females were counted and replaced with similarly aged females. The male and 10

females were then transferred to a new plate and allowed to mate for another 12 hrs. This was repeated for 72 hrs.

The copulation endurance assay was analyzed in multiple ways. For example, we quantified the percent of males who mated per time point. For a male to be considered successful they would have had to mate into a single female during the specific time point. In order to quantify the number of females impregnated we summed the total number of females impregnated in a time point across all males. We then divided by the total number of females present across all males assayed (10 females were made available to each male). Approximately 25-35 % of females were impregnated by 10 wild type males during the first 12 hours of the assay.

Mating Interference (MI) Assay

A single day 1 male was transferred to an NGM assay plate with a 5 mm diameter lawn of OP50 and three 1-day-old *let-23(sy1);unc-64(e246);lite-1(ce314)* hermaphrodites. The latency to copulation was determined from the time the male was transferred to the plate, to when he started backwards locomotion behavior. Blue light (475 nm) was then applied after the male had attempted to continuously mate for 1 min. Time was recorded when the male disengaged from the hermaphrodite. Each worm was tested once.

Construction of Plasmids and Transgenic Strains

FAT-6 Crisper/Cas9 Plasmids, Expression Plasmids and Transgenics

To generate the *fat-6* CRISPR/CAS 9 guide RNA plasmid pJG74 and pJG75, the 19 bp guide RNA sequence to the *fat-6* 3' untranslated region (UTR) (5' cggaacgcccggggtttcc 3') and 5' 1st exon (5' gagacgcaatatctcgccg 3'), was added to the CRISPR/CAS 9 guide RNA/ enzyme plasmid pDD162 using PCR and the primers, forfat6_2cas9; cggaacgcccggggtttccgttttagagctagaaatagcaagt, forfat6cas9; gagacgcaatatctcgccggttttagagctagaaatagcaagt, and sgRNA(universal)REV; CAAGACATCTCGCAATAGG. Sequence errors were checked using primer SEQpDD122-sgRNA (universal); CTGCTGAGACCTGAAAATAGC.

The *fat-6* repair template used for CRISPR/CAS 9-mediated recombination was generated by PCR-amplifying from genomic DNA a ~ 4.5 kilo base pair (kb) fragment containing the promoter and gene. This fragment was amplified using the primers For_ATTB_fat6Prom; GGGGACAAGTTTGTACAAAAAAGCAGGCTACCATCTTCATCAATCTTGCGCC CACGAACC and Rev_fat6_ATTB; GGGGACCACTTTGTACAAGAAAGCTGGGTCATGATTGATTTTCCTCGTTGAA TATCACAT. The fragment was then recombined into pDG15 by Invitrogen BP clonase to generate pJG45. To fuse YFP to the *fat-6* gene a second recombination occurred between pJG45 and pGW322YFP by Invitrogen LR clonase to generate pJG61. The YFP was not directly fused by the recombination reaction and so the primers linfat6yfp;

atgagtaaaggagaagaacttttccactggagttgtccca and reverse_fat6_nostop; catgattgattttcctcgttgaatatcacatccatgattggatac were used to correct the frameshift to generate pJG62. To create greater homology, we PCR-amplified the *fat-6* 3' UTR using primers

fat6forutr_yfp; tggatgaactatacaaataggatactgttccgtattcactcaaataagag and fat6revutr_unc54; gcacgggcgcgagatgctgagcgtacttctcgtttatttcacatttgacttac. We also linearized pJG62 using primers fat6forlin_pjg62; gaaataaacgagaagtacgctcagcatctcgcgcccgtgcctc and fat6revlin_pjg62; agtgaatacggaacagtatcctatttgtatagttcatccatgccatgtgtaatcccag. Using the In-Fusion HD-cloning, we fused the PCR fragment *fat*-6 3' UTR to the last codon of YFP in the plasmid pJG62 generating pJG63. A single loxp site were added to pJG63 by using the primers fat6for5primeloxp; accatatacgaagttatgacatcgagtagtcgaacatttcatgtcaactgtc and fat6rev5primeloxp; accatatacgaagttatgctgatcacattgatcagaactgataagacgacac. Quick ligase was used to join homologous ends to generate pJG64. This was repeated for the second loxp site using primers fat6for3primeloxp; accatatacgaagttatgatactgttccgtattcactcaaataagag and fat6rev3primeloxp; accatatacgaagttatctatttgtatagttcatccatgccatgtgtatc. Quick ligase was used to join homologous ends to generate pJG65. The PAM sites located at the 3' UTR were mutated using primers fat6for3primepammut; gtttcccatatcacagacgaaccccac and fat6rev3primepammut; cccgggcgttccggtttgcaaatc. Quick ligase was used to join homologous ends to generate pJG66. The PAM sites located at the 5' 1st exon were mutated using primers fat6for5primepammut; gacgcaatatctcgccgtagatccaaatg

fat6rev5primepammut; tctgggccgccgtccttctcaatc. Quick ligase was used to join homologous ends to generate pJG67. Plasmids were sequenced and repaired for mutations that arose during the construction to generate pJG76.

Plasmids Used For Conducting Tissue-Specific Rescue of fat-6(lf)

The plasmid pJG76 had the *fat*-6 promoter removed and the Invitrogen Gateway ATTR cassette B was cloned in using In-Fusion HD-cloning creating pJG89. The cassette was PCR amplified using primers for_fat6_attr1_ccdb; tgcctgcaggtcgactctagatcaaacaagtttgtacaaaaaagctgaac and rev_ccdb_attr2_fat-6; tgtttgaacgagtttttaccgtcataccactttgtacaagaaagctgaac. pJG76 was linearized using primers rev_lin_fat6_attr1; tcagctttttgtacaaacttgtttgatctagagtcgacctgcaggcatgcaagcttatc and for_lin_fat6_attr2; cttgtacaaagtggtatgacggtaaaaactcgttcaaacatcgcaaaaaagattgag. For intestinal expression, the gateway entry plasmid pBL63 (LeBoeuf, Gruninger et al. 2007) was used to recombine in the gtl-1 promoter (Teramoto, Lambie et al. 2005) to generate pJG90. For epidermal expression, the gateway entry plasmid pXG76 was used to recombine the dpy-7 promoter (Gilleard, Barry et al. 1997) to generate pJG91.

Injection mixes, containing 50 ng/µl of pJG90 and/or pJG91 and up to 150 ng/µl of pUC18 filler DNA, were injected into the germline of *fat-7(lf);fat-5(lf)* hermaphrodites. Stable transgenic lines that heritably transmit YFP fluorescence were then used to generate the integrated lines; *fat-5(tm420);fat-7(wa36) rgIS48 [P_{gtl-1};fat-6::YFP] and fat-5(tm420);fat-7(wa36) rgIS50[P_{gtl-1};*FAT-6::YFP *, P_{dpy-7};fat-6::YFP]*. Then *fat-7(wa36);him-5(e1490) males were crossed into fat-5(tm420);fat-7(wa36)*

rgIS48 [P_{gtl-1};fat-6::YFP] to generate fat-7(wa36);him-5(e1490); rgIS48[P_{gtl-1};fat-6::YFP]. The fat-7(wa36);him-5(e1490); rgIS48[P_{gtl-1};fat-6::YFP] males were then crossed into *fat-6(tm331);fat-7(wa36);him-5(e1490)* to generated *fat-6(tm331);fat-7(wa36);him-5(e1490); rgIS48[P_{gtl-1};fat-6::YFP]*. Similarly, *fat-6(tm331);fat-7(wa36);him-5(e1490)* males were crossed into *and fat-5(tm420);fat-7(wa36) rgIS50[P_{gtl-1};*FAT-6::YFP , *P_{dpy-7};fat-6::YFP]* to generate *fat-6(tm331);fat-7(wa36);him-5(e1490); rgIS50[P_{gtl-1};*FAT-6::YFP , *P_{dpy-7};fat-6::YFP]*.

CRISPR/Cas9-mediated Recombination of YFP into Genomic *fat-6*

The CRISPR/Cas9 plasmids and protocols established in Dickinson *et al*. 2013 were used in this report (Dickinson, Ward et al. 2013). To generate the genomic FAT-6::YFP knock-in, a hundred ~ 5 to 10 hour old adult *N2* hermaphrodites were microinjected with 50 ng/µl of the CRISPR/CAS9 plasmids pJG74 and pJG75, and 50 ng/µl the FAT-6::YFP repair template pJG76. In the F2-F3 generation, fluorescent animals were picked and analyzed by PCR and sequencing to verify homologous recombination between the repair template and the genomic *fat-6* locus. The *fat-6*::YFP knock-in allele is referred to as *fat-6*::YFP. We also validated the knock-in of loxp by expressing *Pges-1:Cre* and we observed a reduction in FAT-6::YFP between 54-60% during larval development. The remaining FAT-6::YFP was highly mosaic and did not result in obvious mutant phenotypes.

CRISPR/Cas9-mediated Mutation of *him-5(e1490)*

The *him-5(e1490)* mutation is a G-to-A transition affecting the splice acceptor site at the start of exon 4 (or at the end of intron 3). To generate the *him-5(e1490)* CRISPR/CAS 9 guide RNA plasmid, the 19 bp guide RNA sequence to the *him-5 (e1490)* slice acceptor site (5' cggaacgcccggggtttcc 3') was added to the CRISPR/CAS 9 guide RNA/ enzyme plasmid pDD162 using PCR and the primers, ForHim5Cas9sgRNA; /5Phos/TTATTTTCCAGGCAAAGCTCGTTTTAGAGCTAGAAATAGCAAGT and sgRNA(universal)REV; CAAGACATCTCGCAATAGG to create pJG33. Sequence errors were checked using primer SEQpDD122-sgRNA (universal); CTGCTGAGACCTGAAAATAGC. The repair template used was the oligo him-5(e1490) Oligo; CCTTTCTATGTTAGTAATTTTTAAAAACATGGAATTTTACTGATTATTTTCCA AGCTAAGCTCCGTAAAGCTAACTCCAAGTATTCCTCAAAGCCCAAAGAAAG AGA.

To generate the mutation of *him-5(e1490)*, a hundred ~ 5-10 hour old adult *fat-7(lf)* hermaphrodites were microinjected with 50 ng/µl of the CRISPR/CAS9 plasmids, and 50 ng/µl of the oligo repair template. In the F2-F3 generation, males were picked and allowed to mate into *fat-7(lf)* hermaphrodites. We verified the *him-5(e1490)* mutation by PCR and sequencing.

Gonad Ablation

We laser-ablated the gonad precursor cells in L1 animals. We could not tell if they were male or hermaphrodites until they reached L4 at which point we picked males and quantified fluorescence in day 1 adults. Agarose pads were 5% Noble agar melted in water. Animals were immobilized with 10mM azide. L1 worms (3 to a pad) were kept on the pad no more than 10 minutes.

Quantification of Fluorescence

Digital images of animals were obtained using a Yokogawa CSU-X1 Spinning Disk Unit (Andor Technology, CT USA) mounted on an Olympus IX81 microscope. Animals were anesthetized using abamectin (Sigma-Aldrich) (Cully, Vassilatis et al. 1994). A 50 mg/ml DMSO stock of abamectin was diluted in M9 buffer to the working concentration of 250 µg/ml. Worms were allowed to soak in 1-5ul of solution. Generally, 1-2 minutes elapsed before the worms became paralyzed. To measure calcium transients' males were mounted using 10% Noble agar containing Polybead polystyrene 0.1 um microspheres. The adults were imaged using the 10X objective for a full body perspective, Nile red staining and YFP, and 100X objective for individual cell resolution (FAT-6::YFP tissue expression and GCAMP). In order to see low expressing tissues, we increased contrast by scaling a selected range of its gray levels to another range. Contrast was not changed when calculating average intensity. We also used Prism

software analysis for normalization described by the equation ((Sample-Min)/ (Max-Min)) where the Min and Max are user chosen but normally refer to the lowest point in the data set and the mean respectively.

Metamorph image software (version 7.8.0.0., Molecular Devices, Sunnyvale CA) was used to quantify average pixel intensity of a region of interest (ROI). To quantify *fat-6::YFP*, a series of rectangular ROI's were drawn across the entire intestine. The average pixel intensity was determined for each ROI and a single average of all ROIs was calculated for the whole intestine. If the intestine was analyzed into differing segments then only the average pixel intensity for a specific set of ROIs was averaged. For example, the anterior intestine was composed of the first ~5 intestinal rectangular ROI's. The pixel intensity was averaged for each ROI and then a single average was calculated from the subset. Nile red staining also used only the first 5 ROI's (see Nile Red staining and quantification).

SimplePCI imaging software was used to quantify average pixel intensity of regions of interest. In every male, ROI's were drawn for 12 cholinergic neurons and fluorescence was collected across time. We were able to draw matching ROI's for every neuron in both strains. Wavelength was approximated using Prism Software analysis. Amplitude was measured by taking the difference between a local max and local min of every individual peak. To quantify signal duration, we used the average fluorescence across time to set a threshold. Every male had an individual calcium wave with a unique threshold. Using the threshold as the minimum, we then measured the distance between both sides of a single peak. Every male had 3 peaks quantified.

We collected G-CaMPV6 and DsRed fluorescence from Immobilized males using a Dual View Simultaneous Image Splitter (Photometrics, AZ) and a Hamamatsu ImagEM Electron multiplier (EM) CCD camera. The recordings were analyzed in Hamamatsu SimplePCI software (version 6.6.0.0) and Microsoft Excel.

We could not observe changes in SPC/PCB/PCC but we did observe changes in cholinergic neurons in the ventral cord including CA8, VB11, DB7, AS10, DA7, CA9, VA11, AS11, and VA12. Given the dynamic changes seen we generated Region-of-Interests (ROI's) of equal areas around the ventral cord neurons in Simple PCI software. These neurons were never obscured by other tissues but some ventral cord neurons were mosaic in that they did not always express. As such we labeled the neurons appropriately and kept track of their location. ROI's were used to measure the background signal, fluorescent signal from green emission channel and the fluorescent signal from red emission channel. Males were immobilized so ROI's remained in position but if there was movement ROI's were moved in accordance with position. The mean pixel intensity was then transferred into Microsoft Excel and background signal was subtracted from neuronal signal.

Photo bleaching artifacts caused unwanted fluorescent changes. A higher rate of mDsRed photo bleaching, relative to minimal GCaMP photo bleaching, required appropriate signal correction. We described the DsRed bleaching using a one-phase decay curve and fitted it over the data points in GraphPad Prism (version 4.03). The fitted curve described unwanted changes in fluorescent. For every frame the fitted curve was used to correct the background subtracted red channel mean pixel intensity (MPI).

The MPI value was divided by the fitted red value to give a correction value. This was then applied to the green channel MPI for the respective frame. The resulting data solely reflected changes in calcium.

The expression levels of GCaMPV6 differed between wild type and *fat-6(lf);fat-7(lf)* males. To quantify the amplitude of the calcium signal we corrected for transcriptional activity of the promoter of a vesicular acetylcholine transporter (divide by the mean difference in expression).

RT-qPCR

The sequences for primers that anneal to the metabolic genes *sod-4, ctl-1, t20h4.5, cco-1, ech-2, and fat-5* were described previously (Castelein, Hoogewijs et al. 2008). The sequences for primers that anneal to *unc-103* isoforms D and A were for_unc103c; cactagtggcaagatcggga and for_unc103i; tgcgtgcggttctatcactt respectively. When searching through wormbase.org we found discrepancies with previously published work (Reiner, Weinshenker et al. 2006). Of note for this paper wormbase.org labels *unc-103* isoforms A and D as I and C respectively. All *unc-103* isoforms labels have been shifted.

Given the low abundance of *unc-103* isoforms using an Oligo (dT) 18 primer for first strand cDNA synthesis was not possible (primed at the 3' poly A tail of eukaryotic mRNA). A gene specific primer was used to reverse transcribe *unc-103* cDNA and therefore a variety of housekeeping genes were tested. We continued with *unc-15* as a

reference gene as the other gene amplifications resulted in an intense band slightly overlapping with primer dimers (all reference genes were consistent). After synthesizing cDNA (*unc-103* primer only) and then using Taq PCR many of the unc-103 isoforms could be seen by gel electrophoresis (2% @ 100V). When we continued with a mixture of *unc-15* and *unc-103* primers for cDNA synthesis many of the bands for unc-103 isoforms became fainter. Many primer combinations were tried and the best condition was a dilution of 1:10 for the *unc-15* primer (stock 50uM→Diluted to 5uM and final 0.2uM) and 2uM final concentration of unc-103 primer.

General Protocol

Single worm q-RTPCR protocol was adapted from (Ly, Reid et al. 2015). A single microliter of Lysis solution (5mM Tris pH8. 0.5% triton X-100, 0.5% Tween 20, 0.25mM EDTA; 1 mg/ml Protease K) was added to the cap of a PCR tube. Using a eye lash a worm was transferred to the lysis buffer. Using a sharpened platinum pick we cut the worm up in the lysis buffer. Then samples were frozen at -70°C. The samples were then put into a thermocycler to incubate at 65°C for 20 minutes then 85°C for 5 minutes. Once the lysis was complete 10 µl of Turbo DNAse I solution (9 µl nuclease free water, 1µl 10X Turbo DNAse I buffer) was added and allowed to incubate at 37 °C for 20 minutes. We then added 2ul of Turbo DNAse I inactivation beads and incubated 5 minutes. We spun down the solution and gently remove 10 µl of the lysed worm. We then added 1 µl of dNTP and 1 µl of oligo dT and incubated at 65 °C for 5 minutes then put-on ice for 1 minute to anneal. Finally, we added 10 µl of the RT solution containing

(2 µl 10X RT buffer; 4 µl 25mM MgCl2, 2 µl 0.1 M DTT, 1 µl RNAse out; 0.5 µl Superscript II RT; 0.5 µl nuclease-free water) and incubated at 42 °C for 50 minutes and 70 °C for 15 minutes.

Nile Red Staining and Quantification

The following was adapted from (Pino, Webster et al. 2013). L4 males from non-crowded OP50 spotted NGM plates were separated, 15 males per plate, and allowed to reach adulthood. For assays in which various ages were tested males were transferred onto new plates on a daily basis. On the day of the assay 30-50 males were transferred using 25ul of PBS with 0.01% triton X-100 (Sigma-Aldrich) to a 1.5 mL Eppendorf tube. Animals were then fixed using 150µL of 40% isopropanol and incubated at room temperature for 3 min. During this incubation, 1 mL of Nile Red (Invitrogen™ Molecular Probes™) stain was prepared using 6µL Nile Red stock solution (0.5 mg/ml in acetone) per 1 mL of 40% isopropanol. Males were pelleted by centrifugation and the supernatant was aspirated leaving 25ul. To each worm pellet, 150µL of Nile red staining solution was added and males were stained in the dark for 2 hours. Males were then collected by centrifugation and supernatant was aspirated leaving 25ul. Males were incubated with 150µL of PBS with 0.01% triton X-100 in the dark for 30 minutes. Males were centrifuged and supernatant aspirated leaving 25ul. Prior to imaging 1-5 males were transferred to a glass slide with 2% noble agar pad.

Males were imaged on a Yokogawa CSU-X1 Spinning Disk Unit mounted on an Olympus IX81 microscope (514 nm laser) using a 10X objective. Metamorph imaging software was used to quantify the average intensity of intestinal neutral lipid stores. To quantify Nile Red staining a series of rectangular ROI's were drawn across the entire intestine. The average pixel intensity was determined for the first 5 ROI's and a single average of all ROIs was calculated. Nile Red staining was occluded by hermaphrodite eggs therefore we treated hermaphrodites and males similarly by only calculating average intensity using the first five segmented ROI's.

Oxygen Consumption Assay

AD instruments Research Powerlab records voltage changes in solution. These voltage changes can give us approximate changes of oxygen in solution. A 1.5ml Eppendorf tube had a hole punched out of the cap. Then 50 males were added in 50ul of s-basal to the bottom of the Eppendorf tube. The voltage meter was dropped through the Eppendorf cap and sealed with clay and vacuum grease. The respirometers were not handled during the experiment.

Aldicarb Assay

Aldicarb were prepared in distilled water and kept frozen at –20°C as 100 mM. Aldicarb was then diluted with concentrations ranging from 5-20mM. Media, 500ul of

NGM with aldicarb, was allowed to solidify in a Pyrex round-bottom, three-well titer dish. Then ten day 1 adult virgin males were transferred to the solid media. Males were scored if they protracted their spicules for more than 10 seconds.

CHAPTER IX

SUMMARY OF EXPERIMENTS AND DISCUSSION

Summary of Experimental Results

Previous research had established a metabolic shift occurring from day 1 to day 2 of adulthood in *C. elegans* males that affects mating behavior performance. We validated increases in fatty acid desaturase gene expression, encoded by *fat-5/6*, from day 1 to day 2 of adulthood. Contrary to the increased gene transcription of *fat-6* in aging males, FAT-6::YFP protein levels decreased with age in specific segments of the intestine in males. We found that food deprivation mimicked FAT-6 degradation patterns. We hypothesized that during bouts of food deprivation, ingestion of saturated fat decreases and catabolism of stored fuel occurs. Under this condition, we expected fatty acid desaturases to play a minimal role.

We further established the role of stearoyl CoA desaturases (SCD) in early aging males by studying *fat-6(lf);fat-7(lf)* mutant males. We found that SCDs played a role in maintaining intestinal lipid storage and wild type mitochondrial respiration. In *fat-6(lf);fat-7(lf)* mutant males we measured moderate compensatory mechanisms including increases in gene expression of *fat-5*,the remaining SCD, and *sod-4*, a superoxide dismutase which converts reactive O_2^- and O_2 into H_2O_2.

Food deprivation dependent FAT-6 protein degradation suggested that well-fed day 2 wild type males decrease their feeding behavior. Indeed, we found that bacterial

consumption was decreased in day 2 males relative to day 1 males. This suggested that lower ingested saturated fat could account for reduced need for fatty acid desaturase function. The day 2 wild type male's reduction in food ingestion prompted us to make probabilistic predictions, using Markov Modeling, of the male's feeding, exploring, and mating behavioral states. We used a second order model that was based on 15 secs of behavioral history and the male's present behavior. We concluded that day 2 wild-type males reduced their feeding and increased their exploratory behavior. This combination of behavioral changes resulted in increased mating incidence.

We then addressed how lipid over-catabolism alters the males feeding, mating, and exploring states. We found that the *fat-6(lf);fat-7(lf)*mutant males differ from wild type in their increased exploring state probabilities on day 1 and unchanged feeding state probabilities on day 2. We expected that catabolizing fat is correlated with sustaining exploring behavior, a state that normally occurs when a starving animal searches for food. Additionally, not storing fat also could be correlated with sustaining feeding behavior, since the males might not be producing food satiety signals.

The discovery that *fat-6(lf);fat-7(lf)*mutant males differ from wild type in their increased exploring state probabilities on day 1 implied a potentially higher incidence of mating. We expected that dysregulated fat metabolism could disrupt neural muscular processes, used in mating behavior, that are tuned to glycolytic-mediated fuel. In order to address whether mating behavior was affected by increased saturated fat oxidation we performed multiple mating behavior assays. Contrary to wild type and single mutants, oleic acid-fed *fat-6(lf);fat-7(lf)* mutant males significantly mated into fewer females after

24 hrs. The period of time after 24 hours was noteworthy, as it coincided with the *fat-6* RNA increases seen in wild type males. These observations suggest that *fat-6* expression in one or more tissues maintains serial mating robustness.

To address which tissues, require *fat-6* transcription, we performed multiple tissue specific behavioral rescues. We found that epidermal FAT-6::YFP expression caused *fat-6(lf);fat-7(lf)* males to mate into an increased number of females. Furthermore, the mating deficit seen in *fat-6(lf);fat-7(lf)* males was due to the inability to maintain posture over the vulva and appropriately insert its spicules. We expected that the double mutant's deficit could be due to a defect in cholinergic motor control of muscles involved in both body posture and spicule motion. After an aldicarb treatment, acetylcholine esterase inhibitor, we found that *fat-6(lf);fat-7(lf)* males increase spontaneous cholinergic release in the spicule protraction circuitry. To further explore the posture deficit, we ascertained the activity of cholinergic motor neurons in the mail tail. We found an exaggerated intensity and shortened duration of cholinergic neural activity.

The increased neurotransmitter release and augmented calcium transients suggested that the potassium channels regulating membrane threshold and repolarization were disrupted. We quantified the expression changes of ERG-like/*unc-103* K^+ channel and found two isoforms, *unc-103* A and D isoforms, were both upregulated in *fat-6(lf);fat-7(lf)*. All other isoforms of ERG-like/*unc-103* K^+ channel were not observable suggesting a down regulation in *fat-6(lf);fat-7(lf)*. We expected the down-regulation of neuronal *unc-103* isoforms could account for the heightened neural excitation and

transmitter release. Furthermore, the upregulation of the muscle-expressed isoform A could mitigate possible downstream muscle spasms from the altered neural activity.

To further explore the role of *unc-103* we created a triple mutant, *unc-103(lf);fat-6(lf);fat-7(lf)*and found that males were suppressed for the *unc-103(lf)*-induced Prc phenotype. This result prompted us to consider earlier work that indicated food stress could induce EAG/EGL-2 K+ channel expression. Since *fat-6(lf);fat-7(lf)* double mutants abnormally catabolize ingested lipids, we asked if the fat mutations synthetically interacted with the *unc-103* deficiency to alter EAG/*egl-2* expression. We found *egl-2* expression was significantly elevated in non-Prc *unc-103(lf);fat-6(lf);fat-7(lf)* triple mutant. We suggested that the levels of unsaturated lipid synthesis and catabolism can alter K^+ channel expression, resulting in differential excitation activity used for spicule insertion behavior. Furthermore given that we know spicule muscle spasms can be reduced by food deprivation through *egl-2* expression, we suggested that the metabolic state of *fat-6(lf);fat-7(lf)*males might share signaling commonalities that occur during food deprivation.

In addition to finding transcriptional increases in *fat-5/6* in aging wild type males we also found the PEPCK genes *pck-1/2*, involved in gluco-glyceroneogenesis. In conjunction with FAT-6's role, we hypothesize that aging adult males increase their gluco-glyceroneogenesis as a compensatory response to continued mitochondrial lipid oxidative metabolism. Expressional studies showed that *pck-1* was neuromuscular and *pck-2* was primarily intestinal and epidermal. We assessed mating performance and found that the loss of each PEPCK was compensated by the others expression on day 1.

This suggested that day 1 wild type males required neuromuscular glycolytic metabolites, either derived from supporting tissues or directly made in neurons and muscles. This was validated by behavioral rescue studies which showed neuronal *pck-1(+)* and epidermal *pck-2(+)* could rescue *pck-1(lf);pck-2(lf)* mutants.

PEPCK enzymatically produces the glycolytic metabolite PEP (phosphoenolpyruvate) from the TCA cycle metabolite OAA (oxaloacetate). We expected that if PEPCK expression increases with age that it may 1) decrease ROS production by removing excess substrates from the TCA cycle or 2) produce glucose and glycerol for stored sugar and triglyceride synthesis. To address these possibilities we supplemented day 1-2 *pck-1(lf);pck-2(lf)* with D-glucose and found a rescue in the number of females mated into only on day 1. This observation suggested that a metabolic shift, during day 1-2, from glycolysis to potentially glyceroneogenesis and triglyceride synthesis maintains mating performance and fitness.

The mating deficits in day 2 *pck-2(lf)* and day1-2 *pck-1(lf);pck-2(lf)* were found to be due to muscle spasms induced by dysregulated membrane excitability. Previous research had shown that food-deprivation, which leads to catabolism of internal sugar and lipid stores, can result in a compensatory increase in *egl-2* K+ channel expression. Given the expected decrease in gluco-glyceroneogenesis in *pck-1(lf);pck-2(lf)* we observed *egl-2* K+ channel expression and found a decrease in sex muscles and neurons on day 1 of adulthood. We hypothesized that gluco-glyceroneogenesis promotes EGL-2 protein levels in the copulatory circuit.

The observation that PEPCK genes compensate for each other's loss lead to the discovery that PCK-2 levels decrease to better match the levels in *pck-1*-lacking tissues. This was surprising but indicated that *pck-1*-deficient neurons and muscles had become overly dependent on mitochondrial respiration resulting in neighboring tissues downregulating gluco-glyceroneogenesis. This was supported by the mutant, found through an EMS screen, *sdha-1(lf)* which showed increased PCK-2 levels. *sdha-1*, encoding a part of Complex II, catalyzes the conversion of succinate to fumarate in the TCA cycle and contributes to the proton motive force. We suggested that disrupted complex II requires PEPCK to shunt metabolites from the TCA cycle and the ETC.

Finally, we addressed what disrupted functions of *sdha-1(lf)* resulted in *pck*-2 increases. After treatments and mutant analysis targeting electron transfer and TCA cycle function of *sdha-1* we found both the TCA cycle and ETC were required to increase *pck-2* levels.

Discussion

In this work we showed that declines in wild type mating behavior is partially due to decreases in feeding behavior and concomitant degradation of FAT-6, involved in lipid synthesis. As a result of changes in feeding and lipid synthesis, fat oxidation prevails during early-mid aging. To support this, we showed that *fat-6(lf);fat-7(lf)* mutants, undergoing increased lipid oxidation, prematurely transitioned off feeding

behaviors. The premature changes in feeding behavior were incurred as an indirect result of increased exploring on day 1 of adulthood.

Transcriptional Responses in fat-6(lf);fat-7(lf) Males

In *fat-6(lf); fat-7(lf)* mutants, insufficient compensation was observed with increases in the transcription of the remaining fatty acid desaturase and no changes in other genes involved in fatty acid oxidation. Despite the insufficient compensation, previous research has shown that under the specific conditions the low fat phenotype of *fat-6(lf);fat-7(lf)* mutants can be reversed. Specifically, a *daf-2* mutation increases the transcription of *fat-5*, more so than in *fat-6(lf); fat-7(lf)*, resulting in increased intestinal lipids. If this is occurring through *daf-16*, we suggest that starvation can trigger a more efficient metabolic reprogramming that allows *fat-6(lf);fat-7(lf)* mutants to partially recover. We suspect that the enhanced starvation response elicits changes in intestinal metabolism and downstream tissues.

The extracellular and membrane bound superoxide, *sod-4*, was shown to increase in the *fat-6(lf);fat-7(lf)*. *sod-4* has been implicated in creating H_2O_2 that inhibits PTP, protein tyrosine phosphatases, dependent inhibition of insulin signaling (Gems D et al. 2009, Doonan R et al. 2008, Goldstein BJ et al. 2005). If insulin signaling is activated under conditions of increased *sod-4*, we expect increases in glycogen and lipid synthesis and decreases in lipolysis and gluconeogenesis. We expect that *sod-4* H_2O_2 signaling may act in conjunction with *daf-16,* as wild type male's age, to maintain mating fitness.

Spatial Regulation of FAT-6 in Males

In aging wild type males the transcriptional response of *fat-6* was spatially regulated throughout different areas of the intestine as seen by FAT-6::YFP. It has been similarly reported that sodium hydrogen exchangers are spatially regulated throughout the intestine. Specifically, transgenes driving GFP from *nhx-6* and *nhx-7* promoters showed diverse anterior and posterior patterns (Nehrke and Melvin 2002). The exclusive posterior expression of *nhx-7*(*pbo-4*) was found to serve a role in regulating posterior body wall muscle contraction (Pfeiffer, Johnson et al. 2008). We hypothesize the continuous expression of FAT-6 in the anterior intestine represents a need to absorb dietary fats (Palmitic acid) and convert them into storage. The posterior intestine expression most likely provides unsaturated fats necessary for sperm development. This was supported by gonad ablation abrogating idiosyncratic levels of FAT-6::YFP. We also observed potential compensatory increases of FAT-6, near the seminal vesicle, in *fat-5(lf);fat-7(lf)* mutants. Finally, despite minimal epidermal FAT-6::YFP in adults, we were able to restore mating behavior with epidermal *fat-6*. Altogether this suggests that fatty acid desaturases are spatially and temporally tightly regulated to feed a variety of tissues with specific metabolic needs.

Tissue Specific Rescue's Reveal Required Metabolism in the Male Tail

Our work has shown that PEPCK, which promotes gluco-glyceroneogenesis, is required in the epidermis to rescue mating behavior defects. It is suspected that the epidermis is capable of feeding the neuromuscular circuitry in the male tail. While

intestinal *fat-6* expression rescues developmental and morphological defects, specific tissues may never fully recover without their own immediate supply of specialized metabolites. For example, glucose partially rescues mating robustness in PEPCK mutants, *pck-1(lf); pck-2(lf)*, during the first 24 hrs of adulthood. This suggests PEPCK within the first 24 hrs functionally makes glucose for eventual TCA metabolism. It is possible that the epidermis provides neurons with glucose so as to readily use this fuel during day 1 of adulthood. The rescue did not occur when glucose was fed post day 1 of adulthood in *pck-1(lf); pck-2(lf)* mutants. With the diminished reliance on glucose it may suggest fat synthesis increases in the epidermis with age to provide different fuels for the neuromuscular circuitry controlling mating behavior. This aligns with the compensatory transcriptional responses of *fat-6* on day 2 of adulthood. Together with the decline in mating fitness of *fat-6(lf);fat-7(lf)* day 1 males, this suggests a reversal of enhanced fat oxidation during early-mid age delays mating performance decay.

The forms of fat provided by the intestine to the epidermis are currently unknown as are the epidermal lipid-based fuels used by the neurons and muscles in the male tail. It is possible that the epidermis uses unsaturated fat made by the intestine and pools it for a variety of signaling processes. This was disproved by the intestinal *fat-6* rescue insufficiently feeding the neuromuscular circuitry through the epidermis. The intestine may also feed saturated fat directly to the epidermis. Ultimately, we hypothesize that a pool of intestinal saturated and unsaturated fats is made available to the epidermis and then this tissue becomes an intermediate in determining the needs of surrounding tissues responsible for spicule intromission; neurons and muscles.

Fuel Utilization in the Neurons and Epidermis of the Male Tail

Previously published work has shown that medium chain fatty acids contribute ~20% to the neuronal acetyl-CoA pool (Ebert, Haller et al. 2003). Labeling of octanoate (C_8) and glutamine isotopomer analysis, glutamine synthetase is astrocyte-specific, revealed that a majority of medium chain fatty acids are metabolized in astrocytes (Ebert, Haller et al. 2003). Glutamine is indirectly made in astrocytes from the catalysis of a TCA cycle metabolite, alpha ketoglutarate, to glutamate. Given this information, we hypothesize that in wild type males the epidermis may act similarly to astrocytes resulting in a significant contribution of neuronal acetyl CoA.

In day 2 wild type males, the contribution of fatty acid derived neuronal acetyl CoA by the epidermis is exacerbated by increases in lipid catabolism. In *fat-6(lf);fat-7(lf)* mutants, the rescue of *fat-6(+)* in the epidermis was enough to restore mating fitness. While the epidermal rescue of mating fitness increased across 72 hours, closer observations suggest day 1 mating fitness increased substantially. This may indicate that an appropriate balance between primarily neuronal glucose metabolism and epidermal fat metabolism must be maintained. This is supported by the day 1 rescue of mating fitness in *pck-1(lf);pck-2(lf)* with supplemented D-glucose.

Interestingly, the balance between different fuels and their tissue of origins changes on day 2. For example, the epidermal *fat*-6 rescue in *fat-6(lf);fat-7(lf)* did not substantially increase mating fitness on day 2. Also D-glucose on day 2 did not rescue *pck-1(lf);pck-2(lf)* defects. Previously published work showed that hexokinase, initiates glycolysis, was upregulated on day 2 resulting in potential ROS production. The

possibility exists that increases in hexokinase with D-glucose supplementation exacerbates day 2 ROS generation. *fat-6(lf);fat-7(lf)* excessive fat oxidation byproducts in the epidermis may also result in increased ROS production in neurons despite epidermal *fat-6*. Altogether, a cohesive and coordinated anabolic response is needed to delay mating behavior decay.

Epidermal Support Tissue for Neuronal Fat Accumulation

Previously published work has shown that neurons secrete fatty acids for processing in astrocytes, avoiding activity dependent dysfunction (Ioannou, Jackson et al. 2019). The authors induced neuronal excitotoxicity and measured increases in lipid peroxidation, oxidative radicals reacting with unsaturated fatty acids (Ioannou, Jackson et al. 2019). Subsequently, neuronal lipoproteins then traffic free fatty acids to astrocytes (Ioannou, Jackson et al. 2019). In turn, astrocytes increase cytoplasmic lipolysis during enhanced neuronal activity by sensing glutamate NMDA, glutamate receptor, binding (Ioannou, Jackson et al. 2019). Astrocytic mitochondria are also found with increased loads of saturated fat following enhanced neuronal activity (Ioannou, Jackson et al. 2019). Although we did not observe neuronal death, excitotoxicity, in aging wild type and *fat-6(lf);fat-7(lf)* males we expect that increased cell excitability with age, previously shown in *C. elegans* males, can be exacerbated or caused by increased fat catabolism.

Excitotoxicity is thought to be caused by over activation of glutamate receptors resulting in inward currents of Na^{+} and Ca^{2+} (Dong, Wang et al. 2009). In turn proteases

are activated, by calcium and damage a variety of proteins involved in cytoskeleton and metabolism (Dong, Wang et al. 2009). The calcium activity observed in *fat-6(lf);fat-7(lf)* suggests an exaggerated calcium inward current. Interestingly, the calcium currents, in *fat-6(lf);fat-7(lf),* were extinguished quicker than those seen in wild type males. The ERG-like/UNC-103 and EAG/EGL-2 channels may play a role in repolarizing neurons in *fat-6(lf);fat-7(lf)* avoiding excitotoxicity.

Functionally Diverse Neuron and Muscles in the Male Tail

The circuit responsible for spicule insertion is composed of multiple sensory-motor neurons. The neurons control complex muscles capable of fast and slow twitch like responses. For example, proprioceptive neurons, upon sensing the vulva, normally elicit a continuous high frequency spicule prodding motor response encompassing multiple muscles. Vital to the process of spicule prodding is the continuous contraction and relaxation of protractor muscles. When the spicules partially penetrate the vulval slit, the SPC proprioceptive motor neurons induce sustained spicule muscle contraction, which forces the spicules through the vulva. This highlights the multifaceted nature of the protractor muscles capable of high frequency contraction and sustained contraction; fast and slow twitch like muscle.

The sensory-motor neurons, controlling fast and slow twitch like muscles, are also electrically and chemically connected to other tissues, e.g., necessary for sperm release. The extensive connections between neurons and other tissues require temporal regulation of differing motor programs (LeBoeuf, Correa et al. 2014). Therefore, we can

expect a high degree of complexity in regulating appropriate responses under the burden of a concurrent mating behavior. Maintaining the appropriate responses also requires energy demanding regulation of ions by leak channels. We hypothesize a substantial metabolic requirement for the intromission circuitry to quickly respond to the vulva and maintain extended sessions of mating. Also, the precise temporal regulation of motor programs most likely requires external metabolic support. While this support may be heavily glucose dependent on day 1 of adulthood, we suggest a constant requirement of saturated and unsaturated lipid pools in the epidermis. A constant supply of unsaturated fat may support long sessions of fatiguing complex motor responses. This may also help maintain membrane thresholds used in triggering rapid on-and-off motor responses during extended stretches of copulation.

Neuronal Morphological Changes with Age

Neurons have recently been shown to morphologically change with early age resulting in hypersensitive responses to stimuli. For example, the URX neuron increases dendritic arborizations by day 4 of adulthood in hermaphrodites. Changes in dendritic structure result in increases in calcium responses and oxygen sensitivity (Cohn, Cebul et al. 2020). We showed that males undergoing increased saturated fat oxidation have hyperactive cholinergic transmission and enhanced transient cholinergic neural activity. Dysregulated neuronal calcium activity results in compensatory upregulation of potassium channels which increase the threshold to neuronal activation. While we show no evidence of morphological neuronal deficits it could be possible that males

undergoing enhanced fat oxidation also eventually develop changes in arborization or neuronal architecture that result in sensory deficits.

Locomotor Motor Neurons and Spicule Circuitry Connectivity

A-class motor cholinergic excitatory neurons, producing rhythmic calcium transients, are regulated by activated premotor AVA interneurons in the head and result in backward movement (Wen, Gao et al. 2018). Conversely B-class motor neurons are regulated by activated AVB interneurons in the head resulting in forward movement (Wen, Gao et al. 2018). The mating deficit of the *fat-6(lf);fat-7(lf)* males is in part due to instability in body posture during spicule insertion. We found enhanced transient calcium activity in several A-class motor neurons including VA12, and DA7. This would suggest that neurons regulating forward locomotion were becoming increasingly activated and repolarized faster than the same neurons found in wild type males. We expect this would lead to locomotive stuttering resulting in insufficient stabilization for spicule insertion.

Several of the A and B-class motor neurons are connected either through a gap junction or synapse to neurons involved in spicule insertion. For example, VB11, DB7 and VA11 are connected to the PDB, PDC, or PVV neurons controlling copulatory locomotion and posture after sensing the vulva through HOA or HOB. PVV neurons in turn also connect either through synapse or gap junction to PCB controlling appropriate sensing of the vulva and spicule insertion. Some of the remaining neurons we observed, male specific CA9, with higher calcium transients are indirectly connected either by gap

junction or synapse to the spicule insertion cholinergic neurons SPC, PCB, and PCC. Altogether we suggest that locomotor behavior and tail positioning on the vulva are regulated together with spicule insertion.

Future Experiments

Transcriptional Responses in fat-6(lf);fat-7(lf) Males

RNA-seq can provide whole worm metabolic dynamics across age. Unfortunately, whole worm RNA-seq would most likely be biased towards larger tissues, intestine. Alternatively, it would provide information that would not represent individual tissues but a mixed signal incorporating varied metabolic responses across multiple tissues. Recent work has combated this problem by sorting cells into distinct clusters and then assigning cell types by comparing gene expression patterns reported in the literature.

Alternatively, to perform tissue specific analysis would require single cell RNA-seq and the use of microfluidic cell sorting. The simple nervous system of the *C. elegans* male is composed of approximately 385 neurons and at least ~118 neuronal classes. Recent single cell RNA-seq in hermaphrodites conducted on larval animals could only cluster ~23 neuronal classes (Cao, Packer et al. 2017). Without more cell specific promoters, analyzing RNA-seq data may prove difficult.

The epidermis is a multinucleate tissue, >100 nuclei spanning the whole worm, presenting a problem when it comes to analyzing local changes near the neurons and

muscles of the male tail. If we could isolate posterior epidermis and isolate cholinergic neuronal populations across day 1-2 adult males, it may allow us to observe native differences in metabolic gene expression. For example, the expression of PDHC is known to be upregulated in neurons and downregulated in astrocytes. This unique expression profile determines which tissue it most likely to convert glucose into pyruvate and consequently acetyl CoA. If cholinergic neuronal PDHC is higher in the male tail on day 1 than glucose will most likely be made into acetyl CoA. Any metabolic changes of PDHC across age may hint at a metabolite flow change across tissues. If neuronal PDHC is lower with age than pyruvate may be preferentially converted to lactate and taken up by the epidermis.

Spatial Regulation of FAT-6 in Males

A CRISPR/Cas9 YFP knock is a powerful tool which in conjunction with an EMS screen could elucidate mutations that result in spatially and temporally dysregulated FAT-6. Of interest would be how the intestine is metabolically compartmentalized. Not only does the gonad potentially regulate the posterior intestine but *fat-5(lf);fat-7(lf)* mutants clearly show increases in FAT-6 in the posterior intestine. Given the clear and obvious expression pattern increases in specific compartments of the intestine, we should be able to dissect expressional dynamics easily. Additionally, the FAT-6 protein degradation occurring in the head and tail epidermis during adulthood is drastic. Any mutation that would result in a 2-fold or higher increase in FAT-6 in the epidermis would be identifiable.

Our work showed that tissue specific rescue's required glycolytic metabolites in the day 1 male Tail. The types of metabolites required to sustain mating behavior with age are unknown. Despite glucose improving *pck-1(lf);pck-2(lf)* mating fitness, we do not know which metabolites are required for day 2. Conducting a screen, using FAT-6::YFP or PCK-2::YFP expressional changes, of well-known metabolites exchanged between astrocytes and neurons could reveal information on the metabolic needs of these tissues with age. For example, any metabolite that results in the increase of day 1 FAT-6 or PCK-2 could indicate a specific metabolic flux occurring on day 2. We could then proceed with characterized mutations in the metabolic genes responsible for the specific metabolite production. Alternatively, if metabolite supplementation decreases the expression of FAT-6 or PCK-2, we could observe mating fitness with age under metabolite supplementation.

Epidermal Support Tissue for Neuronal Fat Accumulation

Published papers have suggested that changes in fat metabolism can result in neighboring tissues increasing lipid droplets and lipase activity. In some cases, lipids are transferred using lipoproteins and undergo mitochondrial β-oxidation. I propose using a variety of neutral lipid stains and ROS dyes to specifically characterize the tissues of the male tail. Previous research has used a myriad of fluorescent dyes to determine ROS levels; including 2′,7′-dichlorodihydrofluorescein diacetate (H2DCFDA), dihydroethidium (DHE) and CellROX® Deep Red (Tao, Wu et al. 2017). The objective would be to characterize male tail tissue specific changes taking place across day 1-2.

The use of stains and dyes in combination with metabolite supplementation may indicate how neighboring tissues are reacting to aging neurons and muscles.

In addition, we can measure the formation of lipid peroxides in *C. elegans*, using the sensor BODIPY581/591 undecanoic acid (BODIPY581/591-C11) (Beaudoin-Chabot, Wang et al. 2019). The sensor emission peak shifts from 590 to 510 nm when the polyunsaturated butadienyl domain is oxidized. With continued innovation in BODPIY staining of *C. elegans*, new tissue specific patterns of lipid storage may be revealed. For example, a new hybrid probe was recently created showing more specific staining of lipids in the posterior end of a hermaphrodite (Mota, Correa et al. 2018).

Conclusion

In my work I found epidermal fat synthesis and gluco-glyceroneogenesis plays a role in supporting neighboring tissue metabolism such that behavioral fitness is maintained during early adulthood in male *C. elegans*. Evidence of transcriptional metabolic switches during days 1-2 of adulthood was validated with compartmentalized FAT-6 protein maintenance. The dynamics of FAT-6 protein levels informed differences in local metabolism and regulation dependence on feeding state. Furthermore, wild type feeding, exploring, and mating behavioral switches were found to be a driving force of metabolic shifts and behavioral fitness outcomes. Similarities between increased saturated fat oxidation and food deprivation culminated in compensatory increases in potassium channel expression. In mutants incapable of gluco-

glyceroneogenesis the opposite was seen with decreases in day 1 potassium channel expression. The impact of increased saturated fat was evaluated through observation of neural activity and found to be defined by enhanced acute calcium transients. Further work will have to be done to uncover how differences in fuel usage result in local changes in tissue specific metabolism.

REFERENCES

Alberici, L. C., H. C. Oliveira, P. R. Patrício, A. J. Kowaltowski and A. E. Vercesi (2006). "Hyperlipidemic mice present enhanced catabolism and higher mitochondrial ATP-sensitive K+ channel activity." Gastroenterology **131**(4): 1228-1234.

Alfonso, A., K. Grundahl, J. S. Duerr, H. P. Han and J. B. Rand (1993). "The Caenorhabditis elegans unc-17 gene: a putative vesicular acetylcholine transporter." Science **261**(5121): 617-619.

Alfonso, A., K. Grundahl, J. R. McManus, J. M. Asbury and J. B. Rand (1994). "Alternative splicing leads to two cholinergic proteins in Caenorhabditis elegans." J Mol Biol **241**(4): 627-630.

Alfonso, A., K. Grundahl, J. R. McManus and J. B. Rand (1994). "Cloning and characterization of the choline acetyltransferase structural gene (cha-1) from C. elegans." J Neurosci **14**(4): 2290-2300.

Amtul, Z., M. Uhrig, R. F. Rozmahel and K. Beyreuther (2011). "Structural insight into the differential effects of omega-3 and omega-6 fatty acids on the production of Abeta peptides and amyloid plaques." J Biol Chem **286**(8): 6100-6107.

Appel, L. J., F. M. Sacks, V. J. Carey, E. Obarzanek, J. F. Swain, E. R. Miller, 3rd, P. R. Conlin, T. P. Erlinger, B. A. Rosner, N. M. Laranjo, J. Charleston, P. McCarron and L. M. Bishop (2005). "Effects of protein, monounsaturated fat, and carbohydrate intake on blood pressure and serum lipids: results of the OmniHeart randomized trial." Jama **294**(19): 2455-2464.

Ballard, F. J. and R. W. Hanson (1969). "Purification of phosphoenolpyruvate carboxykinase from the cytosol fraction of rat liver and the immunochemical demonstration of differences between this enzyme and the mitochondrial phosphoenolpyruvate carboxykinase." J Biol Chem **244**(20): 5625-5630.

Beal, M. F. (2005). "Mitochondria take center stage in aging and neurodegeneration." Ann Neurol **58**(4): 495-505.

Beaudoin-Chabot, C., L. Wang, A. V. Smarun, D. Vidović, M. S. Shchepinov and G. Thibault (2019). "Deuterated Polyunsaturated Fatty Acids Reduce Oxidative Stress and Extend the Lifespan of C. elegans." Front Physiol **10**: 641.

Biswas, A., P. I. Oh, G. E. Faulkner, R. R. Bajaj, M. A. Silver, M. S. Mitchell and D. A. Alter (2015). "Sedentary time and its association with risk for disease incidence, mortality, and hospitalization in adults: a systematic review and meta-analysis." Ann Intern Med **162**(2): 123-132.

Brenner, S. (1974). "The genetics of *Caenorhabditis elegans*." Genetics **77**(1): 71-94.

Brock, T. J., J. Browse and J. L. Watts (2006). "Genetic regulation of unsaturated fatty acid composition in C. elegans." PLoS Genet **2**(7): e108.

Brock, T. J., J. Browse and J. L. Watts (2007). "Fatty acid desaturation and the regulation of adiposity in Caenorhabditis elegans." Genetics **176**(2): 865-875.

Cao, J., J. S. Packer, V. Ramani, D. A. Cusanovich, C. Huynh, R. Daza, X. Qiu, C. Lee, S. N. Furlan, F. J. Steemers, A. Adey, R. H. Waterston, C. Trapnell and J. Shendure (2017). "Comprehensive single-cell transcriptional profiling of a multicellular organism." Science **357**(6352): 661-667.

Castelein, N., D. Hoogewijs, A. De Vreese, B. P. Braeckman and J. R. Vanfleteren (2008). "Dietary restriction by growth in axenic medium induces discrete changes in the transcriptional output of genes involved in energy metabolism in *Caenorhabditis elegans*." Biotechnol J **3**(6): 803-812.

Chen, T. W., T. J. Wardill, Y. Sun, S. R. Pulver, S. L. Renninger, A. Baohan, E. R. Schreiter, R. A. Kerr, M. B. Orger, V. Jayaraman, L. L. Looger, K. Svoboda and D. S. Kim (2013). "Ultrasensitive fluorescent proteins for imaging neuronal activity." Nature **499**(7458): 295-300.

Cohn, J. A., E. R. Cebul, G. Valperga, L. Brose, M. de Bono, M. G. Heiman and J. T. Pierce (2020). "Long-term activity drives dendritic branch elaboration of a C. elegans sensory neuron." Dev Biol.

Cully, D. F., D. K. Vassilatis, K. K. Liu, P. S. Paress, L. H. T. Van der Ploeg, J. M. Schaeffer and J. P. Arena (1994). "Cloning of an avermectin-sensitive glutamate-gated chloride channel from *Caenorhabditis elegans*." Nature **371**(6499): 707-711.

De Meyts, P. (2000). The Insulin Receptor and Its Signal Transduction Network. Endotext. K. R. Feingold, B. Anawalt, A. Boyce et al. South Dartmouth (MA), MDText.com, Inc.
Copyright © 2000-2021, MDText.com, Inc.

Dickinson, D. J., J. D. Ward, D. J. Reiner and B. Goldstein (2013). "Engineering the *Caenorhabditis elegans* genome using Cas9-triggered homologous recombination." Nat Methods **10**: 1028.

Dong, X. X., Y. Wang and Z. H. Qin (2009). "Molecular mechanisms of excitotoxicity and their relevance to pathogenesis of neurodegenerative diseases." Acta Pharmacol Sin **30**(4): 379-387.

Doonan, R., J. J. McElwee, F. Matthijssens, G. A. Walker, K. Houthoofd, P. Back, A. Matscheski, J. R. Vanfleteren and D. Gems (2008). "Against the oxidative damage theory of aging: superoxide dismutases protect against oxidative stress but have little or no effect on life span in Caenorhabditis elegans." Genes Dev **22**(23): 3236-3241.

Ebert, D., R. G. Haller and M. E. Walton (2003). "Energy contribution of octanoate to intact rat brain metabolism measured by 13C nuclear magnetic resonance spectroscopy." J Neurosci **23**(13): 5928-5935.

Evans, J. G. (1993). "Metabolic switches in ageing." Age Ageing **22**(2): 79-81.

Garcia, L. R., P. Mehta and P. W. Sternberg (2001). "Regulation of distinct muscle behaviors controls the C. elegans male's copulatory spicules during mating." Cell **107**(6): 777-788.

Garcia, L. R. and P. W. Sternberg (2003). "Caenorhabditis elegans UNC-103 ERG-like potassium channel regulates contractile behaviors of sex muscles in males before and during mating." J Neurosci **23**(7): 2696-2705.

Gems, D. and R. Doonan (2009). "Antioxidant defense and aging in C. elegans: is the oxidative damage theory of aging wrong?" Cell Cycle **8**(11): 1681-1687.

Gems, D. and D. L. Riddle (2000). "Defining Wild-Type Life Span in Caenorhabditis elegans." The Journals of Gerontology: Series A **55**(5): B215-B219.

Glenn, C. F., D. K. Chow, L. David, C. A. Cooke, M. S. Gami, W. B. Iser, K. B. Hanselman, I. G. Goldberg and C. A. Wolkow (2004). "Behavioral Deficits During Early Stages of Aging in Caenorhabditis elegans Result From Locomotory Deficits Possibly Linked to Muscle Frailty." The Journals of Gerontology: Series A **59**(12): 1251-1260.

Goldstein, B. J., K. Mahadev and X. Wu (2005). "Redox paradox: insulin action is facilitated by insulin-stimulated reactive oxygen species with multiple potential signaling targets." Diabetes **54**(2): 311-321.

Goncalves, J., Y. Wan, X. Guo, K. Rha, B. LeBoeuf, L. Zhang, K. Estler and L. R. Garcia (2020). "Succinate Dehydrogenase-Regulated Phosphoenolpyruvate Carboxykinase Sustains Copulation Fitness in Aging C. elegans Males." iScience **23**(4): 100990.

Gruninger, T. R., D. G. Gualberto and L. R. Garcia (2008). "Sensory perception of food and insulin-like signals influence seizure susceptibility." PLoS Genet **4**(7): e1000117.

Gruninger, T. R., D. G. Gualberto, B. LeBoeuf and L. R. Garcia (2006). "Integration of male mating and feeding behaviors in Caenorhabditis elegans." J Neurosci **26**(1): 169-179.

Guo, X. and L. R. García (2014). "SIR-2.1 integrates metabolic homeostasis with the reproductive neuromuscular excitability in early aging male Caenorhabditis elegans." eLife **3**: e01730-e01730.

Guo, X., A. Navetta, D. G. Gualberto and L. R. García (2012). "Behavioral decay in aging male C. elegans correlates with increased cell excitability." Neurobiology of Aging **33**(7): 1483.e1485-1483.e1423.

Herndon, L. A., P. J. Schmeissner, J. M. Dudaronek, P. A. Brown, K. M. Listner, Y. Sakano, M. C. Paupard, D. H. Hall and M. Driscoll (2002). "Stochastic and genetic factors influence tissue-specific decline in ageing C. elegans." Nature **419**(6909): 808-814.

Herndon, L. A., P. J. Schmeissner, J. M. Dudaronek, P. A. Brown, K. M. Listner, Y. Sakano, M. C. Paupard, D. H. Hall and M. Driscoll (2002). "Stochastic and genetic factors influence tissue-specific decline in ageing C. elegans." Nature **419**(6909): 808-814.

Hodgkin, J. and T. Doniach (1997). "Natural variation and copulatory plug formation in Caenorhabditis elegans." Genetics **146**(1): 149-164.

Hodgkin, J. A., H. R. Horvitz and S. Brenner (1979). "Nondisjunction mutants of the nematode *Caenorhabditis elegans*." Genetics **91**: 67-94.

Huang, C., C. Xiong and K. Kornfeld (2004). "Measurements of age-related changes of physiological processes that predict lifespan of Caenorhabditis elegans." Proc Natl Acad Sci U S A **101**(21): 8084-8089.

Ioannou, M. S., J. Jackson, S. H. Sheu, C. L. Chang, A. V. Weigel, H. Liu, H. A. Pasolli, C. S. Xu, S. Pang, D. Matthies, H. F. Hess, J. Lippincott-Schwartz and Z. Liu (2019). "Neuron-Astrocyte Metabolic Coupling Protects against Activity-Induced Fatty Acid Toxicity." Cell **177**(6): 1522-1535.e1514.

Jabr, R. I. and W. C. Cole (1993). "Alterations in electrical activity and membrane currents induced by intracellular oxygen-derived free radical stress in guinea pig ventricular myocytes." Circ Res **72**(6): 1229-1244.

Jee, C., J. F. Goncalves, B. LeBoeuf and L. R. Garcia (2016). "CRF-like receptor SEB-3 in sex-common interneurons potentiates stress handling and reproductive drive in C. elegans." Nat Commun **7**: 11957.

Kirkwood, T. B. L. (1977). "Evolution of ageing." Nature **270**(5635): 301-304.

LeBoeuf, B., T. R. Gruninger and L. R. Garcia (2007). "Food deprivation attenuates seizures through CaMKII and EAG K+ channels." PLoS Genet **3**(9): 1622-1632.

LeBoeuf, B., X. Guo and L. R. García (2011). "The effects of transient starvation persist through direct interactions between CaMKII and ether-a-go-go K+ channels in C. elegans males." Neuroscience **175**: 1-17.

Liang, B., K. Ferguson, L. Kadyk and J. L. Watts (2010). "The role of nuclear receptor NHR-64 in fat storage regulation in Caenorhabditis elegans." PLoS One **5**(3): e9869.

Ly, K., S. J. Reid and R. G. Snell (2015). "Rapid RNA analysis of individual Caenorhabditis elegans." MethodsX **2**: 59-63.

Maronpot, R. R., K. Yoshizawa, A. Nyska, T. Harada, G. Flake, G. Mueller, B. Singh and J. M. Ward (2010). "Hepatic enzyme induction: histopathology." Toxicol Pathol **38**(5): 776-795.

Matthews, C. E., S. M. George, S. C. Moore, H. R. Bowles, A. Blair, Y. Park, R. P. Troiano, A. Hollenbeck and A. Schatzkin (2012). "Amount of time spent in sedentary behaviors and cause-specific mortality in US adults." Am J Clin Nutr **95**(2): 437-445.

Mattson, M. P., W. A. Pedersen, W. Duan, C. Culmsee and S. Camandola (1999). "Cellular and molecular mechanisms underlying perturbed energy metabolism and neuronal degeneration in Alzheimer's and Parkinson's diseases." Ann N Y Acad Sci **893**: 154-175.

Mota, A. A. R., J. R. Correa, L. P. de Andrade, J. A. F. Assumpção, G. A. de Souza Cintra, L. H. Freitas-Junior, W. A. da Silva, H. C. B. de Oliveira and B. A. D. Neto (2018). "From Live Cells to Caenorhabditis elegans: Selective Staining and Quantification of Lipid Structures Using a Fluorescent Hybrid Benzothiadiazole Derivative." ACS Omega **3**(4): 3874-3881.

Murphy, M. P. (2009). "How mitochondria produce reactive oxygen species." Biochem J **417**(1): 1-13.

Perez, C. L. and M. R. Van Gilst (2008). "A 13C isotope labeling strategy reveals the influence of insulin signaling on lipogenesis in C. elegans." Cell Metab **8**(3): 266-274.

Pino, E. C., C. M. Webster, C. E. Carr and A. A. Soukas (2013). "Biochemical and high throughput microscopic assessment of fat mass in *Caenorhabditis elegans*." J Vis Exp(73): 50180.

Reiner, D. J., D. Weinshenker, H. Tian, J. H. Thomas, K. Nishiwaki, J. Miwa, T. Gruninger, B. LeBoeuf and L. R. Garcia (2006). "BEHAVIORAL GENETICS OF CAENORHABDITIS ELEGANS UNC-103-ENCODED ERG-LIKE K+ CHANNEL." Journal of Neurogenetics **20**(1-2): 41-66.

Rumora, A. E., S. I. Lentz, L. M. Hinder, S. W. Jackson, A. Valesano, G. E. Levinson and E. L. Feldman (2018). "Dyslipidemia impairs mitochondrial trafficking and function in sensory neurons." Faseb j **32**(1): 195-207.

Schedl, T. and J. Kimble (1988). "*fog-2*, a germ-line-specific sex determination gene required for hermaphrodite spermatogenesis in *Caenorhabditis elegans*." Genetics **119**(1): 43-61.

Schnabel, H. and R. Schnabel (1990). "An Organ-Specific Differentiation Gene, pha-1, from Caenorhabditis elegans." Science **250**(4981): 686-688.

Schrack, J. A., N. D. Knuth, E. M. Simonsick and L. Ferrucci (2014). ""IDEAL" aging is associated with lower resting metabolic rate: the Baltimore Longitudinal Study of Aging." J Am Geriatr Soc **62**(4): 667-672.

Shi, C., A. M. Runnels and C. T. Murphy (2017). "Mating and male pheromone kill Caenorhabditis males through distinct mechanisms." Elife **6**.

Stark, R. and R. G. Kibbey (2014). "The mitochondrial isoform of phosphoenolpyruvate carboxykinase (PEPCK-M) and glucose homeostasis: has it been overlooked?" Biochim Biophys Acta **1840**(4): 1313-1330.

Stark, R., F. Pasquel, A. Turcu, R. L. Pongratz, M. Roden, G. W. Cline, G. I. Shulman and R. G. Kibbey (2009). "Phosphoenolpyruvate cycling via mitochondrial

phosphoenolpyruvate carboxykinase links anaplerosis and mitochondrial GTP with insulin secretion." J Biol Chem **284**(39): 26578-26590.

Swerdlow, R. H. and S. M. Khan (2004). "A "mitochondrial cascade hypothesis" for sporadic Alzheimer's disease." Med Hypotheses **63**(1): 8-20.

Tangney, C. C., H. Li, Y. Wang, L. Barnes, J. A. Schneider, D. A. Bennett and M. C. Morris (2014). "Relation of DASH- and Mediterranean-like dietary patterns to cognitive decline in older persons." Neurology **83**(16): 1410-1416.

Tao, J., Q. Y. Wu, Y. C. Ma, Y. L. Chen and C. G. Zou (2017). "Antioxidant response is a protective mechanism against nutrient deprivation in C. elegans." Sci Rep **7**: 43547.

Taubert, S., M. R. Van Gilst, M. Hansen and K. R. Yamamoto (2006). "A Mediator subunit, MDT-15, integrates regulation of fatty acid metabolism by NHR-49-dependent and -independent pathways in C. elegans." Genes & development **20**(9): 1137-1149.

Tracey, T. J., F. J. Steyn, E. J. Wolvetang and S. T. Ngo (2018). "Neuronal Lipid Metabolism: Multiple Pathways Driving Functional Outcomes in Health and Disease." Front Mol Neurosci **11**: 10.

Van Gilst, M. R., H. Hadjivassiliou, A. Jolly and K. R. Yamamoto (2005). "Nuclear hormone receptor NHR-49 controls fat consumption and fatty acid composition in C. elegans." PLoS Biol **3**(2): e53.

Vincent, A. M., J. M. Hayes, L. L. McLean, A. Vivekanandan-Giri, S. Pennathur and E. L. Feldman (2009). "Dyslipidemia-induced neuropathy in mice: the role of oxLDL/LOX-1." Diabetes **58**(10): 2376-2385.

Watts, J. L. and J. Browse (2000). "A palmitoyl-CoA-specific delta9 fatty acid desaturase from Caenorhabditis elegans." Biochem Biophys Res Commun **272**(1): 263-269.

Yang, F., B. W. Vought, J. S. Satterlee, A. K. Walker, Z. Y. Jim Sun, J. L. Watts, R. DeBeaumont, R. Mako Saito, S. G. Hyberts, S. Yang, C. Macol, L. Iyer, R. Tjian, S.

van den Heuvel, A. C. Hart, G. Wagner and A. M. Näär (2006). "An ARC/Mediator subunit required for SREBP control of cholesterol and lipid homeostasis." Nature **442**(7103): 700-704.

Yuan, Y., P. Hakimi, C. Kao, A. Kao, R. Liu, A. Janocha, A. Boyd-Tressler, X. Hang, H. Alhoraibi, E. Slater, K. Xia, P. Cao, Q. Shue, T. T. Ching, A. L. Hsu, S. C. Erzurum, G. R. Dubyak, N. A. Berger, R. W. Hanson and Z. Feng (2016). "Reciprocal Changes in Phosphoenolpyruvate Carboxykinase and Pyruvate Kinase with Age Are a Determinant of Aging in Caenorhabditis elegans." J Biol Chem **291**(3): 1307-1319.

Yuan, Y., C. S. Kadiyala, T. T. Ching, P. Hakimi, S. Saha, H. Xu, C. Yuan, V. Mullangi, L. Wang, E. Fivenson, R. W. Hanson, R. Ewing, A. L. Hsu, M. Miyagi and Z. Feng (2012). "Enhanced energy metabolism contributes to the extended life span of calorie-restricted Caenorhabditis elegans." J Biol Chem **287**(37): 31414-31426.

APPENDIX

Cell Excitability in *fat-6(lf)*

Many genes are known to be involved in unsaturated fatty acid synthesis. I did a casual screen of the *fat* genes numbering 1-7 for decreases in opacity, proxy for lipid storage, and for ease of propagation. The *fat-6(lf)* and *fat-7(lf)* single mutants seemed like potential candidates. To first determine if cholinergic stimulation of spicule protractor muscle contraction was defective in *fat-6(lf),* I introduced wild type and mutant males to baths containing increasing concentrations of the non-specific cholinergic agonist arecoline and levamisole. We found the single mutant's response to exogenously applied arecoline and levamisole was similar to wild-type, indicating that cholinergic signal transduction and muscle contraction were functional (Fig. 62). I continued with the *fat-6(lf);fat-7(lf)* double mutants for the remained of my research.

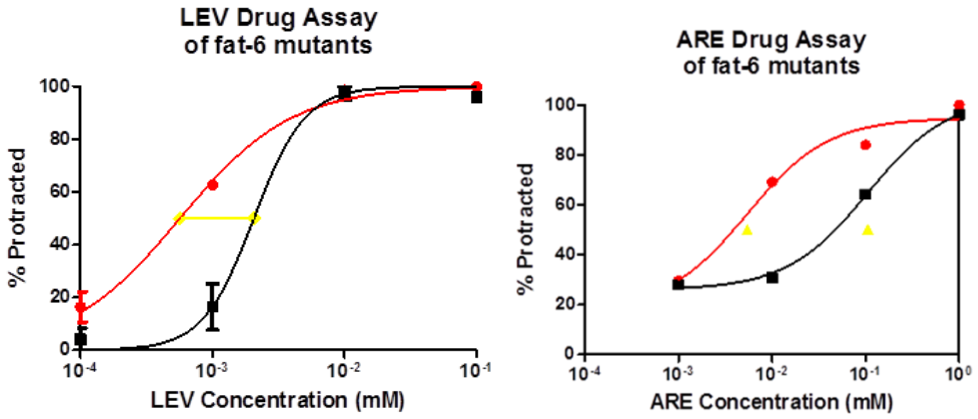

Figure 62 Excitability in *fat-6(lf)* males.
Wild type (black) and *fat-6(lf)*(red) day 1 males were incubated in increasing arecoline and levamisole concentration. We quantified the protraction of the spicule as a proxy for muscle contraction.

fat-6(lf);fat-7(lf) Sensitivity to ROS

fat-6(lf);fat-7(lf) mutants were characterized as having increased mitochondrial respiration. In order to address whether *fat-6(lf);fat-7(lf)* mutants were sensitive to mitochondrial ROS production, we treated males with paraquat and measured rate of death and suicide. Paraquat is reduced by an electron donor, accepts electrons, and is oxidized by dioxygen, transfer of electrons, producing superoxide (ROS). The oxidized form of paraquat is regenerated after creating ROS and is made available to shunt electrons continuously. *fat-6(lf);fat-7(lf)* mutants were found to be as sensitive as wild type males, supporting potential compensatory mechanisms to deal with increased ROS generation (Fig. 63).

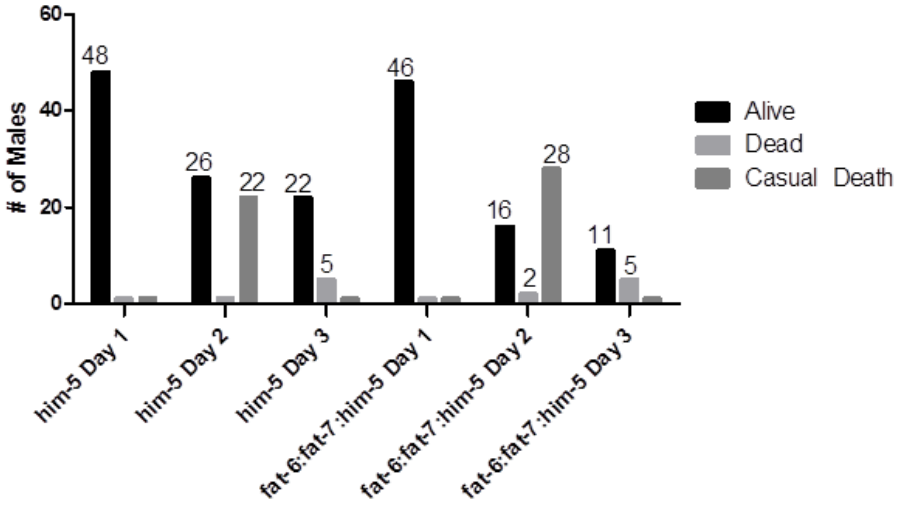

Figure 63 Paraquat Survival in *fat-6(lf);fat-7(lf)* males.
NGM plates were supplemented with 10mM paraquat. Males were incubated for prolonged period of time, day 1-3 of adulthood. Corpses and missing animals were quantified as dead and casual death respectively.

PEPCK Expression in *fat-6(lf);fat-7(lf)*

Given that the fat mutants were hypothesized to have increased fat oxidation and TCA cycle flux, we addressed whether *pck-2*::YFP, in hermaphrodites, increased in *fat-7(lf)*, *fat-6(lf)*, and *fat-6(lf);fat-7(lf)*. PEPCK could potentially shunt metabolites away from the TCA cycle ameliorating increased fat oxidation. I observed no significant difference in PCK-2::YFP expression in any of the mutant background except for *fat-7(lf)* (Fig. 64). The main compensatory mechanisms in *fat-7(lf)*, increases in *fat-5(lf)* and *fat-6(lf)*, have been characterized through RT-qPCR in hermaphrodites. It is possible that many more anabolic processes are upregulated maintaining the phenotypically wild type *fat-7(lf)* male. More work needs to be done to address initial observations as well as

potential increased PCK-2::YFP expression in the first few segments of the anterior intestine in *fat-6(lf);fat-7(lf)*.

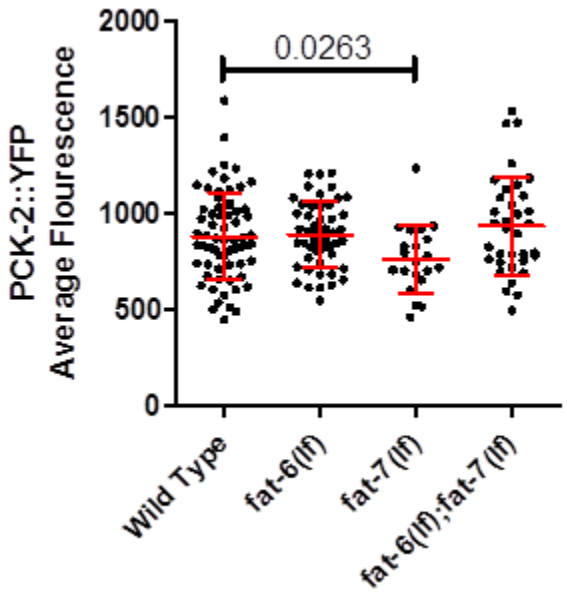

Figure 64 The expression of PEPCK in *fat* mutants.
The average fluorescence of PCK-1::YFP was obtained through the entire intestine using a series of square-like ROI's. Mann Whitney t-test was used to compare *fat-7(lf)* and wild type.

Mating Latency and Disengagement of *fat-6(lf);fat-7(lf)*

In searching for mating defects, I addressed whether *fat-6(lf);fat-7(lf)* mutant males were more prone to disengaging from mating behavior than wild type. Previous work had established the use of a mating interference (MI) assay where 475-nm (blue) light was used to disrupt male's mating behavior (Jee, Goncalves et al. 2016). The blue light acted as a noxious stimulus which *C. elegans* males would avoid. When I

performed the MI assay, wild type males took ~2-3 minutes to begin mating (Fig. 65). Upon shining blue light, wild type males disengaged from mating behavior within 50 seconds (Fig. 61). *fat-6(lf);fat-7(lf)* mutants took significantly longer to start mating but once engaged showed similar responses to noxious stimuli (Fig. 65 and 66).

Over the course of mating fitness trials, day 1 and day 2 males were competed against each other to gauge fitness with age. Preliminary data suggested that day 1 *fat-6(lf);fat-7(lf)* mutant males could outcompete older day 2 *fat-6(lf);fat-7(lf)* mutants (Fig. 67). After more trials we found that wild type day 2 males could mate similarly to day 1 males. Altogether this suggested that mating fitness can be maintained on day 2 for wild type males through increases in *fat-6/7* gene expression.

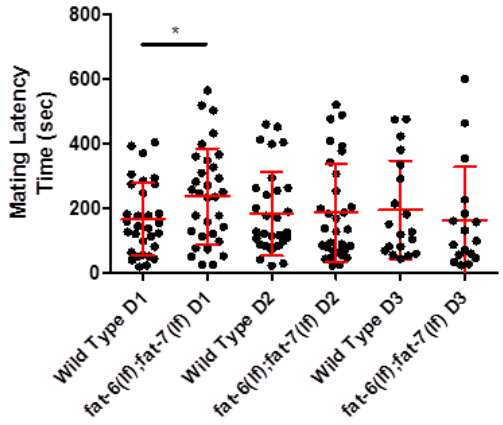

Figure 65 Mating Latency of *fat-6(lf);fat-7(lf)*.
NGM plates containing a small OP50 lawn were used in combination with a single hermaphrodite to gauge the amount of time it would take a male to mate. Man Whitney t-test.

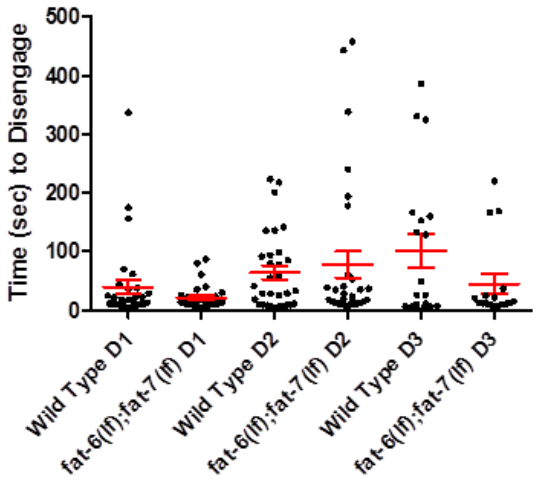

Figure 66 Mating Disengagement of *fat-6(lf);fat-7(lf)* males.
Blue light, with an average intensity of 3980 uW/cm^2, was used to determine the time to disengagement during mating behavior.

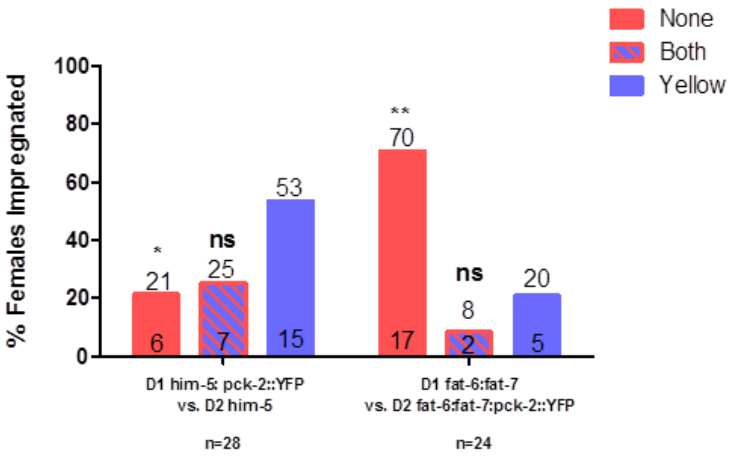

Figure 67 Competitive fitness declines in *fat-6(lf);fat-7(lf)*.
PCK-1::YFP was used to track paternity between day 1 and day 2 *fat-6(lf);fat-7(lf)* males competed against each other (Unpaired t-test). Number of animal's assay listed at the bottom of the bars. Percent of females impregnated listed on the top of the bars.

Behavioral Switches of Starved Males

Behavioral alterations to food-seeking and copulation preference were initially analyzed in well fed and starved wild type males. After designing mating arenas to monitor the male's choice to feed, mate, or explore its environment (Fig. 18), we assayed starved males. Males in each frame of the one-hour video were given a different arbitrary value if they were feeding, mating or exploring. These values were color-coded and plotted across time per male (Fig. 19 and 68). From first approximation, day 1 males who had been starved spent more time eating than mating, compared to day 1 males who had been well fed (Fig. 68).

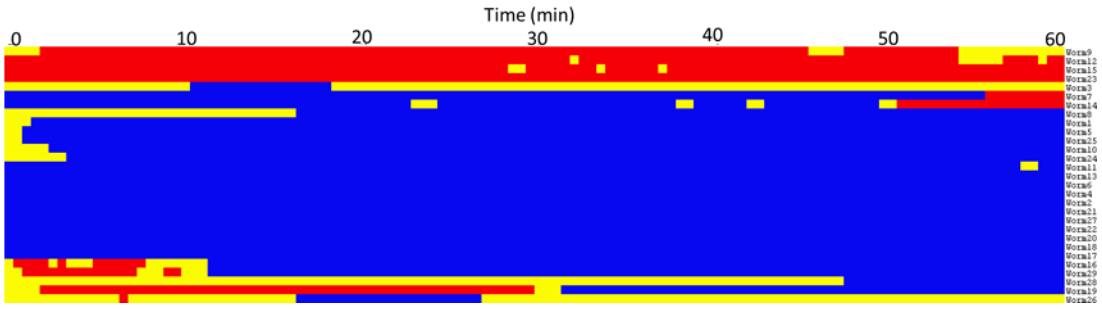

Figure 68 Visualized feeding, mating, and exploring behaviors in starved males. Raw data colorized in blue, yellow, and red for feeding, exploring, and mating behaviors respectively. The vertical axis corresponds to individual males. The horizontal axis corresponds to time in minutes.

Artificial Activation of LUA Interneuron

Work had been done that established the role of corticotropin-releasing factor receptor family homologue SEB-3 in activating an LUA interneuron capable of overriding environmental stimuli in favor of mating (Jee, Goncalves et al. 2016). At the reviewer's request, the first author asked that I attempt to induce an artificial activation of the interneuron LUA using an overexpression of *egl-30(gf)*.

egl-30 encodes an ortholog of the heterotrimeric G protein alpha subunit Gq (Gq/G11 class) that affects viability, locomotion, egg laying, synaptic transmission, and pharyngeal pumping. Gαq/11 stimulates the membrane-bound phospholipase C (beta isotype), which then cleaves PIP2 (phospholipid phosphatidylinositol 4, 5-bisphosphate) into two second messengers, IP3 (inositol 1, 4, 5-trisphosphate) and DAG (diacylglycerol). IP3 then diffuses through the cytosol to bind to IP3 receptors, particularly calcium channels in the smooth endoplasmic reticulum (ER). This causes the cytosolic concentration of calcium to increase, causing a cascade of intracellular changes and activity.

I specifically made an *egl-30 (tg26gF)* cDNA:SL2:GFP, including 4th intron, construct driven from four promoters including *rab-3*, *tph-1*, *gpa-10*, and *QUAS*. Preliminary work showed that the pan neuronal expression of in *egl-30(gf)* increased the onset of paralysis as gauged by aldicarb treatment (Fig. 69). Aldicarb inhibits acetylcholine esterase, an enzyme responsible for degrading acetylcholine at the synaptic cleft (Rand and Russell 1985, Nguyen, Alfonso et al. 1995, Miller, Alfonso et al. 1996).

Under inhibition, spontaneous release from cholinergic neurons leads to acetylcholine buildup and can result in sex muscle contraction and spicule protraction.

In addition I attempted to rescue *seb-3(lf)* with injections of *pseb-3*:hCRF1::GFP, *pseb-3* containing the beginning of exon 1;hCRF1;;GFP, and *pseb-3*:hCRF1:SL2:GFP into *pha-1; him-5; seb-3(lf)*. Preliminary lines appeared to possibly be rescued for *seb-3 (lf)*.

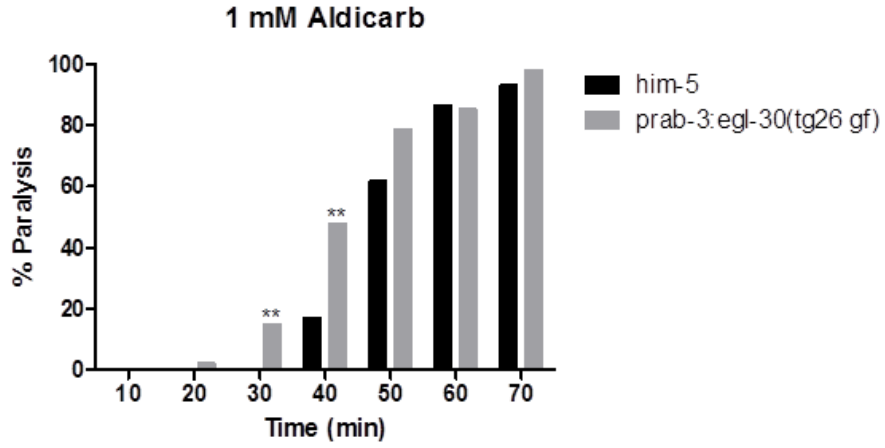

Figure 69 Artificial Activation of LUA Interneuron.
Transgenic expression of *egl-30(gf)* in wild type animals resulted in neuronal activation. The severity of activity was gauged by treatment with an acetylcholine esterase inhibitor, aldicarb, at 10mM.

Ca^{2+} Imaging of the Cholinergic Ventral Cord

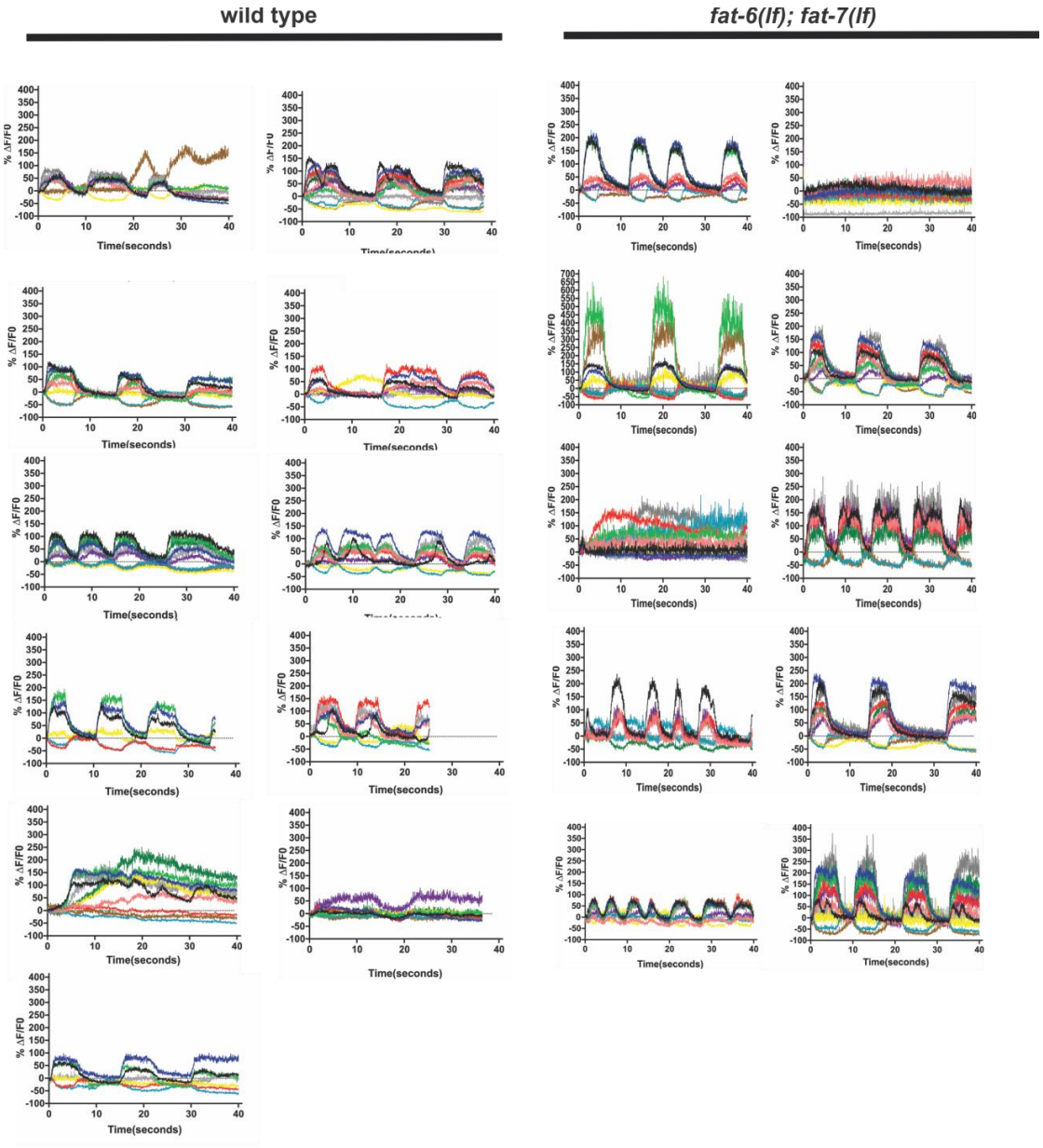

Figure 70 Complete Cholinergic Calcium Transients in *fat-6(lf);fat-7(lf)*
ROI's were drawn for 12 cholinergic neurons and fluorescence calcium waves were recorded across time.